Biomimetic approaches to pneumatic fiber-reinforced soft actuators for thumb motion support

August 2022

Yuanyuan WANG
Graduate School of Science and Engineering
CHIBA UNIVERSITY

CHIBA UNIVERSITY

DOCTORAL THESIS

Biomimetic approaches to pneumatic fiber-reinforced soft actuators for thumb motion support

Author:
Yuanyuan WANG

Supervisor:
Professor Wenwei YU

(千葉大学審査学位論文)

A thesis submitted in fulfillment of the requirements for the degree of Doctor of Engineering

in the

Department of Medical Engineering
Graduate School of Science and Engineering

August 2022

CHIBA UNIVERSITY

Abstract

Department of Medical Engineering
Graduate School of Science and Engineering

Doctor of Engineering

Biomimetic approaches to pneumatic fiber-reinforced soft actuators for thumb motion support

by Yuanyuan WANG

Soft pneumatic actuators have been widely used in hand rehabilitation and supportive devices due to their greater compliance than motor-driven actuators. Most existing soft robotic gloves provide adequate finger flexion support, whereas insufficient independent thumb abduction or opposition support limits their applicability in practical use. Previous studies focused on the mechanical functionality of soft actuators for four-finger but failed to account for the thumb's inherent biomechanical traits.

Unlike the other four fingers, the thumb has a more complicated degree of freedom, unique range of motion requirements, and larger intrinsic functional hand muscles. Prosthetic hands were developed with biomimicry endeavors. They did, however, focus on the thumb's multi-DoF demand, a general kinematic feature, with less regard for the other thumb characteristics since they can neglect the device's interaction with a hand. To improve the thumb support efficiency of soft robotic gloves, we developed biomimetic actuators that take advantage of the thumb's unique biomechanical features. The objective was to develop new methodologies for fiber-reinforcement soft thumb actuators capable of achieving independent flexion and abduction, opposition, and a considerable thumb-tip pinch force for practical usage.

Our approach included: 1. Optimizing the geometry of soft actuators for two thumb support approaches: one that mimicked hand muscle morphology and the other that coped with kinematics features of the thumb; 2. Designing reinforcement fibers of multi-chamber actuator mimicry in the anatomical structure of skeletal muscle. 3. Comparing three biomimetic approaches, the two proposed approaches and a modular approach, for demonstrating their pros and cons and practical usage.

The novelties and contributions were: 1. Designing novel geometrical structures and reinforcement fiber layouts for soft thumb actuators based on a comprehensive view of the thumb's unique mechanical properties; 2. Enabling soft thumb actuator to provide adequate support in thumb flexion, abduction, and opposition. 3. Developing a systematic evaluation method for measuring both the kinematic aspect of the thumb and thumb-tip pinch force. This Doctoral project contributes to the field by providing critical insights into the implementation of various biomimetic concepts in soft thumb actuators. The findings offer multiple viable solutions for thumb motion support, which aid in the development of soft robotic gloves for practical application.

Acknowledgements

In the beginning, I would like to thank my supervisor, Professor Yu, for his dedicated support and guidance. Professor Yu continuously provided encouragement and was always willing and enthusiastic to assist in any way he could throughout the research project. He is my mentor and a better advisor for my doctorate study beyond the imagination. Additionally, this endeavor would not have been possible without the generous support from the Iwatani International Scholarships and LOTTE Fundation.

I would also like to thank my defense committee, Professor Nakagawa, Professor Shimomura, and Professor Namiki, who generously provided knowledge and expertise. A special thanks to Professor Shaoying Huang at Singapore University of Technology and Design and Technology and Professor Ya-Hsin Hsueh at National Yunlin University of Science and Technology for their valuable inputs and suggestions throughout this project. Thanks should also go to the laboratory's secretary, Osugi. Without her help, the acquisition of experimental tools and materials would not have gone so smoothly.

Many thanks to all my labmates for providing a friendly and active research environment. Especially Kokubu, Zhou, Tortós Vinocour, and Lu, who provided experimentation assistance and editing help, and shared their insightful suggestions with me.

Lastly, but not least, my heartfelt thanks go to my family, friends, and boyfriend, for their tremendous support, never-ending encouragement, and for always being there for me. Their belief in me has kept my spirits and motivation high during this process.

Chiba, June 6, 2022

Yuanyuan Wang

Contents

List of Figures

List of Tables

List of Abbreviations

RoM	**R**ange **o**f **M**otion
DoF	**D**egree **o**f **F**reedom
FEM	**F**inite **E**lement **M**ethod
DS	**D**ragon**S**kin
DIP	**D**istal **I**nter**P**halangeal (joint)
PIP	**P**roximal **I**nter**P**halangeal (joint)
MCP	**M**eta**C**arpo**P**halangeal (joint)
IP	**I**nter**P**halangeal (joint)
CMC	**C**arpo**M**eta**C**arpal (joint)
DP	**D**istal **P**halanx (segment)
MP	**M**iddle **P**halanx (segment)
PP	**P**roximal **P**halanx (segment)
Fan-ACT	**Fan**-shaped **ACT**uator
3C-ACT	**3 C**hamber **ACT**uator
E-type	**E**terior fiber-reinforced **type** of 3-chamber actuator
I-type	**I**nterior fiber-reinforced **type** of 3-chamber actuator
IE-type	**I**nterior and **E**terior hybrid fiber-reinforced **type** of 3-chamber actuator
IE-ACT	**I**nterior and **E**terior hybrid fiber-reinforced of 3-chamber **ACT**uator in DragonSkin 20
M-ACT	**M**odular finger **ACT**uator

Chapter 1

Introduction

1.1 Preface

This chapter presents an overview of the doctoral study's research background, research challenges, goals, limitations, and contributions. The state-of-the-art in robotic gloves for daily living and rehabilitative support is classified in Section 1.2. The biomechanical features of the thumb are described in Section 1.3. The devices that deal with these features are summarized in Section 1.4. Sections 1.5 and 1.6 focus on thumb-specific supporting devices, identify challenges for thumb actuators, and point out weaknesses in existing devices. The goals, limits, and contributions of this doctoral work are discussed in Section 1.7.

1.2 Robotic gloves for hand motion support and rehabilitation

According to a World Stroke Organization report, over 80 million people have experienced a stroke in their lifetime, and the number is growing rapidly [1]. One of the most common stroke sequelae is hand impairment, which manifests as muscular weakness, joint stiffness, and the inability to create force with the fingertip [2][3][4]. Physical exercises can help to strengthen muscles and re-develop fine motor skills. In comparison to arm and leg recovery following stroke, hand recovery following stroke may be more difficult and time-consuming due to the complexity of finger movements. Additionally, due to a labor shortage of rehabilitation therapists, it becomes necessary to utilize an assisting device to achieve the required high repetition for hand rehabilitation and to assist with daily hand manipulation.

Researchers have developed a variety of robotic gloves over the last three decades, powered by either rigid electrical motors or soft pneumatic actuators. Studies have preliminary confirmed the efficacy of robotic-glove-assisted rehabilitation in redeveloping hand function and motor recovery [5][6][7][8].

1.2.1 Rigid motor-driven gloves

The rigid systems often depend on servomotors or pneumatic pressure to produce pulling of linkages and tendons that are fixed on joints and finger segments, thus activating finger movements [9], such as X-Glove [5], J-Glove [10], and BiomHED [11]. Most of these motor-driven gloves could produce coordinated finger movements like a human finger would. Nevertheless, they often have a rigid accessory brace on the forearm where the cables are connected to a motor, making the system bulky and uncomfortable for long-term use. Also, the motor-driven systems would be easier to induce fatigue in joints due to their lack of compliance with the user and

their environment. Therefore, rigid motor-driven systems would not be optimal for either long-term daily use or rehabilitation scenarios.

1.2.2 Soft robotic gloves

Because of their lightweight, soft interface and high compliance to the user and surroundings, soft pneumatic actuators made of silicone rubber (e.g., WACKER ELASTOSIL®, smooth-on Inc. Dragon SkinTM Series, and EcoflexTM Series) have been widely used in robotic gloves.The existing soft actuators can be further classified according to their geometrical characteristics into Pneu-Net, bellow-shaped, and fiber-reinforcement types.

Pneu-Net actuator

The Pneu-Net actuator consists of a strain-limited bottom layer and an elastomer body embedded with multiple air bladders connected in series [12]. The air bladder expands while the strain-limited portion does not during air inflation, thereby enabling the actuator to bend. The dimensions and oblique angle of air bladders are carefully designed to achieve coupled deformations. For example, Polygerinos et al. [12] and Yap et al. [13] designed actuators with parallel air bladders which can provide support for finger flexion, one DoF motions. Gu et al. [14] and Yap et al. [15] developed actuators with oblique air bladders that can achieve a coupled deformation of bending and twisting during air pressurization, enabling the support in partial thumb opposition.

The bending performance of Pneu-Net actuators is determined by the geometrical design of the silicone body and the material property of silicone. Therefore, using the minimum potential energy method and the continuum rod theory [14], analytical models with a high degree of reduction and prediction of the relationship between design parameters and bending performance can be constructed. Also, they are suitable for automatic 3D printing due to their pure silicone configuration. Nevertheless, this type of actuator is frequently bulky [12], particularly when pressurized. Those with a compact size and appropriate for finger size can only produce a small force output, such as 0.5 N in [16], 1.2 N in [12].

Bellow-shaped actuator

The bellow-shaped actuator typically has a structure of stacked V-shaped bellows, the zig-zag angle of which becomes flat under air pressurization. The even (simultaneous) change of the peripheric zig-zag angle results in elongation, an extending deformation, of the actuator, whereas the uneven peripheral change results in radius bending [17][18][19].

The bellow-shaped modules are arranged above the finger joints and connected in series. Superior to most of the existing prototypes, this actuator type can achieve both flexion and extension with air inflation and air extraction, respectively [20].

In addition to having the same advantages as Pneu-Net actuators, the bellow-shaped actuator is capable of extension during air extraction. However, the finger-sized bellow-shaped actuator has a relatively small force output in the flexion direction, e.g., 1.5 N in [21].

Fiber-reinforced actuator

The fiber-reinforced actuator features a tube-shaped body with one or more pneumatic chambers modeled longitudinally within. The reinforcement fibers are coiled in various patterns (single-helix, double-helix, single loop, and two-directional hitching [22]) outside the body or on the inner chambers to direct the desired deformation of the actuator (bending, twisting, and extending trajectories). In comparison to Pneu-Net and bellow-shaped actuators, this actuator type has additional design parameters related to the reinforcement fiber, such as fiber material, winding pattern, fiber loop interval, and fiber position (wrapped on interior chambers or on the exterior main body surface). These extra design parameters of the reinforcement fibers allow more freedom in the design of a soft actuator. Therefore, this doctoral project explored the fiber-reinforced soft actuator.

The fiber-reinforced actuator with a single elastomeric chamber usually has a strain limiting layer at the bottom for facilitating bending performance [23] [24]. Using a combination of multiple woven patterns determined based on the range of motion (RoM) and degree of freedom (DoF) requirements of each finger joint, the single chamber fiber-reinforced actuators have the potential to deform to fit the outline of human fingers [25].

The fiber-reinforced actuator with multiple inner chamber bends due to the asymmetry of the structure caused by air inflation [22]. Additionally, there should be no restriction at the bottom layer to allow for deformations in orthogonal directions (e.g., flexion vs. abduction); thus, multi-chamber actuators are not necessary to have a strain limiting layer. A multi-chamber fiber-reinforced actuator could be innovated in terms of the geometrical design of the silicone body and fiber patterns.

In comparison to the other two types of actuators, fiber-reinforced actuators have additional design parameters related to the reinforcement fiber, allowing for more complex deformation, such as segmented multi-DoF deformation. Furthermore, this type of finger actuator has the potential for high force output, as it can generate 8.5 N in [22]. On the other hand, the effects of fiber winding are difficult to reproduce in mathematical models, especially when the winding method is complex, i.e., with nodes. But the FEM simulation technique can help to overcome this difficulty to some extent.

This study focused on the development of fiber-reinforced actuators due to their high degree of freedom in design.

The functional elements of fiber-reinforced soft actuators are as follows:

1) Geometrical design of a silicone body or chambers, with consideration of finger joint support methods (modular type or whole-finger type actuator, combination of multiple actuators).

2) The wrapping method of reinforcement fibers.

3) The fixation of soft actuators to a hand (directly attach to the finger or use sockets).

4) Control methods of soft actuator and the interface of robotic gloves.

Limitation in existing soft pneumatic actuators

All the existing soft actuators can provide adequate support for a full RoM of finger flexion and assist with rudimentary grasping actions. Nevertheless, they are insufficient in thumb abduction and opposition support.

Some soft robotic gloves have attempted to realize partial thumb opposition support through the geometrical design of the elastic main body and fiber wrapping methods. For example, the Pneu-Net in [15], which has air bladders arranged obliquely, and the fiber-reinforced actuators in [23], [25], and [26], which has fibers wrapped in single-helix at the root half, can impel a coupled motion of flexion and twisting of the root part of the thumb; however, they are incapable of providing independent abduction and independent flexion support, which limited their possibility in thumb support.

Few studies have included an additional module to augment the multi-DoF support efficiency of their soft gloves. For example, Wang et al. [16] and Hu et al. [20] placed a minimized version of their actuators transversely between the metacarpophalangeal (MCP) joint of the thumb and index finger to provide thumb abduction support. Their robotic gloves may be capable of supporting both independent flexion and abduction; however, the initial angle/length of the actuator module would prohibit the thumb from contacting the lateral side of the index finger, limiting the thumb's abduction RoM.

In general, there are hardly any studies that use soft actuators to support full RoM of independent thumb flexion, independent thumb abduction, and complete thumb opposition.

1.3 Thumb function and importance for daily living

1.3.1 Thumb vs. four-finger in DoF requirements

Among the three joints of the thumb, the interphalangeal (IP) and MCP joints are in a hinge structure that allows mobility in only flexion and extension (one DoF). The carpometacarpal (CMC) joint, located at the base of the thumb, is a saddle joint that allows movements in two directions: abduction and adduction in a plane perpendicular to the palm; flexion and extension in the radial-ulnar direction of the hand (the direction refers to [27]) [28] [29] [30] [31].

Similarly, the distal interphalangeal (DIP) and proximal interphalangeal (PIP) joints of four-fingers are in a hinge structure, permitting them for One-DoF motion. The MCP joints, however, are condyloid joint, which allow flexion-extension and a very limited RoM of abduction-adduction [32].

1.3.2 Thumb vs. four-finger in RoM requirements

Soft actuators designed based on the requirements of the four-finger may not be suitable for the thumb because the thumb has unique RoM requirements.

In terms of flexion RoM, the maximum flexion angle is observed at the DIP joint and the minimum at the CMC joint (Table 1.1). The four-finger digits, on the other hand, have the maximum flexion angle at the PIP joint and the minimum at the DIP joint [33]. As for the abduction RoM, the thumb's CMC joint has a significantly larger abduction RoM (50-71° [34]) than the MCP joint of the other fingers (20° [35]).

1.3.3 The importance of the thumb

According to an Australian government guide [36], the loss of the thumb is rated at 23% whole-person impairment (WPI), which is higher than that of the other four fingers (5 to 10% WPI). The absence of the thumb was also estimated to cause a 40% loss of hand function [37].

TABLE 1.1: Range of motion of five fingers [°].

	Joint(thumb/ fingers)	Thumb	Index	Middle	Ring	Small
Flexion RoM	IP/DIP	81	68	70	66	69
	MCP/PIP	61	104	107	107	104
	CMC/MCP	49	80	85	87	86
Abduction RoM	CMC/MCP	60		20		

The data is presented as a mean value.

In practice, the RoM of thumb abduction determines the largest object that a hand can manipulate. The flexion and abduction forces of the thumb have a significant influence on the magnitude of pinching and gripping strength. Furthermore, thumb opposition, which is a combination of active flexion, active abduction, and passive rotation, is essential for effective handling and manipulation of small items [37]. It is estimated to account for 50 to 60% of thumb function [38].

Therefore, a functional rehabilitation or assistive robotic glove must be able to provide enough support for independent thumb abduction and flexion, as well as thumb opposition motions.

1.4 Challenges for a thumb support actuator

The difficulties in achieving full functional thumb support lie in the spatial constraints of the hand's dorsal side and the intrinsic complexity of thumb movements.

The soft actuators for rehabilitation gloves are mounted on the dorsal side of the finger digits and usually extend from the middle of the metacarpal to the fingertip. Considering the spatial limitation of the hand's dorsal side, thumb actuators could be positioned within a triangular area between the 1st and 2nd metacarpals. Therefore, the structure of soft actuators needs to be elaborately designed to satisfy the multiple DoFs of thumb movement and fit within the restricted area.

Soft actuators for multi-DoF support usually have multiple modules, each responsible for a different DoF, or a single actuator with multiple inner chambers. The deformation of one of the modules or chambers upon pressurization would affect its neighboring one, thereby causing an unintended deformation of the entire actuator. The interference among either the multiple soft actuators with a single DoF or multiple DoFs within one single soft actuator would deviate the thumb movement from the desired one, making independent flexion or abduction impossible.

Furthermore, evaluation for a single DoF is carried out in terms of bending RoM and force output. However, there is a lack of evaluation methods for accessing multi-DoF deformation as well as interference between different DoFs. The opposition performance was evaluated only by whether the thumb could touch the other fingertips, with no quantitative evaluation. Therefore, we must develop comprehensive methods for measuring not only the RoM and force output of the actuator in flexion, abduction, and their coupled motions, but also the kinematic aspect of thumb opposition and the tip-to-tip pinching force for a practical evaluation.

1.5 Actuators for thumb motion support

Most of thumb exoskeletons [39][40][41][42][43] achieved thumb abduction-adduction and opposition support by rigid mechanical systems that are activated by servomotors. As a compromise, Shiota et al. [44] used a parallel cable-driven mechanism

which was activated by 3 Mckibben-typed pneumatic artificial muscles to drive thumb motions in palmar (flexion), ulnar (abduction), and dorsal (extension) directions, respectively. Similar to other cable-driven gloves, the accessory on the upper arm makes it unpleasant to use, and the cable system would generate an excessive moment on the thumb with the change of joint angle, potentially causing safety issues.

To the best of our knowledge, only Maeder-York [26] designed the soft actuator specifically for thumb rehabilitation. Their actuator has a single-chamber structure with reinforcement fiber wrapped in single-helix at the position corresponding to the metacarpal of the thumb and double-helix at the rest. It can, however, only support a coupled movement of abduction and twisting at the CMC joint, incapable of independent flexion and abduction.

Soft actuators capable of supporting multi-DoF of the thumb are designed for prosthetic hands that do not take into account the biomechanical characteristics of a natural hand. The soft prosthetic hands developed by Zhou et al., [45] and Wang et al., [46] have an extra bending actuator installed transversely at the palm to facilitate abduction and opposition of the thumb's CMC joint. This strategy, however, cannot be applied to a robotic glove due to the limited hand space available for thumb actuators. Even though these prostheses display independent flexion and abduction motions, they may fail to do so when coactivated with a real hand due to the viscoelasticity of the finger joints and sliding between the actuator and fingers.

1.6 Biomimetic approaches of robotics gloves

1.6.1 Introduction to biomimetic approach

Nature has evolved a wide variety of highly adapted mechanisms. Biomimetics approaches aim to utilize biological principles to create new technologies or to mimic the structures and algorithms that living creatures use to solve problems and carry out tasks [47].

Soft robotics for various applications have been developed using biomimetic approaches. A portion of the research mimicked animal morphology and locomotion patterns. Shintake et al. [48] developed fish-shaped dielectric elastomer actuators that mimic a fish for underwater environmental monitoring and control of living fish. Gu et al. [49] created micro-to-millimeter-scale aquabots that mimic the shape and swimming motion of an octopus and sperm for underwater monitoring and drug delivery. To meet the demands for segmented multi-DoF deformations, some studies developed continuum actuators that mimicked the snake [50], the elephant's trunk [51], the octopus' tentacles [52], [53] for surgery instruments, stick climbing robots, or grippers. Inspired by the distinctive locomotion of inchworms, Wang et al. [54] and Hu et al. [55] developed soft robots capable of two-way linear and turning movement, as well as climbing on curved surfaces, using shape memory alloy.

Another portion of biomimetic soft robotics integrates the features of living creatures into their actuator designs for improvement. For example, based on the fact that the angle of the pangolin's scales and skin changes the surface hardness, Sun et al. [56] modified the conventional Pneu-Net actuator into a toothed actuator with small teeth that mimicked pangolin scales, arranged at the surfaces between bladders, realizing a variable stiffness in their actuators. Jiang et al. [57] developed an actuator that is similar to a fiber-reinforced actuator. They used a fish-bone-liked frame instead of reinforcement fiber to constrain the radius of expansion of the silica

body, and when combined with the strings that thread through the fish-bones, their actuators can achieve both finger flexion and extension.

1.6.2 Soft robotic gloves with biomimetic design

Basically, all prostheses and robotic gloves have been implemented with biomimetic design that considers shape-related parameters of the hand, such as finger dimension and fundamental RoM requirements of finger joints, because they are used as a substitute for missing limbs or direct contact with the hand to impel hand movement. For example, the length and width of the fiber-reinforcement actuator in [22], the chamber length of the Pneu-Net actuator in [16] and [58] were designed based on a healthy participant's hand. The fiber angle and wrapping method in [25] [26] [22] were determined depending on the joints' RoM and DoF requirements. Almost all the existing soft actuators are size-adjustable to fit the wearer's finger.

Few studies have designed or improved finger actuators by taking into account the morphology of functional muscles and their algorithm for implementing muscle force. To the best of our knowledge, only Jiralerspong et al. [21] designed a V-shaped actuator which may be similar to the contours of muscles that relevant to thumb abduction. The actuator was secured between the metacarpal bone of the thumb and index finger to propel thumb abduction. Nevertheless, this study ended with the abduction actuator generating a very limited force (0.9 N at 50 kPa of air inflation) without delving further into their optimal design. They also lack a reliable assessment of their actuator's thumb abduction and opposition support capabilities. As a result, the physiological and mechanical characteristics of the hand have not been completely exploited, and thumb abduction and opposition support remains inadequate.

1.6.3 Possibility of using biomimetic in thumb actuator design

When designing a soft thumb actuator, biomimetic design may be able to overcome the difficulties demonstrated in Section 1.4.

The hand muscle distribution or morphology may provide inspiration for coping with the spatial constraint of the hand's dorsal side. Numerous functional muscles responsible for hand movement are located within the palm of the hand, which are distributed between bones or across multiple bones. So if we mimic the muscle structure and shape, we may be able to overcome the space limitation.

Soft finger actuators usually perform well in multi-DoF deformation during free bending (bending with actuator only). When equipped on the dorsal side of the hand, its flexion force is applied vertically to the back of the finger, but its abduction force is tangential to the finger surface, resulting in poor force transmission. To enhance force transmission efficiency, we can mimic how abductor muscles generate and exert force in the same location.

Furthermore, human muscles are made up of many tiny muscle fiber bundles wrapped in a membrane, and muscles are adhered to and staggered to one another in the human body, but they do not interfere with one another significantly. The structure and algorithm of skeletal muscles may provide inspiration for improving inter-chamber interference in soft actuators.

1.7 Goals, limitations, and contributions

1.7.1 Goals

An incompetent thumb limits a patient's ability to perform daily activities and essential motor skill development. To achieve a more functional hand assist of the existing soft robotic gloves, the main goal was to develop new methodologies for fiber-reinforced pneumatic actuators capable of providing sufficient support in independent thumb flexion (the 1st DoF), independent abduction (the 2nd DoF), opposition motions (a coupled motion), and a considerable thumb-tip pinch force for practical usage.

We aimed to develop the fiber-reinforced soft actuators with multiple inner chambers in terms of both the geometrical design of the silicone main body and the design of the reinforcement fibers while coping with the biomechanical characteristics of the thumb and taking advantage of the physiological kinematic mechanism of the thumb, e.g., muscle morphology, muscle force application algorithm, etc.

Various fiber-reinforced soft actuators with novel geometrical structures and fiber wrapping methods were designed, fabricated, and evaluated through repeated trial and error. The COMSOL-based finite element method (FEM) was used to predict the bending performance of a part of the proposed design and to analyze interior deformation that could not be observed in a prototype experiment. Through this approach, new biomimetic thumb soft actuators were developed and new evaluation methods were developed for evaluating both the kinematic aspect of thumb support performance and thumb-tip pinch force.

1.7.2 Limitations

The proposed actuators' thumb support performance was evaluated using a dummy hand that replicated the dimensions, DoF, and RoM of a healthy participant's hand, with finger joints simplified into hinge and ball joints. This dummy hand reproduced the majority of the real-world hand reactions. However, the dummy hand lacks the viscoelasticity of the finger joints, muscles, and tendons, rendering it incapable of representing the hand with certain degrees of disability, such as extreme joint stiffness and muscle spasm. Helical torsion springs can be used to reproduce joint stiffness, elastic rubber with high stiffness can be used to reproduce muscle spasms. The performance of actuators when supporting a dummy hand with symptoms, a real hand, or even a real patient's hand will differ from that being evaluated using the dummy hand , which deserves consideration as a new research topic.

The air pressure was manually adjusted via a regulator. Multi-DoF movements, such as thumb opposition, need to be divided into several different single-DoF movements and executed sequentially. As a result, the generated action resembles a mechanical action rather than a coherent one. For more natural and fluent hand motion support, the mathematical models of the control systems of the thumb actuators need to be established, and control mechanisms with general applicability for multi-DoF actuators need to be further investigated.

Furthermore, 3D printing technology has been used to fabricate the Pneu-Net and bellow-shaped actuators. The fiber-reinforced actuators, on the other hand, are difficult for automatic fabrication because the fiber and the silicone are completely different materials, and in some instances, the two remain nested within one another. During the manuscript procedure, the fiber must be evenly arranged; any misalignment would result in uneven deformation of the actuator. Therefore, 3D automated

printing for fiber-reinforced actuators capable of producing complex fiber windings would be immensely beneficial.

1.7.3 Contributions

The novelty and contribution of this doctoral project were:

1) We designed novel geometrical structures of soft thumb actuators based on not only a basic level of biomimetic design that considered the dimensions and basic kinematic requirements (DoF of finger joints) of the thumb but also a deeper level that dealt with the thumb's unique RoM requirement and principle of force application and transmission of muscle force. The investigations of various designs provide critical insights into the implementation of various biomimetic concepts in soft thumb actuators.

2) We manufactured a variety of thumb actuators out of similar materials that were designed based on different biomimetic perspectives, then tested and compared their effectiveness in thumb support using similar processes, setups, and standards. Multiple solutions for thumb motion support in various scenarios have been offered, which aid in the development of soft robotic gloves for practical application.

3) Interference between chambers is inevitable in semi-cylindrical multi-chamber actuators, manifesting as an actuator bending toward a deviated direction. We evaluated RoM and force output in both desired and undesired directions. Using the FEM analysis, the cause and effect of interference caused by neighboring chambers was investigated for the first time in the finger actuators. Moreover, we evaluated thumb opposition support performance more comprehensively by measuring both the kinematic aspect of the thumb and the thumb-tip pinch force.

Chapter 2

Research methodology

2.1 Fiber-reinforced soft actuator development

2.1.1 Functional requirements of thumb actuators

The thumb actuators should impel the thumb to achieve RoMs as a normal thumb does. The specific values of thumb flexion-extension RoM have been summarized in related studies [33] [34]. However, the abduction-adduction RoM of the thumb's CMC joint varies widely owing to the different initial thumb position, movement types (active or passive), and the use of different measurement tools (e.g., goniometer or Pollexograph®) [59].

This doctoral project designed actuators based on the dimensions of a healthy participant's left hand.The active flexion and abduction RoM of the participant's thumb joints was measured using a goniometer, obeying the methods recommended in [60].

Considering the intrinsic RoM of the participant's thumb joints, we set the RoM requirements as in Table 2.1.

For ease of discussion, thumb opposition could be divided into 2 phases (Fig. 2.1): In phase one, the metacarpal abducts; in phase two, the abducted metacarpal flexes and medially rotates toward other finger digits [62]. Rotation of the metacarpal bone is not considered a third DoF since it cannot be performed independently of the other motions.

2.1.2 Biomimetic design in thumb actuators

Three types of biomimetic thumb actuators were developed in this doctoral study. The biomimetic design concepts of each type are as follows:

1) To compensate for the hand's limited space, fan-shaped actuators for impelling thumb abduction mimicked the morphology and force application mechanism of thumb abduction-related muscles (Chapter 3).

TABLE 2.1: RoM of thumb joints and requirements for thumb actuator.

Joint	Motion	Normal thumb joint RoM [°]	Participant's thumb Joint RoM (°)	Requirement (°)
IP	Extension/Flexion	12 / 88*	- / 90	90
MCP	Extension/Flexion	8 / 60*	- / 35	37
CMC	Extension/Flexion	60*** / 49**	60 / 15	0 / 15
CMC	Abduction	45***	60	60

RoM: range of motion; * Barakat et al. [34]; ** Lee and Jung [33]; *** E-HAND [61]

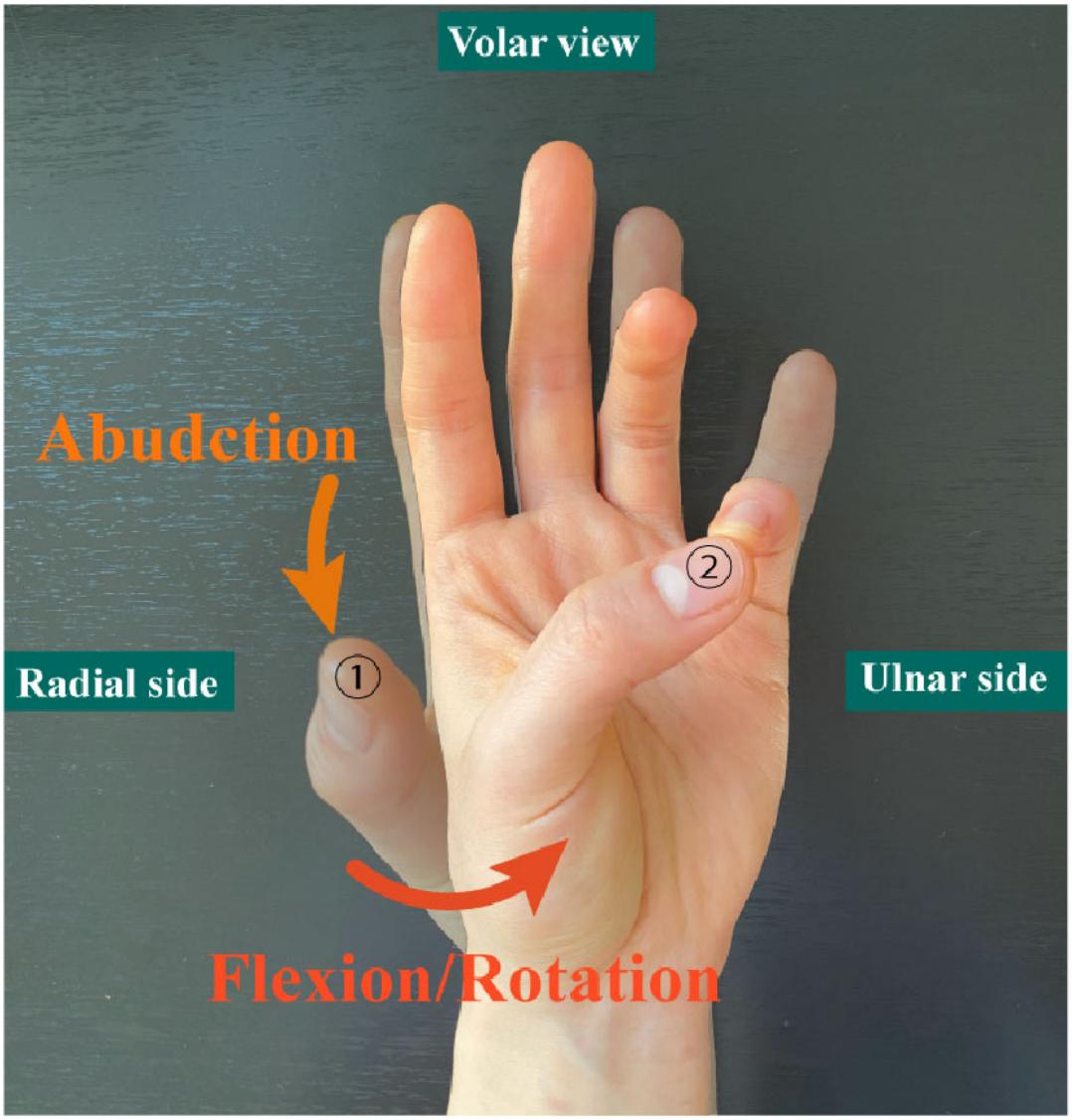

FIGURE 2.1: Two steps of thumb opposition

2) To provide more thumb-compliant support and reduce interference between air chambers, the geometry of the interior air chambers of 3-chamber actuators was designed in accordance with the RoM requirement of thumb joints (Chapter 3).

3) To reduce inter-chamber interference, the fiber wrapping methods of 3-chamber actuators were optimized by mimicking the biological structure of skeletal muscles (Chapter 4).

2.1.3 Actuator design

The tube-shaped fiber-reinforced actuators in this doctoral project were developed based on the multi-chamber actuator designed in a previous study [22]. To begin, the length and width of a participant's thumb joints and finger segments were measured. Then, the design parameters of the actuator's main body, including length, width, and height, as well as inner chamber length, were determined accordingly.

TABLE 2.2: Key properties of silicon rubber.

Material	Density (g/cm^3)	Shore A hardness	Elongation at bread (%)	Tensile strength (MPa)	100% modulus (MPa)
DS* 10 slow	1.07	10	1000	3.275	0.152
DS 20	1.08	20	620	3.792	0.338
Ecoflex 00-30	1.07	00-30	900	1.379	0.0689

*DS: Dragon Skin.

Actuators need to cover the thumb from the fingertip to its CMC joint, and the air chambers need to cover at least the IP and MCP joints.

The wrapping patterns of reinforcement fibers were chosen considering the needs of the DoF requirements and the entire structure of the actuator.

2.1.4 Prototyping

Once the structure of an actuator was determined, its negative molds were built using CAD software (Autodesk Inventor, 2022 Autodesk Inc.). Actuators were fabricated using molds separated into two or more parts, depending on the complexity of the actuator's inner structure. The model file was then sliced by Ultimaker Cura, generating a printer-specific g-code and finally printed out with the Ultimaker 2 Extended+ 3D-printer using PLA filament.

Soft actuators were cast from different platinum-cure silicone rubber (Smooth-On, Inc., Table 2.2). We used Dragon Skin® (DS) 10 Slow or 20 to make the main body of the actuator, depending on its structure and fiber wrapping patterns, and Ecoflex® 00-30 was used for the final coating to fix the reinforcement fibers that wrap around the actuator.

All the rigid accessories of the actuators were printed out by 3D printers.

2.2 Soft actuator evaluation

During the experiments, actuators were mounted on a dummy finger and a dummy hand to simulate the real hand support situation. Compared with direct evaluation using human hands, evaluation with a dummy hand is more objective and therefore suitable in the test of the rehabilitation soft gloves in the preclinical stage.

2.2.1 Dummy hand design

The dimensions and joint RoM of the dummy hand were determined based on a participant's left hand.

The dummy hand consists of a palm that was simplified into a rectangular block. Four-finger digits aligned in parallel (index, middle, ring, and small fingers), and a detachable thumb set slightly in front of the plane of the four-finger (in volar direction), facing toward the palm's ulnar side (Fig. 2.2).

Each finger digit of four-fingers has three bendable finger segments, corresponding to the distal phalanx (DP), middle phalanx (MP), and proximal phalanx (PP) of the real finger. These finger segments were connected by hinge connections, serving as the DIP, PIP, and MCP joints, respectively.

The thumb has three bendable finger segments that correspond to the real thumb's DP, PP, and metacarpal. The IP joint between the DP and PP segments, as well as

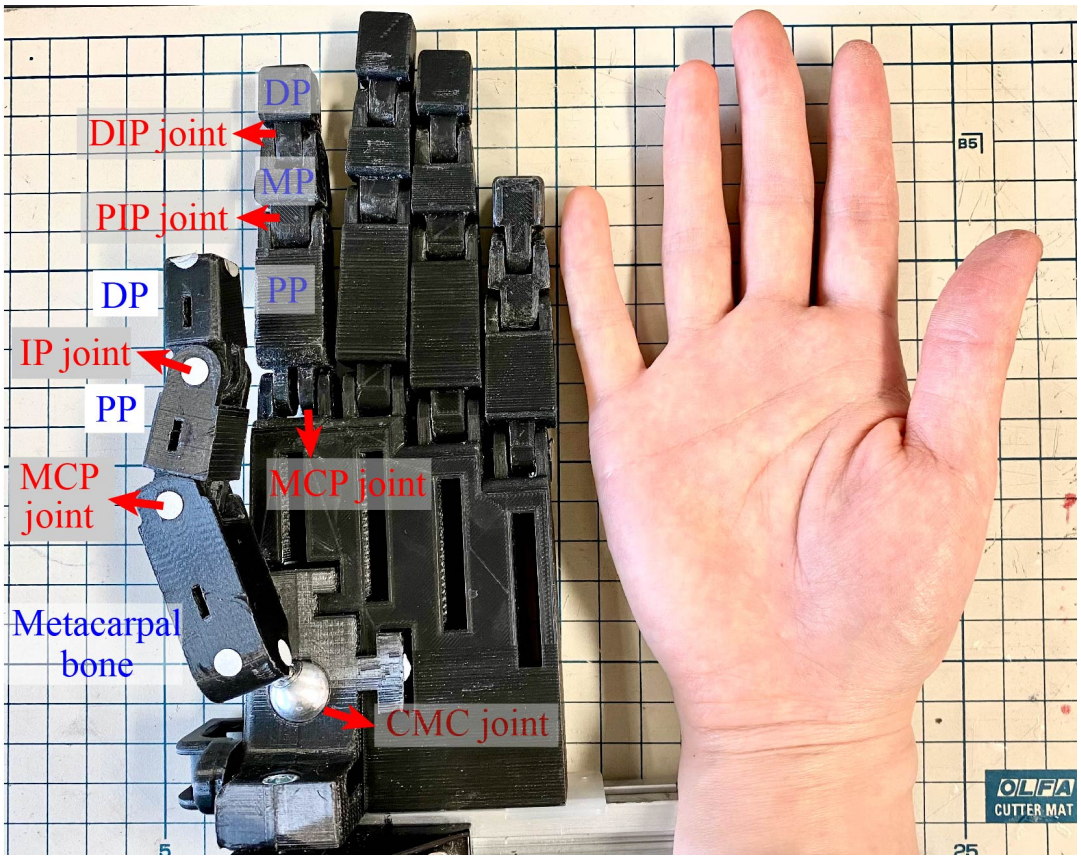

FIGURE 2.2: Dummy hand

the MCP joint between the PP and metacarpal bone, were in hinge connections. The dummy thumb was connected to the palm through a ball joint connection, thereby realizing the multi-DoF of the CMC joint.

The thumb portion of the dummy hand can be detached to measure the actuator's RoM and force output of flexion and abduction. It can be reattached to the palm for the enhanced Kapandji test.

2.2.2 RoM and force output evaluation

The flexion RoM and abduction RoM were measured using either a 2-dimensional (2D) or 3D motion capture system. Details are demonstrated in each chapter.

The force output was measured using a 3-axis load cell (Fig. 2.3, USL06-H5 Load cell, maximum: 100N, Tec Gihan, Japan) to record the force generated in different directions simultaneously.

The finger segment to be measured was wired to the load cell; the other parts were free to move. The flexion force generated in the middle of each thumb segment (DP, PP, and metacarpal) was calculated as the net force of F_Y (elongation force) and F_Z (flexion force). The overall abduction force was measured at the middle of the DP segment since abduction only occurs at the CMC joint. The abduction force was F_Z and the flexion force during an abduction was the net force of F_X (flexion force) and F_Y (elongation force).

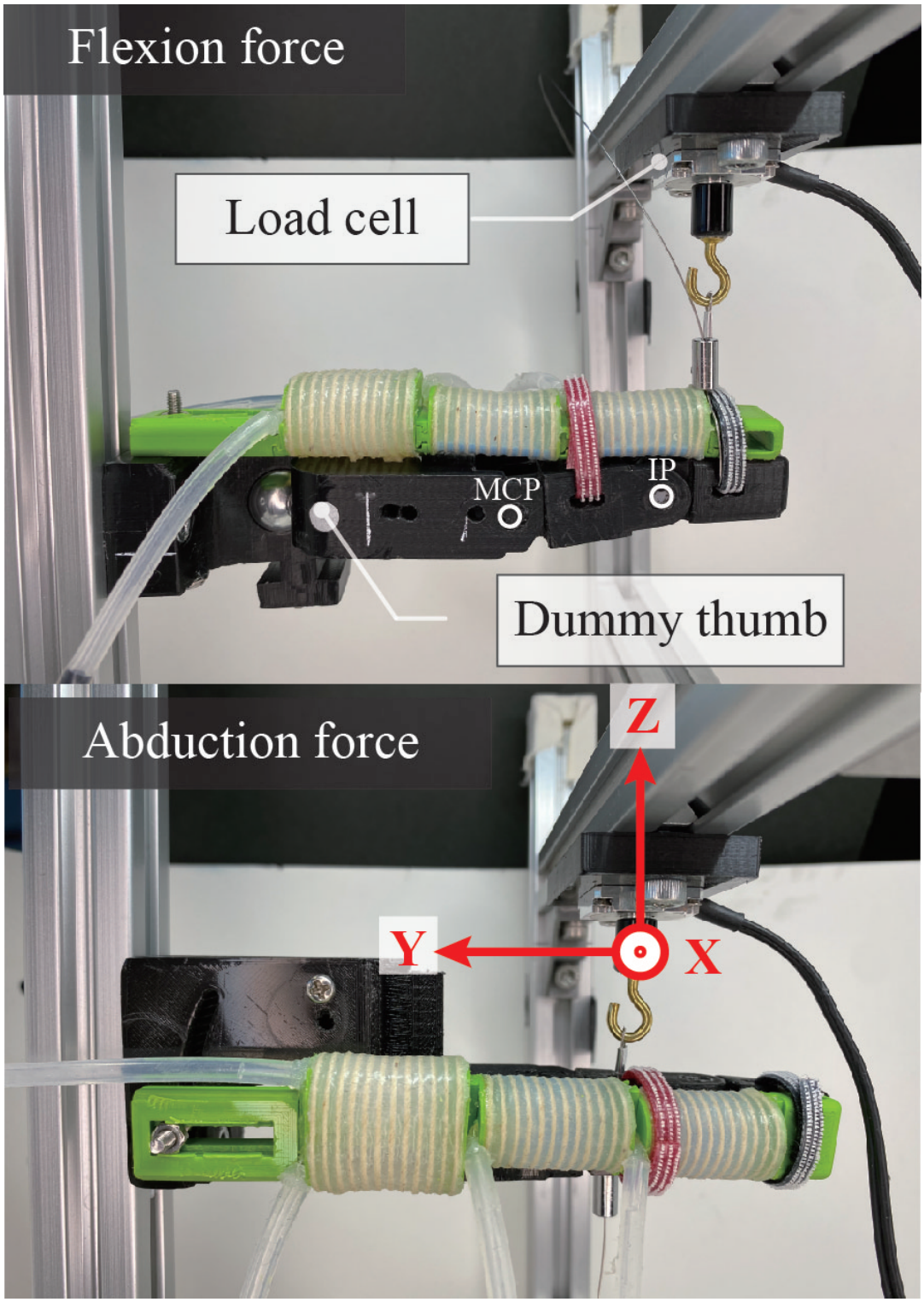

FIGURE 2.3: Force measurement setups.

2.2.3 Thumb opposition evaluation: enhanced Kapandji test

Thumb opposition support performance was evaluated using an enhanced Kapandji test that measured both the Kapandji score, a kinetic aspect of thumb opposition, and the tip-to-tip pinching strength for a practical evaluation.

Kapandji score

The Kapandji test is a clinical test for accessing thumb opposition. It has a score that ranges from 0 to 10, depending on where the tip of the thumb could touch. At the 1st stage, a score of 0-2, the thumb's fingertip touches the lateral side of the index finger. At the 2nd stage, a score of 3-6, the thumb's fingertip touches the other fingertips. At the 3rd stage, a score of 7-10, the thumb's fingertip touches the three joint creases of the small finger and the distal palmar crease [63] (Fig. 2.4 (A)).

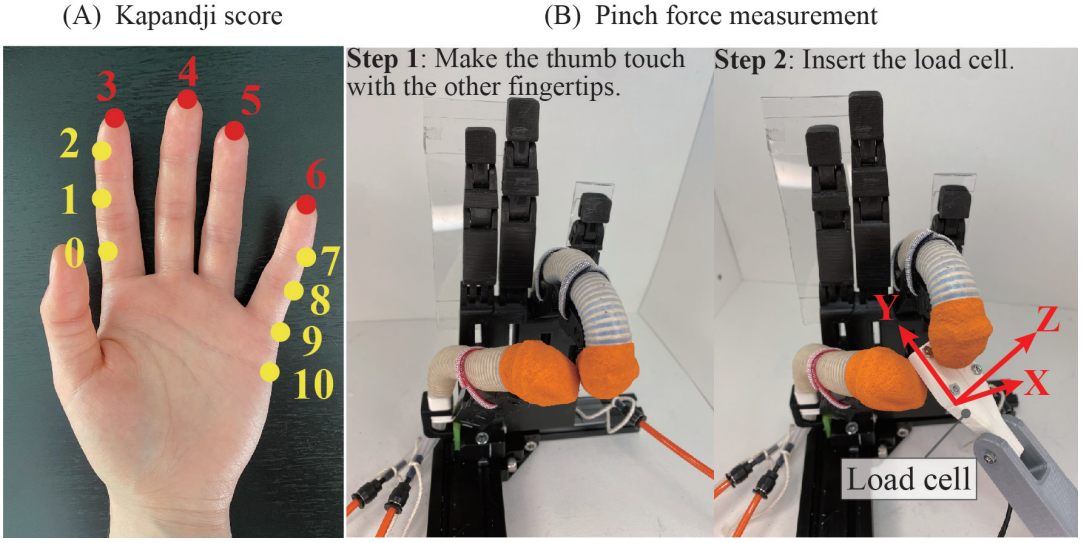

FIGURE 2.4: Enhanced Kapandji test

The Kapandji test was carried out using a dummy hand. It may be difficult to perform movements in the first and third stages due to the dummy hand's restriction in aspects of the initial thumb position and finger joint mobility (e.g., the CMC joint of the ring and little dummy fingers is inflexible). Besides, positions 9 and 10 are hard to reach for a healthy hand. As a result, we assessed the thumb's capability to touch positions 0-8 and measured the magnitude of the pinching strength generated at positions 3-6 (Fig. 2.4 (A), highlighted in red).

Pinching strength

The flexion actuators for four fingers were in a single-chamber structure and had lengths that corresponded to each finger digit.

The designed thumb actuators were mounted on the dummy thumb, and single-chamber soft cylindrical actuators for finger flexion were mounted on the four fingers of the dummy hand. We carefully adjusted the air pressure in the thumb actuator's middle and left side chambers, as well as the four-finger flexion actuator, to make the thumb contact the target positions specified by the Kapandji test. After confirming the thumb-to-finger contact, we inserted the 3-axis load cell between fingers to record the change in pinching force with the pressurization of the middle chamber of the thumb actuator and the four-finger flexion actuator (Fig. 2.4 (B)). The pinching strength was calculated as the net force of force in all three directions.

2.2.4 Finite element analyse

Actuator-only FEA models in COMSOL Multiphysics (COMSOL Inc.) were established for analyzing the interior chamber deformation during free bending in Chapter 6, which cannot be observed in a prototype experiment. The blocked force of a free bending actuator was not investigated since actuators deformed heavily during real-world trials, making reliable measurement and comparison with FEA results unfeasible.

Chapter 3

Design thumb actuators mimicked hand muscle morphology and multi-chamber actuators coped with thumb's kinematics features

3.1 Preface

We (Wang, Kokubu, Zhou, Guo, Hsueh, and Yu) published this study in IEEE Robotics and Automation Letters on August 18th, 2021 [64]. I conducted the design, fabrication, and evaluation of all the prototypes, and the analysis of the results. Prof. Yu provided comments and assistance in editing the manuscript. Other coauthors contributed to the collection and processing of data.

3.2 Introduction

Previous researches on soft robotic glove attempted to realize a portion of thumb motion support by adopting two thumb support approaches: the combination approach and the all-in-one approach.

3.2.1 Related studies on combination approach for thumb motion support

The combination approach uses multiple independent actuators to realize multi-DoF motion support, with each actuator responsible for a different DoF of motion. For example, several studies used a separate soft actuator to assist thumb abduction; Wang et al. [16], Hu et al. [20], and Li et al. [65] reshaped or minimized their soft actuators for finger flexion/extension into a small segment and arranged them transversely between the thumb and the index finger. Jiralerspong et al. [21] designed a unique V-shaped actuator and secured it between the first and second metacarpal bones.

Nevertheless, to transform the actuating force more efficiently to the thumb, most of these actuators were attached above the thumb's MCP joint, which would obstruct grasping and holding. Moreover, these studies did not further discuss the optimum design of the abduction actuators. Most ended up with these actuators generating a very small abduction force (i.e., 0.9 N at 50 kPa air inflation [21]) which would be insufficient for full thumb abduction support. In order to realize part of grasping with only limited DoF, these actuators were designed to have an initial length or angle, so the thumb had been abducted to a certain angle at the initial

state, which limited the thumb abduction range (impossible for a small abduction angle less than the initial angle).

3.2.2 Related studies on all-in-one approach for thumb motion support

Some Pneu-Net actuators or fiber-reinforced actuators have the potential to provide thumb opposition support through the design of the corrugated-fabric layer [15] and the oblique angle of the air bladders [15] [66], or through a novel arrangement of reinforcement fiber in the slender single-chamber actuator [23], [25] [26]. These actuators can achieve a coupled deformation of flexion and abduction with a fixed twisting trajectory, but they cannot adjust the flexion and abduction angles independently.

Several researchers have developed multi-chamber actuators for achieving multi-DoF support. For example, the Pneu-Net actuator developed by Liu Y. et al., [67] and Wang et al., [46] and the reinforced actuator designed by Liu X. [68] have two identical actuators attached at the strain limited layer (the bottom layer). The air inflation of either side-chamber would result in a deformation in the left-right direction (similar to finger abduction-adduction), and the simultaneous inflation of both chambers would result in an up-down deformation (similar to finger flexion). Nonetheless, since these actuators were not developed and evaluated with consideration of the biomechanical characteristics of a real thumb, they would be less applicable for real-hand support.

Furthermore, interference between multiple soft actuators with a single DoF or multiple DoF within a single soft actuator will deviate the thumb movement from the desired one. Yet, there have been few studies that use soft actuators to provide a complete thumb opposition that requires the coordination of independent thumb flexion and abduction-adduction.

3.2.3 Functional thumb muscle morphology

Thumb abduction and opposition are realized by coordinating muscles on the hand (intrinsic muscle) and wrist (extrinsic muscle). Most of the intrinsic muscles are mainly located within the area between the radial side of the 1st and 2nd metacarpals, including flexor pollicis brevis, abductor pollicis brevis, and opponens pollicis (Fig 3.1 (A), marked in red, blue, and green,·respectively) [69][70]. Extrinsic muscles, such as abductor pollicis longus, have tendons attached to the 1st metacarpal bone base. These muscles apply forces directly to the thumb's MCP joint and the 1st metacarpal bone, rolling the thumb away from the palm plane and sliding the distal surface of the metacarpal toward the dorsal side [62].

Notably, the adduction pollicis transversus, a triangular muscle arising by a broad base from the 3rd metacarpal bone, draws the thumb back to the palm through the tendon attached to the thumb's MCP joint (Fig 3.1 (A), marked in pink). Although this muscle works in the opposite direction of an abductor, its morphology is applicable to the design of soft actuators for thumb abduction.

3.2.4 Thumb kinematics characteristics

The thumb has the maximum flexion angle at the DIP joint and the minimum flexion angle at the CMC joint. The abduction movement is mostly produced at the CMC joint, while the other joints have very limited or even no abduction requirements [34].

(A) Morphology of hand muscles

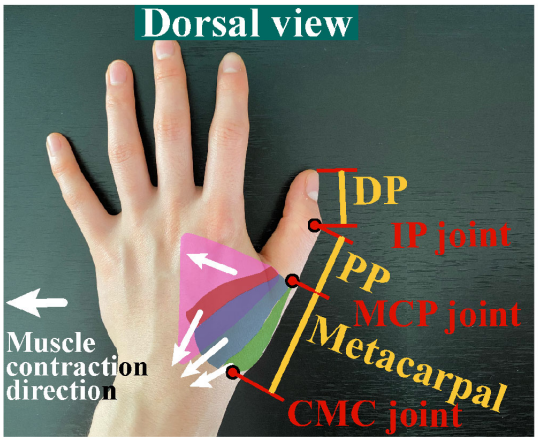

(B) Spatial constrain

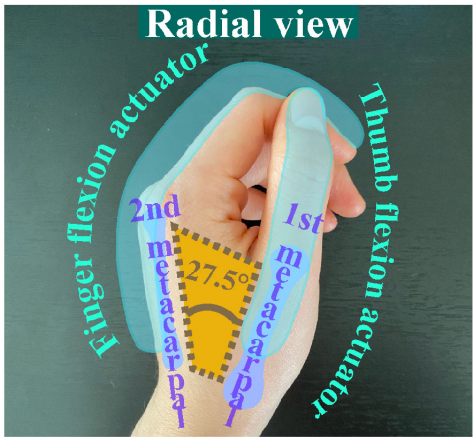

FIGURE 3.1: Hand muscles for thumb abduction and opposition

In general, the thumb's CMC joint requires a more intensive force to impel abduction than to flex the joint. On the contrary, the thumb's DIP joint needs more force for flexion but not for abduction.

3.3 Goals

To achieve a more functional hand assist with the existing soft robotic gloves, we aimed to design and optimize soft actuators for the two approaches for thumb motion support while taking into account the biomechanical characteristics of the thumb. Both approaches need consideration of the hand's spatial limitations and interference between actuators or movements in different directions. We aimed to find out:

1) The optimum design of the two types of thumb actuators.

2) Which thumb assistive approach would be the more effective one.

3.4 Actuator prototyping

3.4.1 Functional requirements

The designed actuators were aimed to achieve the RoM requirements that determined based on a participant's left hand. RoM requirements are shown in Section 2.2.1, Table 2.1.

3.4.2 Combination thumb support approach: fan-shaped actuators

Design concepts of the fan-shaped actuator

The soft actuators of rehabilitation gloves are positioned on the dorsal side of each finger digit and usually extend from the middle of the metacarpal to the fingertip. Given the spatial constraints of the hand's dorsal side, thumb actuators could be located in a triangle area between the 1st and 2nd metacarpals, the same place where abductor muscles are located (Fig 3.1 (B)). This triangular area would remain flat whether the thumb was resting in the same plane as the palm (Fig. 3.1 (A)) or facing the ulnar side of the palm (Fig. 3.1 (B)). To make the most of the limited space, we

developed a fan-shaped actuator (fan-ACT) that mimicked the triangle shape of the adduction pollicis transversus muscle and its force application mechanism, allowing the actuator to provide abduction force directly to the 1st metacarpal bone.

To realize thumb opposition, the fan-ACT needs to collaborate with a single-chamber flexion actuator mounted on the thumb's dorsal side. Thus, the fan-ACT must generate a significant force in the abduction direction while being bendable to allow for extreme flexion of the thumb. To demonstrate the abduction effect of the fan-shape design, we first created Model A with two lateral sides connected in a hinge connection. The junction was then modified into a ball joint connection, allowing the actuator to flex in multiple directions. In addition, to ease expansion in the abduction direction, we limited the thickness expansion of the actuator to two forms: Model B and Model C.

Model A: Original model of the fan-shaped actuator

The actuator consists of three parts: two holding frames, a core unit, and a thickness (volar-dorsal direction) expansion restrictor (Fig. 3.2 (A)). The length of the holding frame was 7 mm less than the 1st metacarpal bone (47.38 mm) so as not to hinder the movements of the thumb's CMC joint. Two holding frames were attached to the core unit's lateral sides using chemical adhesives. They were connected by a hinge connection.

The soft actuator unit takes the shape of an annulus sector. The outer radius was set as the same length as the 1st metacarpal bone and had a radial width of 23/40 of the 1st metacarpal bone (27.4 mm), which was determined empirically. The sector angle was set as 27.5°, which equals the angle formed by the 1st and the 2nd metacarpal bones when the hand rests with the palm's lateral side and the thumb's dorsal side facing upward, and the thumb's fingertip touches the DIP crease of the index finger (Fig. 3.1 (B)).

Reinforcement fiber was coiled longitudinally in a two-directional helix with 3° intervals between fiber loops, causing the actuator to extend sideways (radial-lateral direction). The fiber knots at the shorter arc would facilitate the expansion at the longer arc during inflation, making the actuator open like a fan, thereby propelling the thumb to abduct. The thickness expansion restrictor was also used to facilitate the sideways expansion and alleviate the pressure on the hand caused by thickness expansion.

The hinge connection of the two holding frames was positioned at the CMC joint when setting the fan-ACT onto the hand (Fig. 3.2 (D-E)). One holding frame was secured in alignment with the 2nd metacarpal bone, and the other frame was connected to the MCP joint of the thumb through a ring.

Nonetheless, when working with the single-chamber flexion actuator, whose movement plane is perpendicular to that of the fan-ACT, the original model may inhibit the flexion actuator's movement due to its hinge connection, limiting the RoM of thumb opposition. Following that, we changed the hinge connection into a ball joint connection and realized thickness expansion restriction in two different forms.

Model B: Middle-hole model of the fan-shaped actuator

The core unit of this middle-hole fan-ACT was identical to the original in design and size (Fig. 3.2 (B)). An elliptic hole was placed on the symmetry axis of the actuator unit, near to the outer circle of the annulus sector. The thickness expansion restrictor

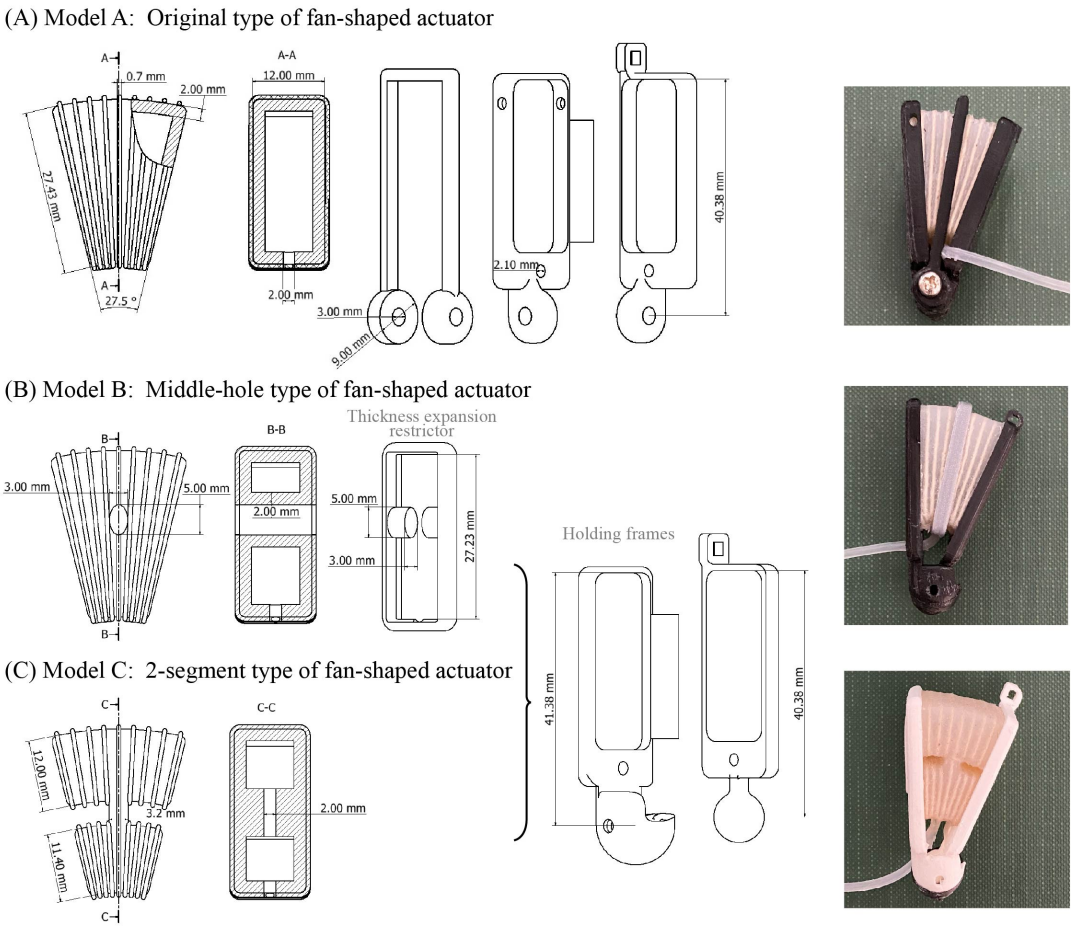

FIGURE 3.2: The three models of the fan-shaped actuator.

was restructured into a rectangular ring with an elliptic bump on each long side in order to be fastened to the core unit.

Model C: Two-segment model of the fan-shaped actuator.

To reduce the rigid accessories on the actuator, we minimized the thickness expansion by modifying the geometric structure of the core unit. A larger surface would deform more. As a result, we separated the fan-shaped core unit of the original

model into two segments to reduce the volar and dorsal surface area of the air bladder; the radial width of the upper and lower segments were 12 mm and 11.4 mm, respectively (Fig. 3.2 (C)).

Separately, reinforcement fiber was coiled around the two segments. Two-directional hitching knots were aligned on the bottom surface of each segment. An air tube (silicone, exterior diameter: 2 mm, inner diameter: 1 mm) was threaded through the lower segment and extended to the upper segment, connecting the two parts and allowing simultaneous inflation.

3.4.3 All-in-one thumb support approach: 3-chamber actuators

The multi-chamber structure is applicable to the thumb actuator because it could realize multiple DoFs simultaneously. In an earlier study, Tarvainen T. et al. [22] developed a semi-cylindrical soft actuator with a composite structure. The MCP joint is covered by a 20mm-long actuator section with three chambers: the middle chamber assists finger flexion, and the two side chambers assist finger abduction and adduction. However, the abduction force generated by the side chamber was less than 2 N, which is inadequate to impel a full thumb abduction.

Design concepts of the 3-chamber actuator

In this thumb assist approach, we adopted the 3-chamber structure for two considerations: First, the three chambers responsible for finger flexion, abduction, and adduction, respectively. Although the material stiffness could realize the thumb adduction to some extent, the side chamber for adduction would be useful for the thumb that has severe stiffness in the CMC joint (such as, zig-zag deformity of the thumb) or problems in the adductor pollicis muscle. Second, to avoid deviated deformation during flexion, the middle chamber should have an axial symmetry shape and be positioned on the symmetrical axis of the actuator. The other chambers should be placed symmetrically inside the actuator, necessitating the use of two identical side chambers, one for each side of the middle chamber.

To augment the abduction force of the 3-chamber actuator (3C-ACT), we designed three models, taking into consideration chamber size, the inner structure of the actuator, and the geometry of the actuator, based on the following principles:

1) To make maximum use of the thumb's dorsal space (total length from CMC joint to the thumb's tip: 103.3 mm, width: 16 mm, height: 12 mm) and the actuator's inner space.

2) To minimize the interference between chambers, the actuator should have an axially symmetrical inner structure.

Model 1: Semi-cylindrical 3-chamber actuator with even chambers

The actuator was designed in a semi-cylinder shape with general dimensions determined based on a healthy participant's thumb, regarding the finger length and width. We maximized the size of three chambers in the limited inner space of the semi-cylinder while keeping the distance between chambers and the chamber wall's thickness at 2 mm. All three chambers run through the root to the tip of the actuator (Fig. 3.3 (A)).

Reinforcement fibers were wrapped on the actuator surface in two patterns: 21 loops of two-directional hitching covered from the tip of the actuator to the position corresponding to the middle of the thumb's proximal phalanx (PP). The knots

(A) Model 1: Semi-cylinder 3-chamber actuator with constant chambers

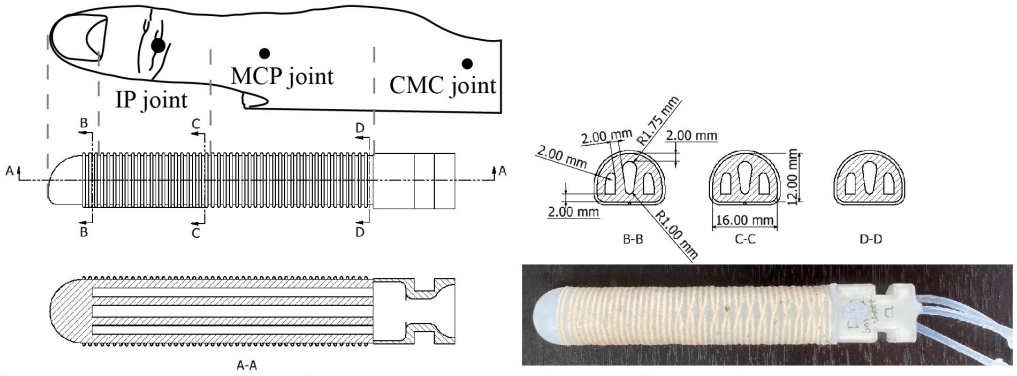

(B) Model 2: Semi-cylinder 3-chamber actuator with gradually changing chambers

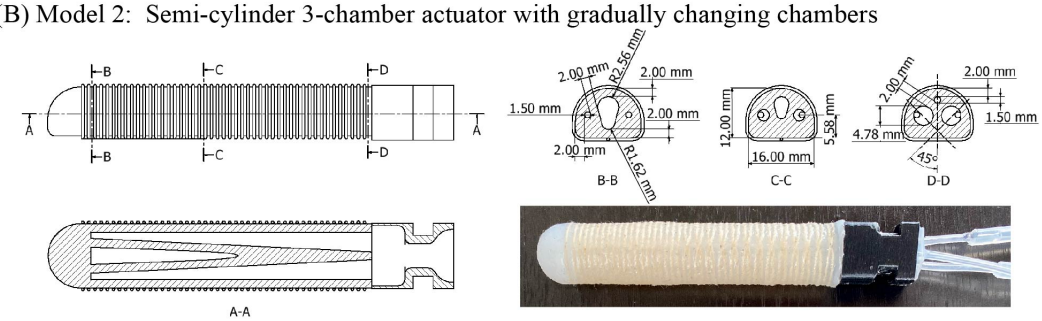

(C) Model 3: Cuboid 3-chamber actuator with gradually changing chambers

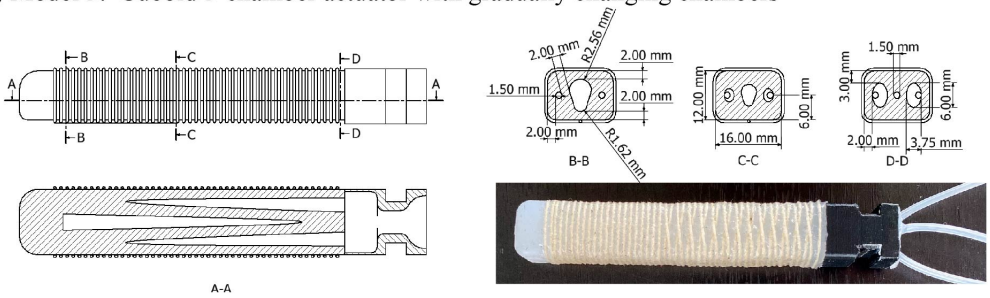

(D) Actuator on dummy hand

(E) Actuator on real hand

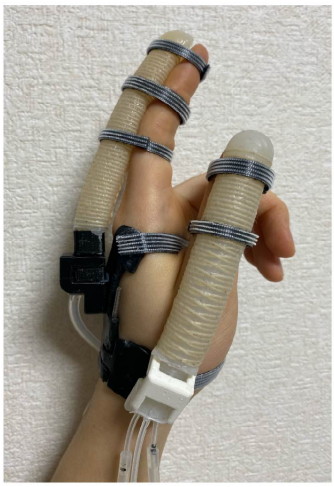

FIGURE 3.3: The three models of the three-chamber actuator.

of two-directional hitching were aligned in the center of the bottom surface, intending to facilitate the flexion of the top half of the actuator. Thirteen sets of double

helix patterns (26 loops) cover the rest, which enables the flexion and abduction-adduction of the lower half of the actuator. Reinforcement fibers were arranged at an interval of 1.5 mm. According to a previous study [22], the fiber loop interval was adjusted between 1.5 and 2 mm to optimise bending performance and prevent excessive silicone bulge between fiber loops.

Finally, the root part of the actuator was designed to be a plastic connector that enabled the actuator to connect to the dummy finger or a supporting orthotic structure on the hand (Fig. 3.3 (E)). The root connector was hollow and had air tubes passing through it. It was secured to the actuator by casting silicon inside its hollow interior [22].

Model 2: Semi-cylindrical 3-chamber actuator with tapering chambers

Unlike the RoM requirements of the other four-finger digits, the thumb's root part requires a more intensive force to impel abduction rather than flexion, whereas the thumb's tip part does the contrary. We proposed a tapering structure based on these biomechanical characteristics.

The two side chambers, assisting the thumb abduction-abduction, are in a tapering down fashion (the maximum cross-sectional area at the root and the minimum at the tip). The middle chamber for thumb flexion support is in a tapering up fashion (Fig. 3.3 (B)). In accordance with the semicircular cross-section of the actuator, which has an axisymmetric shape, the three chambers were also distributed symmetrically inside the actuator. The side chambers were positioned lower than the middle chamber.

Model 3: Cuboid 3-chamber actuator with tapering chambers

A previous study that compared the flexion performance of soft actuators with various cross-section shapes indicated that an actuator with a rectangular cross-sectional has a larger bending resistance than that with a semicircular cross-section [71]. An actuator's flexion capability would be affected by the deformation of the chamber wall opposite to the bending direction. For example, the curved wall of the semi-cylindrical actuator is larger than the upper wall of the cuboid actuator. As a result, the curved wall would show a larger deformation at the same air pressure, making the semi-cylindrical actuator more easily bend.

On the other hand, the cuboid actuator has larger sidewalls opposite the abduction and adduction directions, which might make it suitable for thumb abduction-adduction support. Accordingly, we revised the actuator's geometry in Model 2 to a cuboid actuator with the same length, width, and height as the semi-cylindrical actuators. The middle chamber has the same shape and size as that in the semi-cylindrical Model 2. The side chambers have the same cross-sectional area as that of Model 2 but in an elliptic shape corresponding to the actuator's larger sidewall (Fig. 3.3 (C)). Additionally, in conformity to the actuator's rectangular cross-section, a central symmetric shape, the three tapering chambers were placed central-symmetrically inside the actuator (the centers of the three chambers were aligned at the same level).

3.4.4 Actuator fabrication

The main bodies of fan-ACTs and 3C-ACTs were made from Dragon skin® 10 Slow and 20 respectively. Ecoflex® 00-30 was used for the final coating to fix the reinforcement fibers (cotton thread, 0.7 mm, Shinwa Rules Co.) that surrounded the actuator.

3.5 Thumb support evaluation

The thumb assist performances of the designed actuators were evaluated in terms of RoM, force generation capability, and the enhanced Kapandji test, which was proposed in a previous work [44], for assessing not only the kinematic aspect of opposition but also the pinching strength exerted by the soft actuators. A dummy hand mimicking the participant's hand was used for all the evaluations.

3.5.1 Bending angle measurements (with dummy thumb)

The abduction RoM of fan-ACTs and the flexion and abduction RoM of 3C-ACTs were measured using a 2-dimensional motion capture system (GigE Monochrome Camera System GE60, Library, Japan). The camera was set in front of the movement plane and perpendicular to it.

The measurement of abduction RoM of fan-ACTs. One of the holding frames was fixed to the inclined surface of a wedge-shaped block designed so as to make the initial position of the other holding frame horizontal (Fig. 3.4 (A)). Three reflective markers were attached to the middle of the joint connection and the tip of each holding frame.

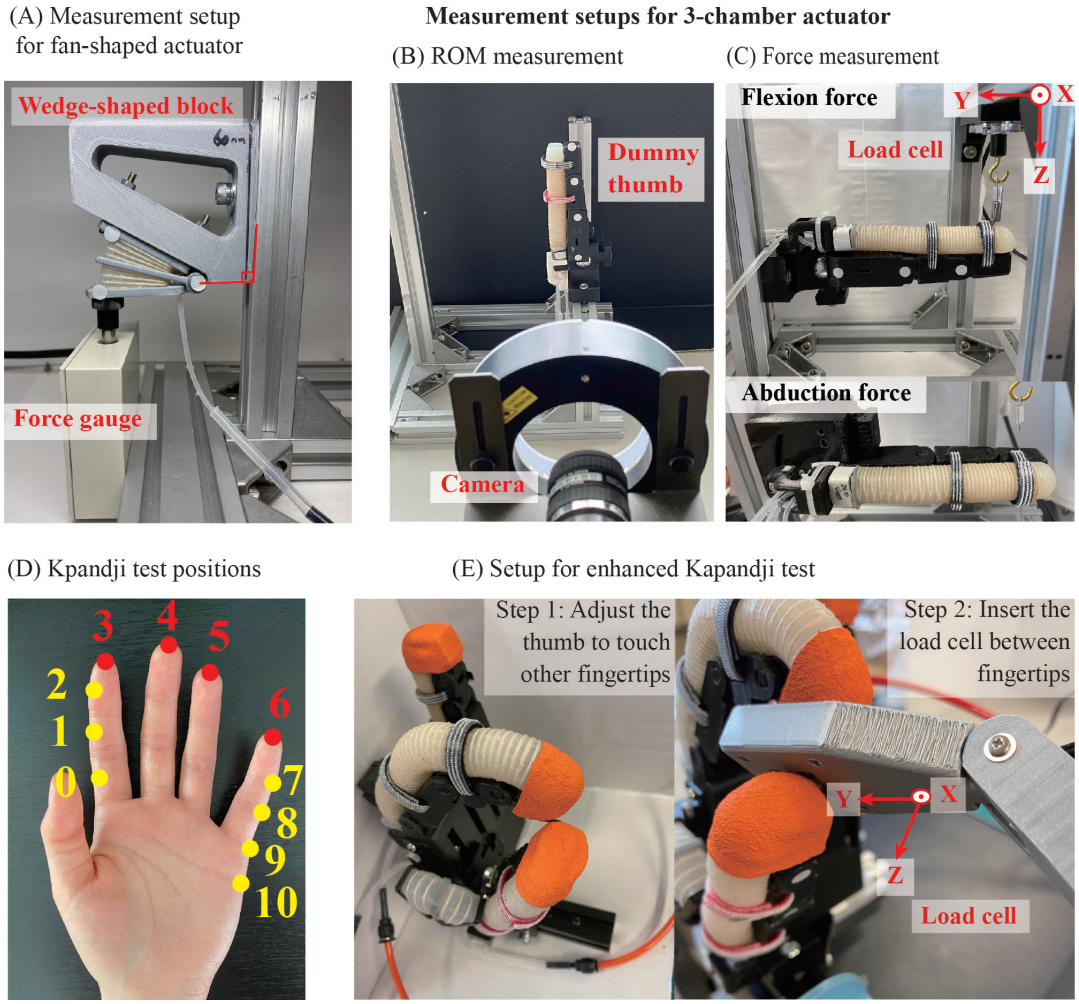

FIGURE 3.4: Experimental setups

.

The measurement of RoM of 3C-ACTs. Actuators were mounted on the dummy thumb with Velcro straps wrapped around the middle of the DP and PP segments. For the flexion RoM measurement, four reflective markers were attached to the dummy thumb's radial side, including the fingertip, IP joint, MCP joint, and the root of the dummy thumb. The camera was positioned at the radial side of the dummy thumb to record the flexion angle of the IP, MCP, and CMC joints during the inflation of the middle chamber (Fig. 3.4 (B)).

The 3C-ACTs might not directly abduct when inflating the side chamber but flex concurrently since the side chamber is away from the symmetrical center of the actuator. Also, the interaction between multiple chambers that are constrained within a common silicon body should be taken into account. Therefore, we measured both flexion and abduction RoMs during the inflation of the left side chamber.

The abduction RoM was measured with a camera placed on the thumb's volar side. Reflective markers were attached to the tip and the root of the dummy thumb. The abducted angle of the segment between the two markers was recorded. The flexed angles of thumb joints during left chamber inflation were recorded using the same method as for flexion RoM measurement.

The RoMs were measured at different air pressure ranges depending on the actuator's extreme air pressure; the fan-ACT measurements were done at 0–200 kPa, the 3C-ACT with constant chambers was at 0–300 kPa, and the 3C-ACTs with tapering chambers were at 0–400 kPa. The air was inflated and then deflated at 10-kPa intervals, repeated two times, and the average was calculated.

3.5.2 Force output measurements (with dummy thumb)

An actuator's force generation capability reflects how well the actuator deformations transform into forces that impel thumb motions [22].

The measurement of abduction force of fan-ACTs. Fan-ACTs were measured using the same setup as for RoM measurement. A force gauge (DPU-50N, IMADA, Japan) was placed beneath the tip of the unfixed holding frame (Fig. 3.4 (A)).

The measurement of force output of 3C-ACTs. 3C-ACTs were measured using a 3-axis load cell (USL06-H5 Load cell, maximum: 100N, Tec Gihan, Japan) to record the force generated in different directions simultaneously. The load cell was fixed facing downwards above the dummy thumb and actuator (Fig. 3.4 (C)). The dummy thumb was connected closely to the load cell through a wire. Only the dummy thumb's root and measurement position (attached to the load cell) were fixed, leaving the other joints free to move. The flexion force generated in the middle of the DP, PP, and metacarpal was measured and calculated as the net force of y-directional and z-directional forces.

The dummy thumb was rotated 90° toward the load cell to measure the abduction force of the 3C-ACTs (Fig. 3.4 (C)). We measured the force generated in the middle of the DP segment (fingertip) since abduction movement occurs mainly at the CMC joint. The z-directional force is recorded as the abduction force, and the net force of the x-directional and y-directional forces is calculated as the flexion force.

3.5.3 Enhanced Kapandji test measurements

Thumb opposition is a coupled movement of abduction and flexion, whereas the thumb-finger pinching strength mainly depends on the flexion of the thumb and

four-finger. Accordingly, the magnitude of pinching strength could reflect the interaction between the actuators (fan-ACTs) or chambers (3C-ACTS) during thumb opposition movements. We used an enhanced Kapandji test that measured both Kapandji score and pinching strength to assess the thumb opposition performance as well as the interference between actuators (or chambers).

The Kapandji score ranges from 0 to 10, depending on where the tip of the thumb could touch. At the 1st stage, a score of 0-2 indicates the thumb's fingertip touches the lateral side of the index finger. At the 2nd stage, a score of 3-6 indicates the thumb's fingertip touches the other fingertips. At the 3rd stage, a score of 7-10, the thumb's fingertip touches the three joint creases of the small finger and the distal palmar crease [63] (Fig. 3.4 (D)).

The Kapandji test was carried out using a dummy hand. It may be difficult to perform movements in the first and third stages due to the dummy hand's restriction in aspects of the initial thumb position and finger joint mobility (e.g., the CMC joint of the ring and little dummy fingers is inflexible). Besides, positions 9 and 10 are hard to reach for a healthy hand. As a result, we assessed the thumb's capability to touch positions 0-8 and measured the magnitude of the pinching strength generated at positions 3-6 (Fig. 3.4 (D), highlighted in red).

For the measurement of the fan-ACT, two semi-cylindrical actuators for finger flexion were set on the dorsal side of the thumb and the other finger digit (Fig. 3.2 (D)). The flexion actuators were in a single-chamber structure. They had the same width and height as the 3C-ACT, while the lengths corresponded to each finger digit. For the Kapandji test of the 3C-ACT, the designed actuator cooperated with one flexion actuator set on one of the four-finger digits (Fig. 3.3 (D)).

The two assisted fingers were upright during the Kapandji tests. To make the two fingertips touch, we first abducted the thumb, then flexed the finger and thumb simultaneously, and lastly fine-tuned the air pressure in each actuator. After confirming that the thumb could touch the target position, we inserted the 3-axis load cell between the two fingertips to measure the change in pinching strength as the air pressure of the two flexion actuators increased (Fig. 3.4 (E)). The position of the load cell was fixed using a 3D-printed frame.

Each flexion actuator's air pressure was increased in 10 kPa increments until it reached its maximum air pressure (at which the actuator twisted). The pinching strength was calculated as the net force of force in all three directions. After one measurement experiment, the fingers were restored to their original position. These procedures were repeated twice, and the mean pinching strength was calculated.

3.6 Results

3.6.1 Bending angle and force output of one-DoF movements

The results of the fan-ACTs and 3C-ACTs were shown separately for comparisons between the three models of each thumb actuator type. We analyzed inflation and deflation data separately where there was a substantial difference between the two, and we analyzed the average of both when the difference was not significant.

Fan-shaped actuators

The results of the abduction RoM and force output of the three models of fan-ACT are shown in Fig. 3.5. The abduction angles of all the three fan-ACTs increased with air inflation (Fig. 3.5 (A)) and achieved the target RoM (60°).

Correspondingly, the force generated by the actuator expansion (or the force that opposes the expansion) also increased with the air pressure (Fig. 3.5 (B)). The original model showed the largest RoM and had the best force generation capability (45 N); the middle-hole model was slightly inferior to the original model (43 N); the 2-segment model had the minimum RoM and generated the least abduction force (32 N).

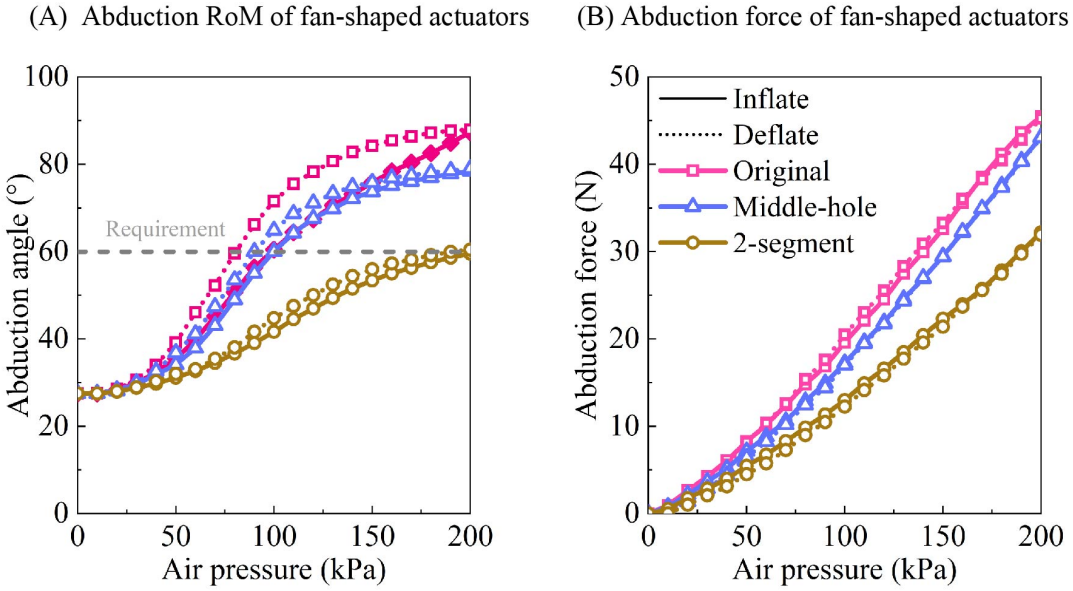

FIGURE 3.5: The abduction RoM and abduction force output of three fan-shaped actuators.

3-chamber actuators

Flexion RoM and force output results. The results of flexion RoM of each thumb joint and force generated at each thumb segment when using the three models of 3C-ACTs are shown in Fig. 3.6 and Fig. 3.7, respectively.

For the flexion RoM result, the IP joint flexed to 85°, an angle close to the limit angle (90°), when using the semi-cylinder 3C-ACT with tapering chambers (Model 2, Fig. 3.6 (A)). In contrast, the maximum angles of the semi-cylinder 3C-ACT with constant chambers (Model 1) and the cuboid 3C-ACT with tapering chambers (Model 3) were far from the requirements. The MCP joint flexed to its limit angle (35°) only when using the Model 2 actuator (Fig. 3.6 (B)). All three models flexed the CMC joint over the required angle (15°) (Fig. 3.6 (C)).

The flexion force results showed that Model 2 generated the largest flexion force at three thumb segments (DP, PP, and metacarpal, Fig. 3.7). Notably, Model 1 showed a different flexion force distribution on the thumb compared with the other models; it generated the maximum flexion force at the PP, the medium at the DP, and the minimum at the metacarpal bone. In contrast, Model 2 and Model 3 generated the maximum flexion force at the DP, the medium at the PP, and the minimum at the metacarpal bone.

Abduction RoM and force output results. The abduction RoM and abduction force results of three 3C-ACTs are shown in Fig. 3.8. All three models had an initial abduction angle of approximately 17° (Fig. 3.8 (A)), which equals the intrinsic angle

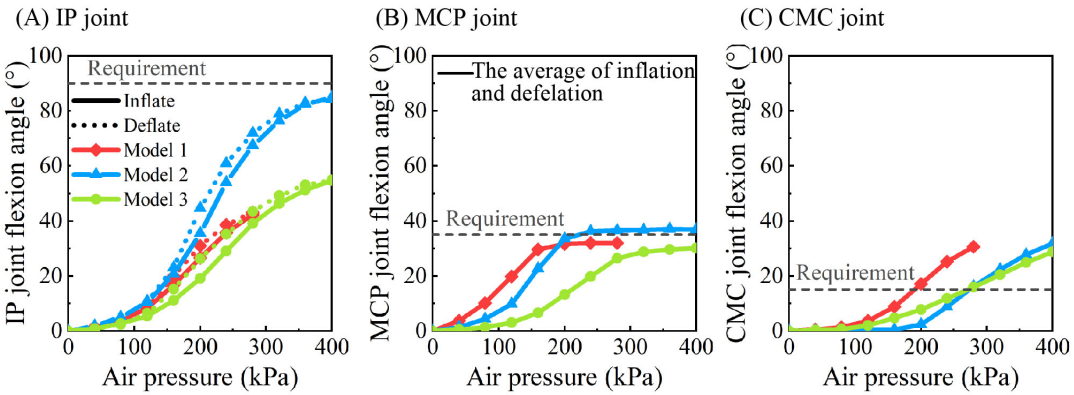

FIGURE 3.6: The flexion RoM of three 3-chamber actuators.

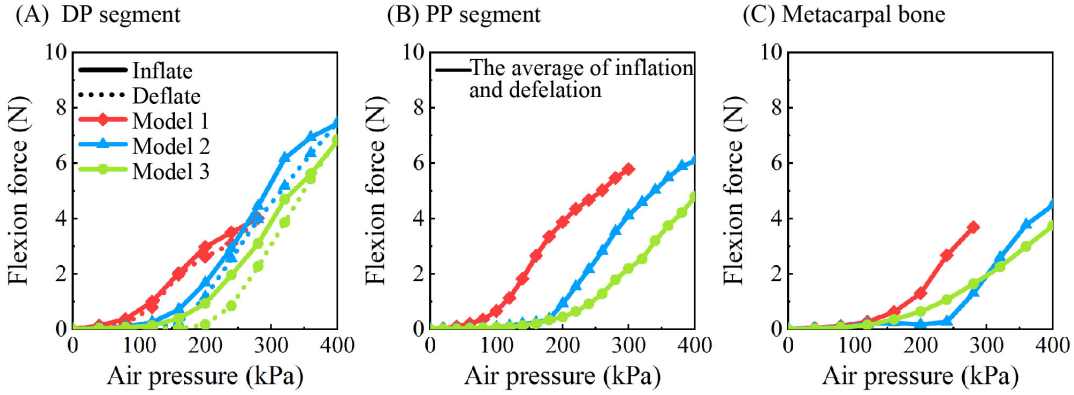

FIGURE 3.7: The flexion force of three 3-chamber actuators.

formed between the 1st and the 2nd metacarpal bones when the thumb adducted closely to the index finger. Model 3, in a cuboid shape, abducted the CMC joint to an angle of 65°, which was larger than the requirement (60°, Fig. 93.8 (A)). In contrast, the abduction angle of Model 2 was slightly less than the requirement, and that of Model 1 was far from satisfying the requirement. The abduction force also showed a similar tendency; Model 3 generated a larger abduction force than the other two models in a semi-cylinder shape. (Fig. 3.8 (B)).

Finger flexion, a movement in a different direction from abduction, was observed during the inflation of the side chamber. The flexion RoM of each thumb joint and the overall flexion force measured at the thumb's DP segment (fingertip) during the thumb abduction are shown in Fig. 3.9.

Modle 3 flexed the least angle and Model 2 the most during side chamber inflation (Fig. 3.9 (A-C)). Since the side chamber was designed to assist the abduction movement, the flexion RoMs generated accompanying the abduction were less than the flexion RoM requirement, especially for the IP joint. In terms of the flexion force generated during the side chamber inflation, Model 2 generated the most flexion force, and Model 1 the minimum (Fig. 3.9 (D)).

Combining the abduction force results (Fig. 3.8 (B)), Model 3 generated a larger abduction force than the flexion force during the side chamber inflation. Model 1 also showed a larger abduction force, but its magnitude was considerably smaller than Model 3. On the contrary, Model 2 generated a larger flexion force than the abduction force during the side chamber inflation.

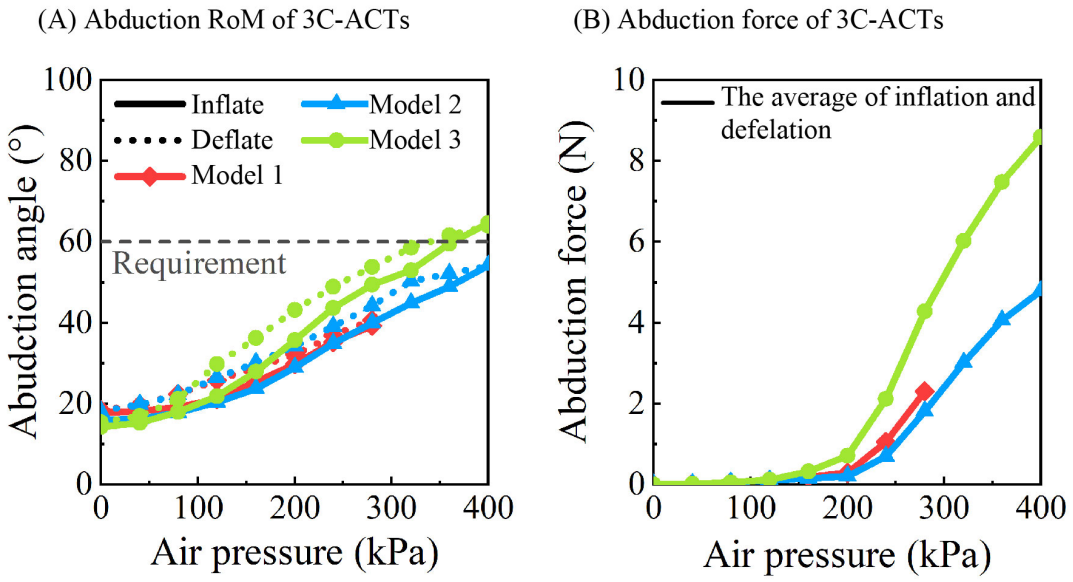

FIGURE 3.8: The abduction RoM and force of three 3-chamber actuators.

3.6.2 Enhanced Kapandji test results

Kapandji score

For the fan-ACTs, Model A (original model) achieved a Kapandji score of 1–5, and both Model B (middle-hole model) and Model C (2-segmented model) achieved a score of 1-6 (Table 3.1, Fig. **??**). All three models could not make the thumb contact the lateral side of the index finger's PP segment (position 0) and the volar aspect of the small finger (position 7-9).

All three models of the 3C-ACT achieved a score of 0–8 (Table 3.1, Fig. **??**), which is a larger score than that of fan-ACTs. The thumb was difficult to reach position 9, the proximal crease of the small finger, due to the limitation of the movability of the dummy hand. As an alternative solution, we measured the distance between the thumb's fingertip and the target position. The results showed a larger distance (22 mm) when using Model 1 with three constant chambers and a smaller distance (12 mm) when using Model 2, a semi-cylindrical actuator with three tapering chambers.

Pinching strength

The original fan-ACT model with a hinge connection could not make the fingertips of the thumb and small finger contact (Table 3.1). We tested and compared the thumb-finger pinching strength when using Model B and Model C of fan-ACT.

For the 3C-ACTs, unlike the other two models, Model 1 with constant chambers was designed without full consideration of the thumb's biomechanical characteristics. Besides, it showed a significantly smaller RoM and force output than the other two models (Fig. 3.6, 3.7, 3.8). Therefore, we compared the pinching strengths of Model 2 and Model 3.

The pinching strength generated between the thumb and different fingers showed varying levels when using the fan-ACTs (Fig. 3.11 (A)). Specifically, the order of thumb-finger pinching strength when using the middle-hole model was: Index < Small < Ring < Middle; when using the 2-segment model, the order was: Index <

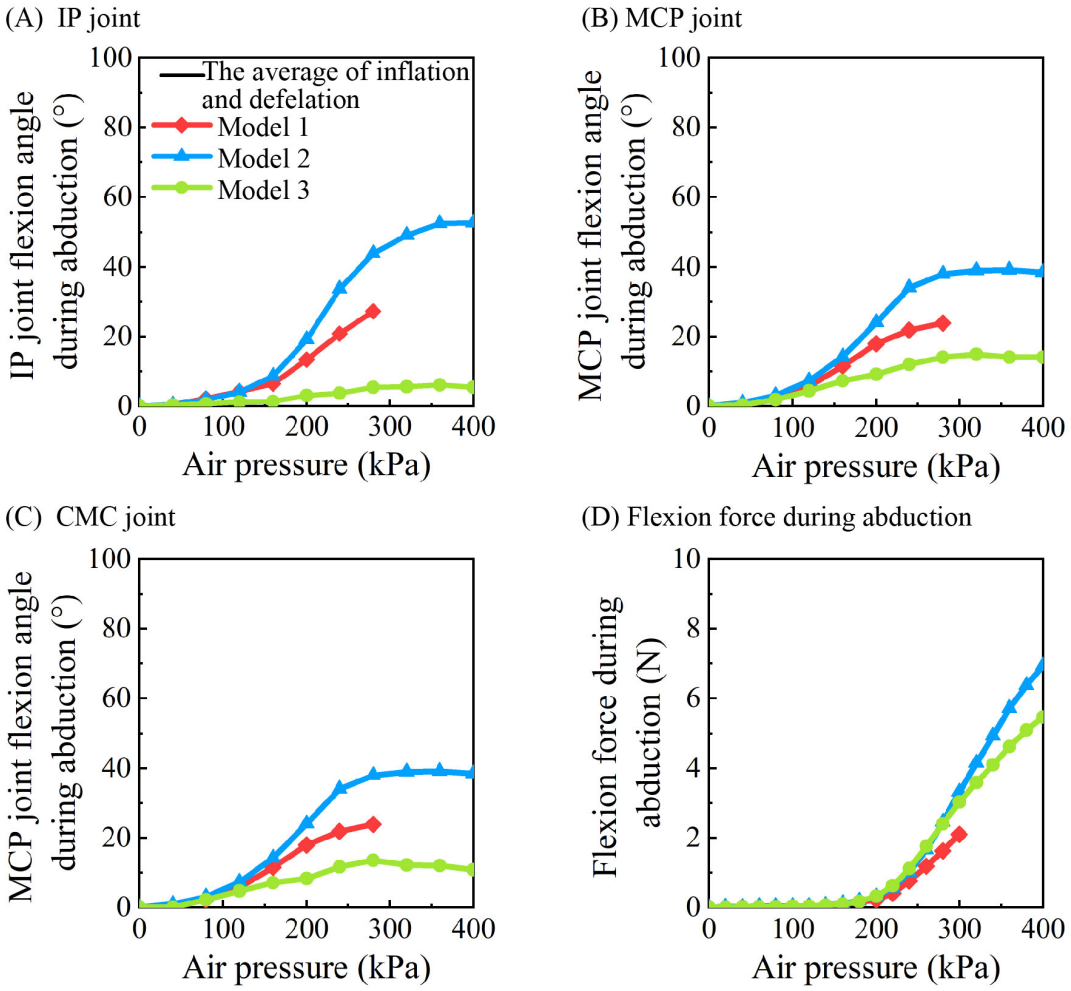

FIGURE 3.9: Flexion RoM of three joints during thumb abduction and the overall flexion force during abduction when using the three 3-chamber actuators.

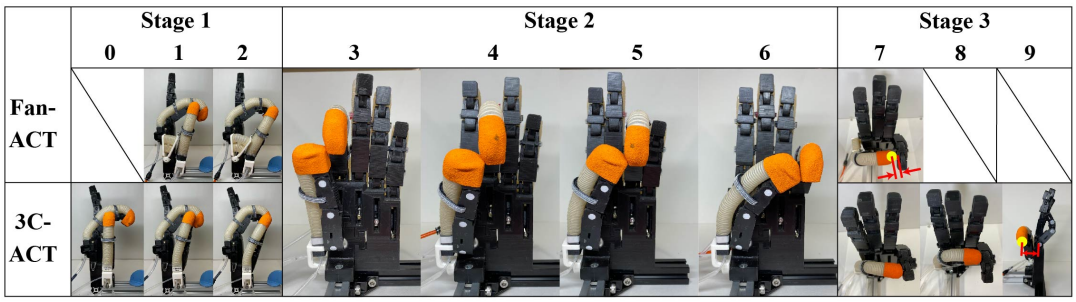

FIGURE 3.10: Thumb opposition support by fan-shaped actuators and 3-chamber actuators.

Small < Middle < Ring. Additionally, the pinching strength of the thumb-index finger and thumb-middle finger, which are fingers close to the thumb, was larger when using the middle-hole model than when using the 2-segment model. For the ring finger and the small finger that are relatively far from the thumb, the upper limit of air pressure of the thumb flexion actuator was smaller when using the middle-hole model. As a result, it demonstrated a lower maximum pinching strength at the ring and small fingers.

TABLE 3.1: The Kapandji score of each actuator [mm].

		Stage 1			Stage 2				Stage 3		
		0	1	2	3	4	5	6	7	8	9
Fan-ACT	Model A	X	O	O	O	O	O	X (11)	X (10)	X	X
	Model B	X	O	O	O	O	O	O	X (8)	X	X
	Model C	X	O	O	O	O	O	O	X (7)	X	X
3C-ACT	Model 1	O	O	O	O	O	O	O	O	O	X (22)
	Model 2	O	O	O	O	O	O	O	O	O	X (12)
	Model 3	O	O	O	O	O	O	O	O	O	X (17)

X: The thumb's fingertip cannot contact the target position; (): the distance in millimeter between the thumb's fingertip and the target position; O: The thumb's fingertip reached the target position; Fan-ACT: fan-shaped actuator; 3C-ACT: 3-chamber actuator.

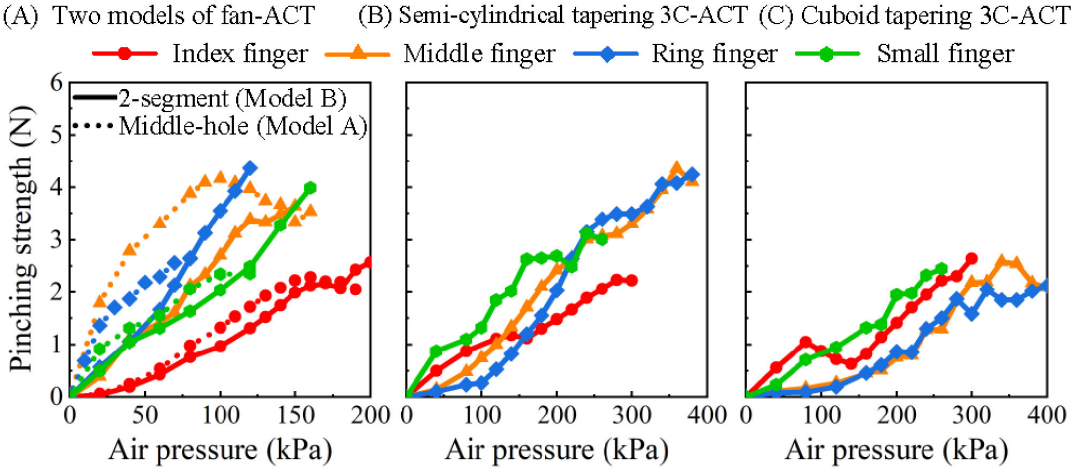

FIGURE 3.11: The thumb-finger pinching strength.

In contrast, the thumb-finger pinching strength level did not vary much with fingers when using the 3C-ACTs (Fig. 3.1 (B) and (C)). The semi-cylinder Model 2 generally showed greater pinching strength than the cuboid Model 3. The magnitudes of the maximum thumb-finger pinching strength were similar to those of the fan-ACTs (for the 2-segment fan-ACT, Index: 2.5 N, Middle: 3.6 N, Ring: 4.3 N, Small: 4.0 N; for Model 2 of the 3C-ACT, Index: 2.2 N, Middle: 4.1 N, Ring: 4.2, Small: 3.0 N).

3.7 Discussions

In this section, we compared the three models of the fan-ACT and 3C-ACT, respectively.

3.7.1 Comparison in terms of abduction and flexion support

Comparison among three models of fan-shaped actuator

All three fan-ACT models, namely, the original, middle-hole, and 2-segment models, satisfied the RoM requirement for a full thumb abduction 3.5 (A)). They generated an abduction force of more than 32 N, close to the maximum abduction force generated by the thumb of a healthy dominant hand (35 N [72]). Certainly, a force of this magnitude might be excessive to assist a healthy thumb to abduct, but it would be useful for assisting the thumb with high joint stiffness.

Original model vs. middle-hole model. The two models were alike in geometrical structure; they only differ in whether there is an elliptic hole in the middle of the core unit or not. The original model has a more consistent and bigger air bladder than the middle-hole model, which might contribute to its slightly larger abduction RoM and force output.

2-segment model vs. other models. The 2-segment model has two air bladders connected in parallel, a different structure to the other two models. When the fan-ACTs achieved a certain abduction angle, e.g., the required angle of 60°, the inflated air pressure of the original and middle-hole models was approximately 90 kPa, the 2-segment was 200 kPa (Fig. 3.5 (A)). Correspondingly, the abduction force generated by the original, middle-hole, and 2-segment models at these air pressures was 17 N, 14 N, and 32 N, respectively (Fig. 3.5 (B)). This abduction force data also indicates the force/energy needed to expand the actuator to a certain angle. Accordingly, the 2-segment model observed greater energy to achieve full thumb abduction than the other two models. Possible reasons include:

1) *Geometrical characteristics:* The pressure exerted on the fan-ACTs' lateral surfaces directly impels the angular expansion of the core unit. The combined area of the two segments' lateral surfaces was smaller than the other two models' lateral surface areas; thus, the 2-segment might have less impelling force for angular expansion at the same inflation pressure. In addition, a couple of actuator surfaces (the surfaces between two segments) increased when separating the core unit into two parts. During air inflation, elastic forces arising from the deformation of these additional surfaces would pull the actuator's lateral sides back toward the symmetrical axis, thus hindering the angular expansion of the actuator sector.

2) *Tighter reinforcement fiber restrictions:* The original and middle-hole models only have fiber knots of two-directional hitching aligned at the bottom surface (the shorter arc of the annulus sector). In contrast, the 2-segment model has two lines of fiber knots, one for each segment's bottom surface. As a result, both surfaces' length extension were restricted by reinforcement fiber, thus making the core unit hard to expand. On the other hand.

In general, all three fan-ACT models have the potential to aid in full thumb abduction.

Comparison among three models of 3-chamber actuator

Flexion performance. According to the flexion RoM results of thumb joints, only the Model 2, a semi-cylindrical tapering actuator, achieved an RoM close to a full

thumb flexion (Fig. 3.6). The slight insufficiency in the IP joint's flexion assist (approximately 5°, Fig. 3.6 (A)) could be improved by enlarging the size of the actuator and air chamber. Model 2 also generated a greater maximum flexion force at each thumb segment compared with the other two models. It had a maximum flexion force at the IP joint of approximately 7.4 N (Fig. 3.7 (A)), which was similar to the minimum force for full flexion of finger joints (7 N, [73]). Accordingly, only Model 2 has the potential to assist with full thumb flexion.

Model 2 and Model 3 have tapering chambers designed based on the RoM requirement of thumb joints. The tapering-up middle chamber was expected to generate the minimum flexion force at the metacarpal bone and the maximum at the thumb's DP segment. In accordance with the expectation, the flexion force results showed that the two models had the minimum force at the metacarpal (Model 2: 4.5 N, Model 3: 3.7 N), the medium at the PP (Model 2: 6.1 N, Model 3: 4.8 N), and the maximum at the DP segment (Model 2: 7.5 N, Model 3: 6.8 N, Fig. 3.7), demonstrating that the tapering chamber design was better in accordance with the biomechanical features of the thumb.

Additionally, Model 2 and Model 3 only differ in the actuator shape. In line with a study that indicated a better flexion performance of the semi-cylindrical actuator [71], results in this study extended this finding and suggested that the semi-cylindrical actuator with multi-chambers (Model 2) has an advantage in finger flexion assist, compared with the cuboid one (Model 3).

In contrast, Model 1, a semi-cylindrical actuator with three constant chambers, had the minimum flexion force at the CMC joint (metacarpal: 4.0 N), the medium at the IP joint (DP: 4.2 N), and the maximum at the MCP joint (PP: 5.8 N, Fig. 3.7). This flexion force distribution was inconsistent with the thumb's flexion RoM requirement; nevertheless, it partially satisfied other four-finger digits' requirements. Specifically, the PIP joint of four-finger digits (corresponding to the thumb's MCP joint) has the largest flexion RoM requirement (Table 1.1). The flexion force exerted on the MP segment of the four-finger (corresponding to the thumb's PP segment) would need a larger flexion force. As a result, Model 1 may not be ideal for thumb assistance; however, it may be suitable for assisting four-finger digit flexion.

Abduction performance. The abduction angle and abduction force results of three 3C-ACT models showed that only Model 3, a cuboid actuator, satisfied the abduction angle requirement (Fig. 3.8), suggesting its potential to realize a full thumb abduction assist.

The three models of 3C-ACT flexed at different angles during the air inflation of the side chamber. When both abduction and its concomitant flexion were considered, the cuboid Model 3 generated a greater force for abduction than flexion (Fig. 3.8 (B) vs. Fig. 3.9 (D)), but the semi-cylinder Model 2 did not. Model 3 flexed thumb joints to a smaller angle than the semi-cylinder Model 1 and Model 2 during side chamber inflation (Fig. 3.9 (A-C)), indicating that Model 3 in a cuboid shape has an advantage in finger abduction assistance compared to the semi-cylinder one.

3.7.2 Comparison in terms of thumb opposition support

In this section, we compared the opposition performance, including the Kapandji score and thumb-finger pinching strength, of the three models of fan-ACT and 3C-ACT separately. The performance of the two types of thumb actuators was then compared.

Comparison among three models of fan-shaped actuator

The original model was inferior in thumb opposition support to the middle-hole and 2-segment models of fan-ACT (Table 3.1). Unlike the ball joint connection of the other two models, the original model's hinge connection constrains its motion in only one direction, making it unsuitable for thumb opposition assistance.

The middle-hole and 2-segment fan-ACTs achieved the same Kapandji score but showed different thumb-finger pinching strengths. The Fan-ACTs only abducted the thumb during the pinching strength measurements, and the single-chamber actuators for thumb and finger flexion were identical for all the measurements. The two models would show similar pinching strength if they had a similar interaction with the thumb flexion actuator. However, the maximum pinching strength of the ring finger and the small finger, which require greater thumb flexion to make the fingertips contact, was smaller when using the middle-hole model (Fig. 3.11 (A)). This result suggests that the flexion force needed to compensate for the twist of the middle-hole model might be much bigger than that for the 2-segment model during the thumb opposition. To testify to this assumption, we measured the twisted angles of the two fan-ACTs, adding weights (0–5 N) to one of their holding frames when the actuators were inflated with the same air pressures as needed for the thumb-finger contact. The results showed that when the two fan-ACTs abducted to a similar angle, the 2-segment model twisted at a larger angle than the middle-hole model at the same loading condition (the differences were approximately 7 to 10°, Fig. A.1). Structurally, unlike the middle-hole model that remained the original model's fan-shaped air bladder, the 2-segment model separated the air bladder into two parts, which reduced the actuator's thickness expansion efficiently, thus making the actuator easier to twist. As a result, the 2-segment fan-ACT could cooperate with the thumb flexion actuator with higher compliance, which resulted in a generally greater pinching strength.

Comparison among three models of 3-chamber actuator

All three models achieved the same Kapandji score, and they all did not make the thumb contact to position 9 (Table 3.1). Since there was no need for thumb abduction to reach position 9, only the middle chamber of each model was inflated to its maximum air pressure. Model 2 and Model 3 had tapering chambers bent to a similar height of position 9; however, they had distance in a volar direction. This distance could be diminished if the metacarpal segment of the small finger of the dummy hand is flexible. Model 1, oh the other hand, did not flex to the height of position 9 due to its inferior flexion capability (less flexion ROM than the other two models, Fig. 3.10), and resulted in the maximum straight-line distance to position 9 (22 mm, Table 3.1).

The flexion forces generated by the middle chamber of 3C-ACTs contributed significantly to the pinching strength. In accordance with the flexion results of the 3C-ACTs, the semi-cylinder Model 2 had a greater pinching strength than the cuboid Model 3 (Fig. 3.11 (B) and (C)). On the other hand, the maximum thumb abduction angle during opposition movements would approximately be 42° (25° [74], adding the initial abduction angle of 17° measured in this study), less than the thumb's maximum abduction RoM (60°). The advantage of Model 3 in abduction support might not be fully present when performing movements that do not require much abduction assistance. Consequently, the semi-cylinder Model 2 would be more suitable

for the thumb opposition assist. In contrast, the cuboid Model 3 might be suitable to assist movements with large abduction requirements, such as grasping large objects.

Comparison between fan-shaped and 3-chamber actuators.

Generally, the fan-ACTs had a smaller Kapandji score than the 3C-ACTs (Table 3.1 and Fig. 3.10). They could not make thumb contact with the position close to the palm, namely, positions 0, 8, and 9, due to their initial angle of 27.5°. Only the thumb flexion actuator was inflated when performing the position 7. The thumb flexed to the same height as position 7 (Fig. 3.10) and formed a horizontal distance. This distance might be caused by the lack of mobility of the small dummy finger's metacarpal segment. Moreover, a part of the flexion force of the thumb flexion actuator would be consumed to twist the fan-ACT when the thumb reaches the ring and the small fingers. Therefore, the interference between independent actuators that support motions in different directions might impair each other's assistive effect, making the combination approach difficult to realize a full thumb opposition support.

In contrast, the 3C-ACTs realized most of the thumb opposition positions. They could achieve motion that contains both abduction and flexion effortlessly by first inflating the side chamber to abduct and flex the thumb to some extent (the flexion coincides during side chamber inflation), then inflating the middle chamber to flex the thumb further if necessary. As a result, the negative interference between chambers might be less significant than that between independent actuators, thus making the full thumb opposition support possible.

3.7.3 Comparison between 2-segment fan-ACT and semi-cylindrical 3C-ACT with tapering chambers

Two-segment fan-ACT and Model 2 of 3C-ACT generally showed superior thumb abduction and opposition support performance, compared with their similar models. These two actuators were compared in this section.

Both actuators could assist the thumb in contacting other fingertips and generated similar levels of thumb-finger pinching strength (Fig. 3.11 (A) and (B)). However, they might be suitable for different scenarios considering their overall performance.

The fan-ACT generated more than 32 N of abduction force (Fig. 3.5 (B)), whereas the 3C-ACT only generated only 4.5 N (Fig. 3.8 (B)). Soft actuators for hand rehabilitation usually need to impel or stretch fingers with severe joint stiffness caused by illnesses or aging at the early stages of robot-assisted rehabilitation. In this case, a 2-segment fan-ACT with more force production capabilities would be desirable.

Although the two kinds of thumb actuators showed similar levels of thumb pinching strength, the 3C-ACT had a wider range of adjustable air pressure. For instance, during the thumb-middle finger opposition, the 2-segment fan-ACT could adjust a pinching strength from 0 to 3.6 N within an air pressure ranging from 0 to 150 kPa (Fig. 3.11 (A)). In contrast, Model 2 of 3C-ACT could adjust a 0 to 4.2 N pinching strength within an air pressure from 0 to 380 kPa (Fig. 3.11 (B)). These results indicated that the same air pressure change in the flexion actuator would cause a more intensive change in pinching strength when using the 2-segment fan-ACT. The pinching strength of the 3C-ACT, on the other hand, could be controlled

more precisely and subtly by adjusting air inflation, suggesting the potential of using Model 2 of 3C-ACT to assist the thumb in performing fine motor movements, such as precision pinching.

3.7.4 Contributions

In this study, soft actuators were designed to realize the thumb opposition with sufficient pinching strength for the first time in the research area. Contributions can be summarized as follows:

About the approaches and realization:

1) Two approaches for thumb support: the combination approach and the all-in-one approach, were accomplished by biomimetic designs and systematically compared.

2) For the combination approach, which combined an abduction fan-ACT and a flexion actuator, multiple constraints (thickness expansion, rotation axis, and spatial) were considered in the prototype design and actuator assembling, which is the first trial to deal with the difficulties due to the combination of multiple actuators for thumb support.

3) For the all-in-one approach, emphasis was given to satisfying the thumb's multiple DoFs and joints' RoM requirements with a single actuator. The design considerations accounting for multiple-chamber interaction that caused DoF differentiation and interference were first addressed in the soft actuator research area.

About evaluation: The thumb opposition support performances of soft actuators were first evaluated thoroughly, concerning the kinematic aspect and the pinching strength of practical thumb opposition.

About findings:

1) Both approaches are applicable for practical use; however, the all-in-one approach (3C-ACTs) is superior in the kinematic aspect of thumb opposition support.

2) The semi-cylindrical tapering 3C-ACT of the all-in-one approach has the potential to assist fine motor movements with proper control.

3) The 2-segment model of the combination approach would be applicable for activating fingers with rigid joints in the early rehabilitation stage.

3.7.5 Future work

Interference between actuators or between inner chambers was observed in this study. We did not analyze the cause and effect of inter-chamber and inter-actuator interference since the focus of this study was on biomimetic design and optimization of actuator geometry. Interference of this type has an impact on the performance of a multi-chamber actuator in independent single-DoF support. It will also make controlling the actuator more challenging.

In the future study, we will continue to develop the 3-chamber actuator. The interference between the chambers could be improved further using design techniques, and the causes and effects of the interference will be investigated using simulation methods.

3.8 Conclusion

This study designed two types of actuators representing different thumb support approaches: The fan-ACTs need to coordinate with a thumb flexion actuator for thumb op-position support; the 3C-ACTs could assist with both thumb abduction and flexion simultaneously. Each actuator type was designed with different models.

The middle-hole and 2-segment fan-ACTs satisfied the abduction RoM and force requirement. However, the 2-segment model would be optimal for assisting the thumb opposition due to its higher compliance with the thumb flexion actuator.

Comparison among 3C-ACTs showed that the flexion force generated by Model 2 and Model 3 with tapering chambers was in accordance with the RoM requirements of a real thumb, whereas Model 1 with constant chambers did not, which testified the validity of the tapering-chamber design. Furthermore, the cuboid model 3 might be suitable for assisting abduction movements owing to its better abduction performance. The semi-cylindrical Model 2 is more applicable for thumb opposition rehabilitation due to its better flexion performance and intensive pinching strength.

A comparison between the two approaches indicates that the combination approach might be suitable for the early stage of rehabilitation due to its intensive abduction force output. The all-in-one approach could assist fine motor movements in the mid-late stage of rehabilitation for its higher Kapandji test score and its potential to control the pinching force exertion more subtly.

Chapter 4

Design soft thumb multi-chamber actuators mimicry in the anatomical structure of skeletal muscle

4.1 Preface

We (Wang, Vinocour, Kokubu, Lu, Zhou, Huang, Hsueh, and Yu) submitted the manuscript of this study to IEEE/ASME Transactions on Mechatronics on January 11th, 2022. The paper was under review at the time of submission. I conducted the design, fabrication, and evaluation of all the prototypes, and the analysis of the results. Prof. Yu provided comments and assistance in editing the manuscript. Other coauthors contributed to the collection and processing of data.

4.2 Introduction

In comparison to Pneu-net and bellow-shaped actuators, fiber-reinforced actuators have additional design parameters related to the reinforcement fiber, such as fiber winding patterns (single-helix, double-helix, single loop, two-directional hitching, etc.), fiber loop interval, and fiber position (wrapped on interior chambers or on the exterior main body surface), allowing for more potential to realize a multi-chamber actuator with less inter-chamber interference.

In Chapter 3, we aimed to accomplish full thumb motion support by optimizing the geometrical structure of the fiber-reinforced actuators. In this study, we attempted to improve the inter-chamber interference in terms of reinforcement fiber design.

4.2.1 Physiological structure of skeletal muscle

Each skeletal muscle is made up of bundles of muscle fibers that are encased in a layer of connective tissue sheath called the epimysium (Fig. 4.1). The perimysium is another layer of connective tissue sheath that binds a group of cylindrical-shaped muscle fibers within that muscle into bundles. The dysfunction of these membranes and proteins between muscle cells may cause muscle weakness and atrophy [75].

The layered composition of skeletal muscle may be useful for reducing inter-chamber interference in a soft multi-chamber cylindrical actuator. The reinforcement fiber of the fiber-reinforced actuator can be wrapped around the inner chamber to

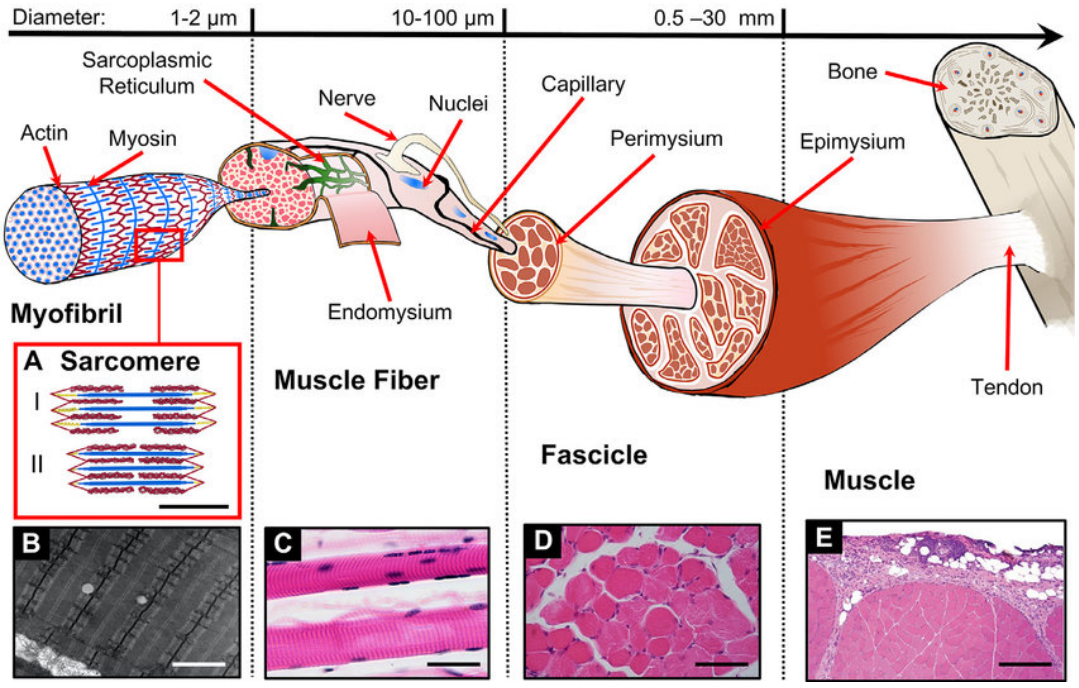

FIGURE 4.1: Structure of skeletal muscle [76]

mimic the perimysium that binds muscle fiber, and the fiber wrapped around the exterior of the entire actuator functions as the epimysium of a muscle bundle.

4.2.2 Related research on soft actuators with exterior and interior reinforcement fiber

The fiber-reinforced continuous soft actuator with multiple air chambers has been extensively explored as it was utilized in minimally invasive surgery and several animal bio-mimicking devices. Decroly et al. [77] and Zhang et al. [78] designed cylindrical actuators with three chambers spaced at 120° intervals along with the cylinder for surgical assistance. Reinforcement fibers are wound in a double-helix pattern on the exterior surface of the actuators. By inflating each chamber with a different pressure, their actuators can (or have the potential to) achieve bending motion in any direction in three-dimensional space.

Another method for achieving multi-DoF is to wrap the reinforcement fiber onto the internal chambers individually and cast them together as the main body of the actuator, such as the octopus robot designed by Fras et al. [52], the surgical robot designed by Abidi et al. [79], and the multi-chamber actuator designed by Nguyen et al. [80]. This interior fiber-reinforced method is helpful for surgical assisting devices because it reduces the interference between chambers while leaving enough space for the additional equipment (camera module and surgical shears) to pass through its center. Nonetheless, actuators for surgical purposes often require only a sufficient RoM (omnidirectional bending) and no force output requirements. Moreover, surgical actuators are frequently assessed by their free bending RoM and force, whose results are less helpful for applications in robotic gloves since hand motion assistance needs a significant force output and RoM when the actuator is bound to a finger. The binding of the actuator would affect its deformation upon pressurization and, therefore, its force and RoM results. The effect of interior and exterior

fiber wrapping methods of soft actuators for hand motion support has not yet been studied.

4.3 Goals

This study aimed to design fiber-reinforced soft actuators with three chambers that could provide sufficient support in thumb flexion, abduction, and opposition support while reducing inter-chamber interference. We designed three types of soft actuators with consideration of the following design parameters:

1) *Fiber winding methods:* Exterior fiber winding on the main body surface; interior fiber winding around each interior chamber; and hybrid exterior-interior winding.

2) *Fiber interval:* The distance between fiber loops needs to be determined depending on fiber winding methods.

3) *The silicone material of the internal chambers and the main body:* The elastic chambers and the actuator's main body are manufactured in separate steps when the reinforcement fiber is wrapped around the internal chambers, allowing the material of the two parts to be changeable.

Actuators' flexion and abduction RoM were preliminarily assessed in terms of free bending angles and Finite Element Analysis (FEA) results. FEA-based simulation results were also used to analyze the internal chamber deformation not visible in experiments and the significance of each design parameter. For the thumb assist evaluation, we compared the flexion, abduction RoM, and force output of the three types of actuators when attached to a dummy thumb. Finally, an enhanced Kapandji test that measured both Kapandji score and tip-to-tip pinching strength was performed with actuators mounted to a bionic dummy hand for a practical evaluation of thumb opposition support. We aimed to (1) find out the optimum design of the fiber-reinforced 3-chamber soft actuator; and (2) clarify the impact of the design parameters related to the fiber winding on bending performance.

4.4 Actuator prototyping

4.4.1 Functional requirements

The designed actuators were aimed to achieve the RoM requirements that determined based on a participant's left hand. RoM requirements are shown in Section 2.2.1, Table 2.1.

4.4.2 Fiber wrapping and actuator design concepts

Design of actuators' silicone body

The thumb actuators are designed in a slender semi-cylindrical shape. Inside the actuators, three identical elastomeric chambers are arranged in parallel around the main body's central axis at 90° intervals. Inflation of the middle chamber bends the actuator toward the bottom surface, providing thumb flexion support, while inflation of the side chambers bends the actuator to the lateral sides, enabling thumb abduction-adduction support.

To facilitate discussion of the effect of reinforcement fibers, we designed air chambers to have a consistent cross-section of a circular sector that runs from the root to the tip of the actuator. We maximized the chamber size while maintaining a 2 mm chamber thickness and a 2 mm distance between neighboring chambers. The width of the actuator was designed to be the same as the width of the IP joint, and the entire actuator length equals the total length of the DP, PP, and the metacarpal bones.

Reinforcement fiber was wound in three methods: exterior winding (E-type), interior winding (I-type), and hybrid winding (IE-type).

Exterior fiber wrapping method

Fibers were wrapped in two patterns on the actuator's exterior surface at 2 mm intervals (Fig. 4.2 (C)), an empirical distance: The top half of the actuator was covered with 21 loops of two-directional hitching to facilitate joint flexion; the rest was wrapped with 13 sets of double-helix patterns (26 loops) to allow flexion and abduction.

Interior fiber wrapping method

Fibers were wrapped with single loops at 4 mm intervals on each chamber (Fig. 4.2 (E)). Compared with the E-type actuator, the I-type actuator had greater radial constraints on actuator expansion due to its three fiber alignments; therefore, it had a greater fiber interval. Greater fiber interval would improve radial bending, but only within a reasonable range, as it would reduce the actuator's force output.

Interior-exterior hybrid fiber wrapping method

Fibers were wrapped in single loops at 8 mm intervals on both the actuator surface and the air chambers. The exterior and interior fiber loops were alternately placed, leading to an overall fiber interval of 4 mm.

Interior and exterior silicone materials

The silicone material for both the interior chamber and the main body is available in two stiffnesses: DS 10 and DS 20. The combination of interior and exterior silicone materials results in four main bodies of variable stiffness (DS 10 (interior chamber material)-10 (exterior material), DS 10-20, DS 20-10, DS 20-20 (DS 20)).

The entire main body of the E-type and I-type actuators was made of DS 20. The IE-type actuator was made in three versions using DS 10-20, DS 20-10, and DS 20 to explore the effects of interior-exterior materials. DS 10-10 was not considered because it is too soft for the IE-type actuators.

In general, five thumb actuators were fabricated for comparison: one E-type and one I-type in DS 20 silicone, and three IE-type actuators made in DS 10-20, DS 20-10, and DS 20, respectively.

Prototyping procedure

The manufacturing steps are demonstrated in Fig. 4.2. The main body of the E-type actuator was cast in DS 20, while the head and root were cast in DS 30, a stiffer silicone, to prevent expansion at both ends of the chamber. The reinforcement fibers (cotton thread, 0.33mm) were secured with Ecoflex 00-30 (Smooth- On, Inc., US) as the final coating.

Three chambers and the main body for the I-type and IE-type actuators were fabricated separately (Fig. 4.2 (D-G)). We started by casting three chambers with a 1 mm wall thickness, then arranging the fiber-wrapped chambers in the mold to cast the remainder of the main body. DS 10 or DS 20 was used to cast the internal chamber and main body.

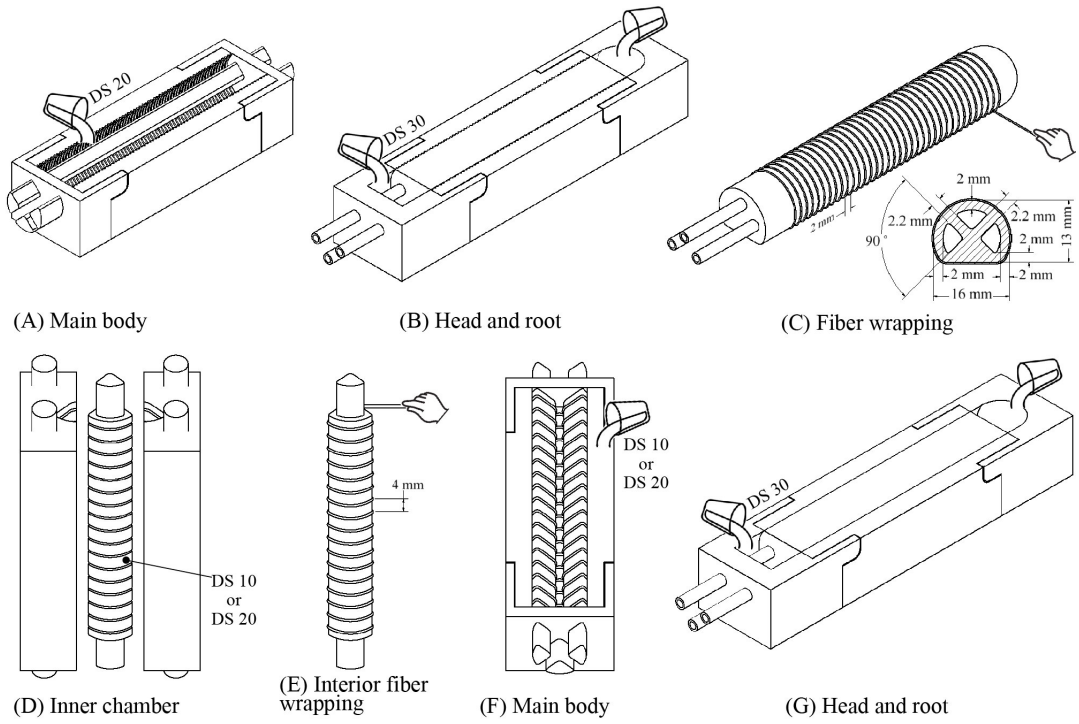

FIGURE 4.2: Illustration of actuator manufacture procedures. E-type fabrication procedure: A-B-C; I-type fabrication procedure: D-E-F-G; IE-type fabrication procedure: D-E-F-G-C.

4.5 Actuator evaluation

The free bending RoM of the designed actuators was measured to validate the FEA simulation. Thumb support performance was evaluated by flexion, abduction RoM, and force output measured with a dummy thumb and an enhanced Kapandji test measured with a dummy hand that mimicked the biomechanical characteristics of a participant's hand.

4.5.1 Finite element analysis

We established actuator-only finite element analysis (FEA) models of the three proposed actuators in COMSOL Multiphysics (COMSOL Inc., Fig. 4.3) to analyze the interior chamber deformation. The blocked force of a free bending actuator was not analyzed since actuators deformed extensively in real experiments, making accurate measurement impossible. The hyperelastic properties of silicone rubber were modeled using the Yeoh's model, which can accurately predict the large deformation of an elastomer material while having a low computing cost [81]. The constitutive model parameters of the materials in [82] were used. The mesh for the entire actuator was built using tetrahedral elements with the default fine setting from COMSOL.

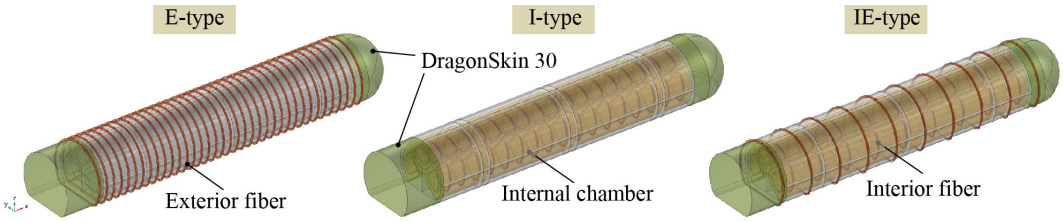

FIGURE 4.3: Finite element analysis modeling.

4.5.2 Free bending measurements

Actuators were held vertically, with two ArUco markers attached at their head and root, respectively (Fig. 4.4 (A)). OpenCV with python was used for camera-based (Intel® RealSense™ Depth Camera D435, US) two-dimensional marker detection and calculation of the angle formed by the left side of the two markers.

(A) Free bending RoM measurement setup

(B) RoM measued with dummy hand

(C) Forece output measurement setup

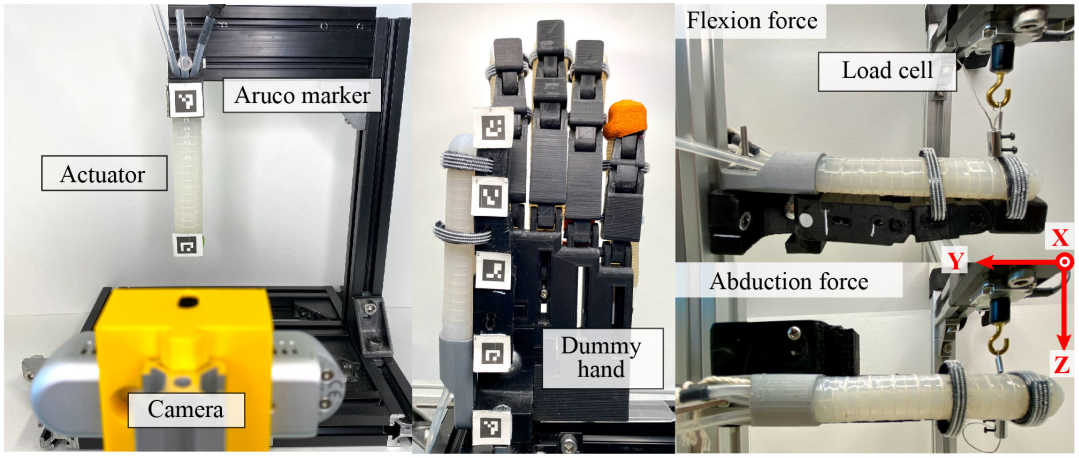

(D) Kapandji score

(E) Setup for pinching strength

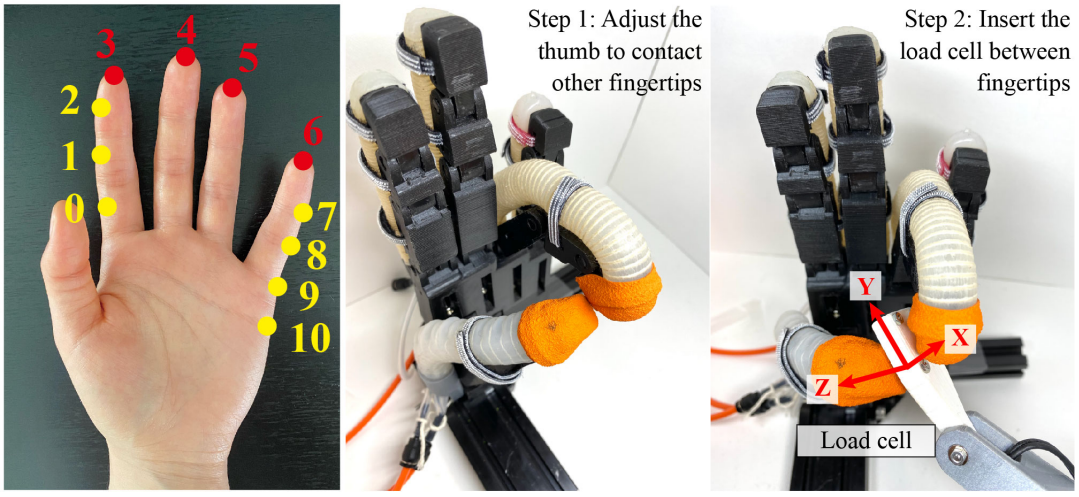

FIGURE 4.4: Experimental setups

4.5.3 Bending angle measurements with dummy thumb

Actuators were mounted on a dummy thumb that was attached with fiver markers (Fig. 4.4 (B)). The angle of the dummy thumb's joints was measured using the same camera-based angle calculator used for free bending RoM measurement. The three-dimensional coordinates of the center point of the markers were recorded, and the angle enclosed by three markers was calculated as the angle of the joint. We calculated the flexion RoM using the x-axis and y-axis data and the abduction RoM using the y-axis and z-axis data.

4.5.4 Force output measurements with dummy thumb

Force output was measured using the same method as demonstrated in Chapter 3. A 3-axis load cell (USL06-H5 Load cell, maximum: 100N, Tec Gihan, Japan, Fig. 4.4 (C)) was used to measure the flexion and abduction forces. The finger segment to be measured was wired to the load cell; the other parts were free to move. The flexion force generated in the middle of each thumb segment (DP, PP, and metacarpal) was calculated as the net force of F_Y (elongation force) and F_Z (flexion force). The overall abduction force was measured at the middle of the DP segment since abduction only occurs at the CMC joint. The abduction force was F_Z and the flexion force during an abduction was the net force of F_X (flexion force) and F_Y (elongation force).

4.5.5 Enhanced Kapandji test measurements

The designed thumb actuators were mounted on the dummy thumb, and single-chamber soft cylindrical actuators for finger flexion were mounted on the four fingers of the dummy hand. We carefully adjusted the air pressure in the thumb actuator's middle and left side chambers, as well as the four-finger flexion actuator, to make the thumb contact the target positions specified by the Kapandji test. After confirming the thumb-to-finger contact, we inserted the 3-axis load cell between fingers to record the change in pinching force with the pressurization of the middle chamber of the thumb actuator and the four-finger flexion actuator (Fig. 4.4 (E)). Pinching strength was difficult to measure in some situations due to the rigid right-angle surfaces of the dummy finger; hence, we added a screw to the load cell to increase the contact of the fingers and sensor.

4.5.6 Measurements and measurands

Actuators were tested in the following order: free bending, RoM with a dummy finger, force output, and the enhanced Kapandji test. If the actuator exhibits a significant disadvantage when measured, it will not proceed to the next measurement. The measurements and measurands are shown in Table 4.1.

4.6 Results

4.6.1 Free bending angle: experiment vs. FEA

For both flexion and abduction RoM, the experiment results showed that the IE-type actuator with DS 10-20 required the least air pressure to fulfill the same angle requirement, while the I-type actuator required the most (Fig. 4.5 (A-B, dot lines)). The same trends were observed in FEA results (Fig. 4.5 (A-B, solid lines)), whereas at smaller values.

TABLE 4.1: Summary of measurements and measurands.

	E-type	I-type	IE-type		
			DS 20	DS 20-10	DS 10-20
Free bending	O	O	O	O	O
FEA	O	O	O	O	O
RoM (dummy thumb)	O	O	O	O	O
Force output	O	O	O	O	
The enhanced Kapandji test	O	O	O		

E-type: exterior fiber winding, I-type: interior fiber winding, IE-type: hybrid fiber winding, DS: DragonSkin, FEA: finite element analysis

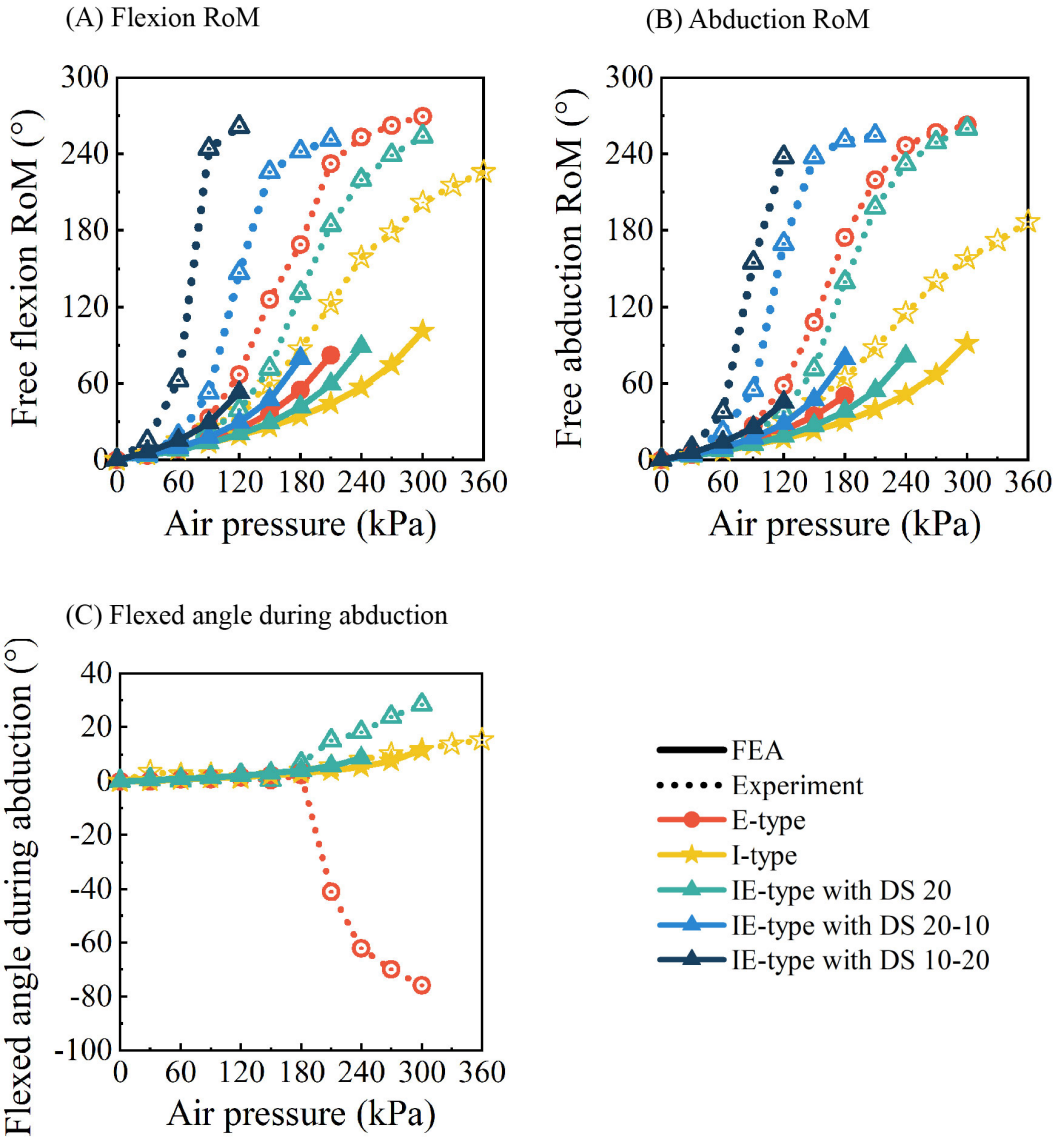

FIGURE 4.5: Experiment results and FEA results of free bending RoM during air inflation in (A) Middle chamber, (B) and (C) left side-chamber.

Both the experiment and the FEA results revealed an unwanted flexion-extension during side chamber pressurization (Fig. 4.5 (C)). In the experiment results, the E-type actuator slightly extended (+) first and flexed (-) later after being pressured

to 210 kPa. However, the FEA results only showed extension since its calculation stopped at 180 kPa because the inflated chamber compressed its adjacent chambers intensely and formed tiny boundaries that were smaller than the mesh, resulting in no convergence of the solution.

4.6.2 FEA of stress distribution and actuator elongation

Middle chamber pressurization

The cross-sections were taken from the location corresponding to the metacarpal's midpoint. The stress distribution was evaluated at the upper and lower surfaces of the middle chamber. The length change was measured at the top and bottom parts of the actuator.

Comparison among E-type, I-type, and IE-type with DS 20: In contrast to the I-type and the IE-type, the E-type actuator showed greater stress at the lower surfaces of its middle chamber when flexed to 82° (the maximum flexion angle of the E-type in FEA results, Fig. 4.6 (upper)). The top and bottom halves of the E-type actuator lengthened during air pressurization, whereas the bottom parts of the other two types shortened slightly (Fig. 4.6 (lower)).

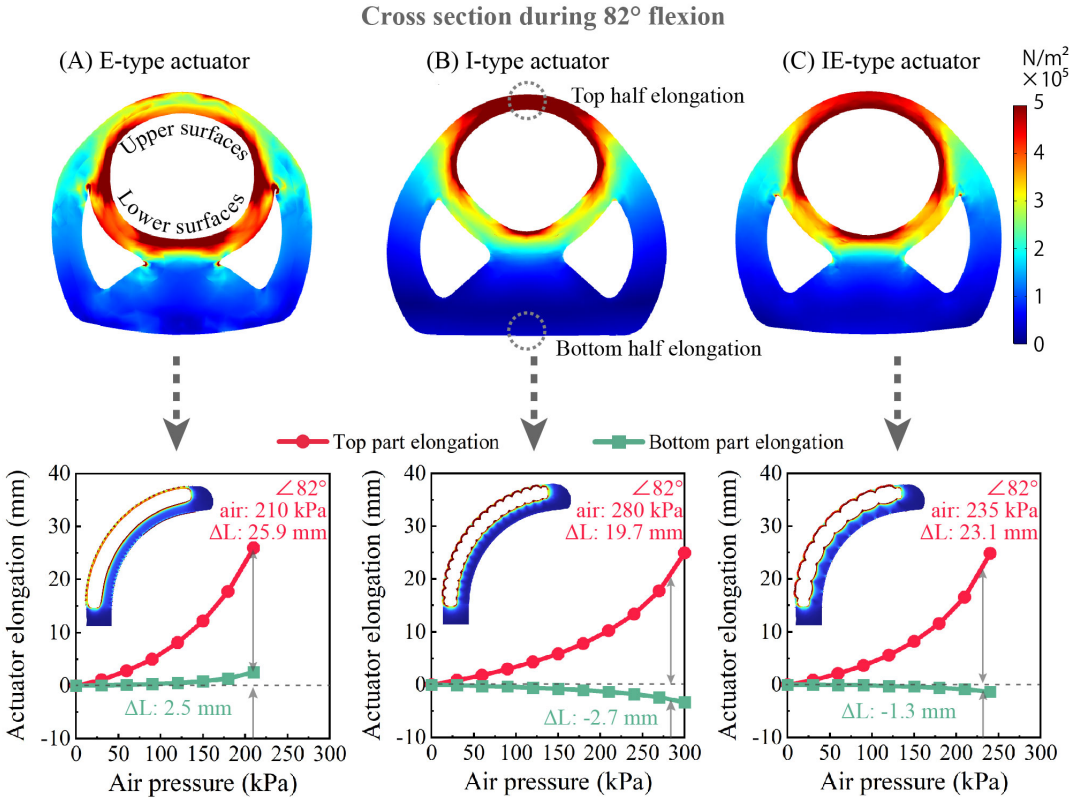

FIGURE 4.6: Stress distribution at the cross section (upper) and actuator elongation during middle chamber pressurization (lower) of E-type, I-type, and IE-type in DS 20.

Comparison between IE-type with DS 10-20 and DS 20-10: The exterior layer of the actuator with DS 10–20 had a larger stress than its interior chamber wall, whereas the actuator with DS 20–10 had the contrary (Fig. 4.7 (upper)). Also, the DS 10-20

had a larger elongation at the same air pressurization than the DS 20–10 (Fig. 4.7 (lower)).

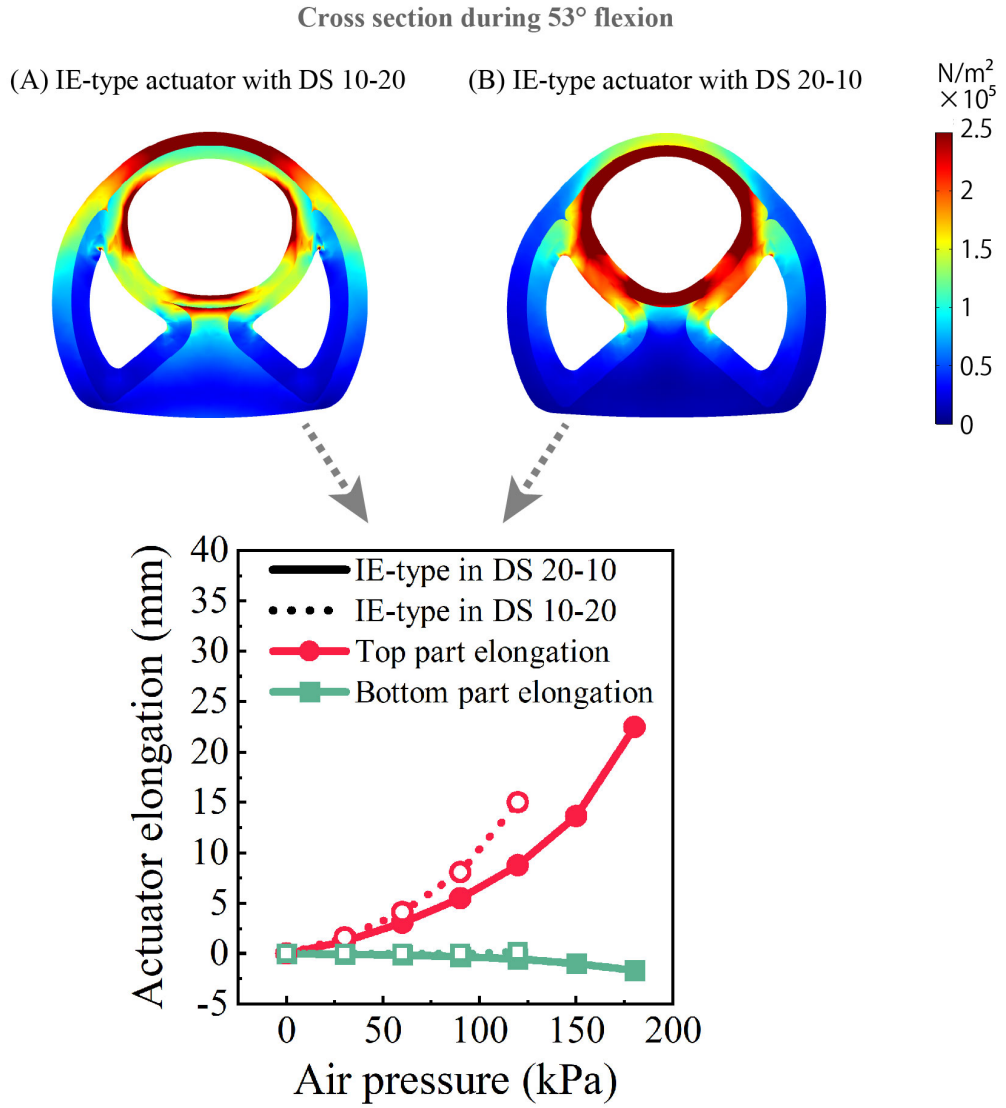

FIGURE 4.7: Stress distribution at the cross section (upper) and actuator elongation during middle chamber pressurization (lower) of IE-type in DS 10-20 and DS 20-10.

Side chamber pressurization

The stress distribution was evaluated at the upper, lower, and lateral surfaces of the side chamber, and the length change was measured at the top, bottom, and lateral parts of the entire actuator.

Comparison among E-type, I-type, and IE-type with DS 20: The I-type actuator had slightly greater stress at the lateral surface of its side chamber. In contrast, the other two types showed higher stress at the upper surface, particularly the E-type (Fig. 4.8 (A-D)). All three actuators had the greatest elongation in their lateral parts and the least in their top parts. The elongation of the top and bottom parts of the E-type actuator was greater than that of the other two types (Fig. 4.8 (E)).

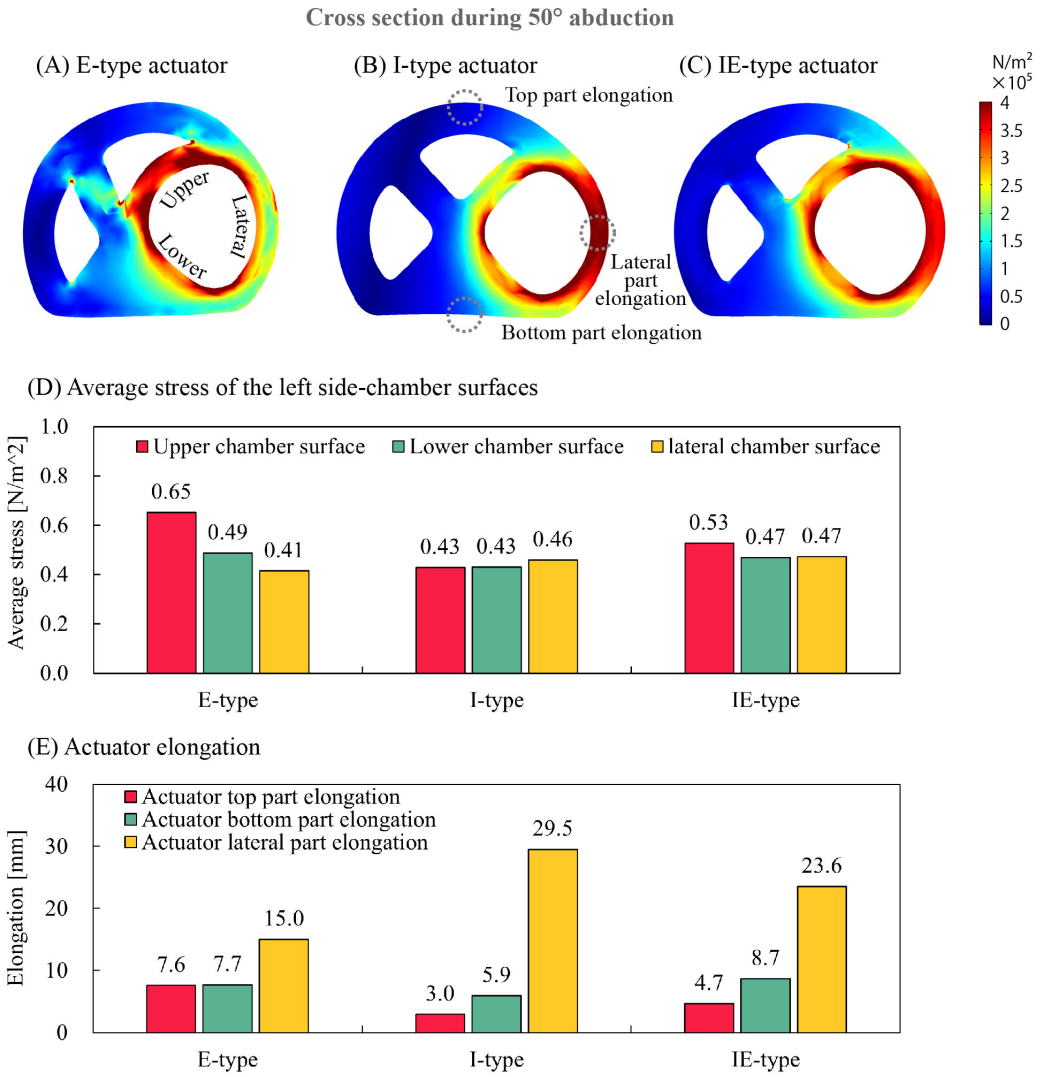

FIGURE 4.8: Stress distribution at the cross section (A-D) and actuator elongation during side chamber pressurization (E) of E-type, I-type, and IE-type in DS 20.

Comparison between IE-type with DS 10-20 and DS 20-10: Similar to the results of middle chamber pressurization, the stress of the two actuators was concentrated at different layers. Moreover, the upper surface of the IE-type with DS 10-20 extruded more intensely into the middle chamber than with DS 20-10 (Fig. 4.9).

4.6.3 Bending angle measured with dummy thumb

Flexion RoM results

The CMC joint flexed to an angle close to the requirement when using the E-type actuator (11°), but it seldom bent when using the other four actuators (Fig. 4.10 (A)). The MCP joint was bent to its limit by all five actuators (Fig. 4.10 (B)). Only the E-type actuator (83°) and IE-type actuators with DS 10-20 (81°) and DS 20 (75°) bent the IP joint to angles close to its maximum flexion angle (Fig. 4.10 (C)).

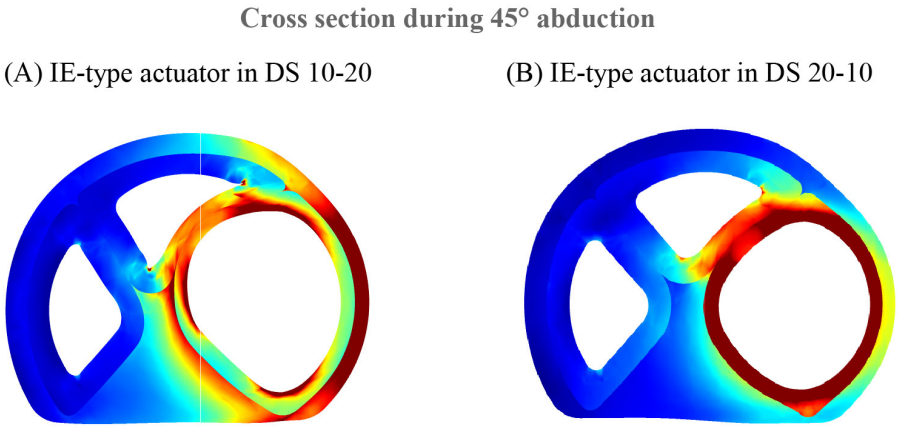

FIGURE 4.9: Stress distribution at the cross section (A-D) and actuator elongation during side chamber pressurization (E) of TE-type in DS 10-20 and DS 20-10.

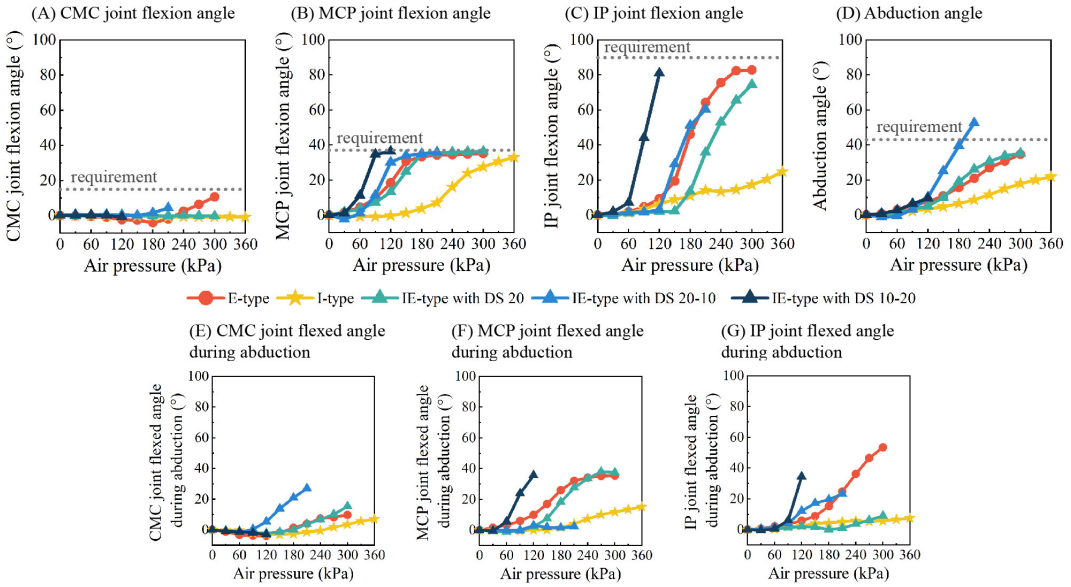

FIGURE 4.10: Flexion RoM (A-C), abduction RoM (D), and flexion RoM during abduction (E-G) measured with a dummy thumb.

Abduction RoM results

Except for the I-type actuator and the IE-type with DS 10-20, all the other actuators abducted the thumb close to the requirement (Fig. 4.10 (D)). However, the E-type actuator produced the greatest unwanted flexion angle during side chamber pressurization, while the I-type actuator produced the least (Fig. 4.10 (E-G)).

4.6.4 Force output measured with dummy thumb

The force measurements of the IE-type with DS 10–20 were excluded since it had a very limited force output due to its low pressurization limit (120 kPa).

Flexion force output results

Similar to the RoM results, the E-type actuator generated the maximum flexion force at the three thumb segments, followed by the IE-type with DS 20, which produced a comparable amount of flexion force, and the IE-type with DS 20-10 and I-type actuator generated the least (Fig. 4.11 (A-C)).

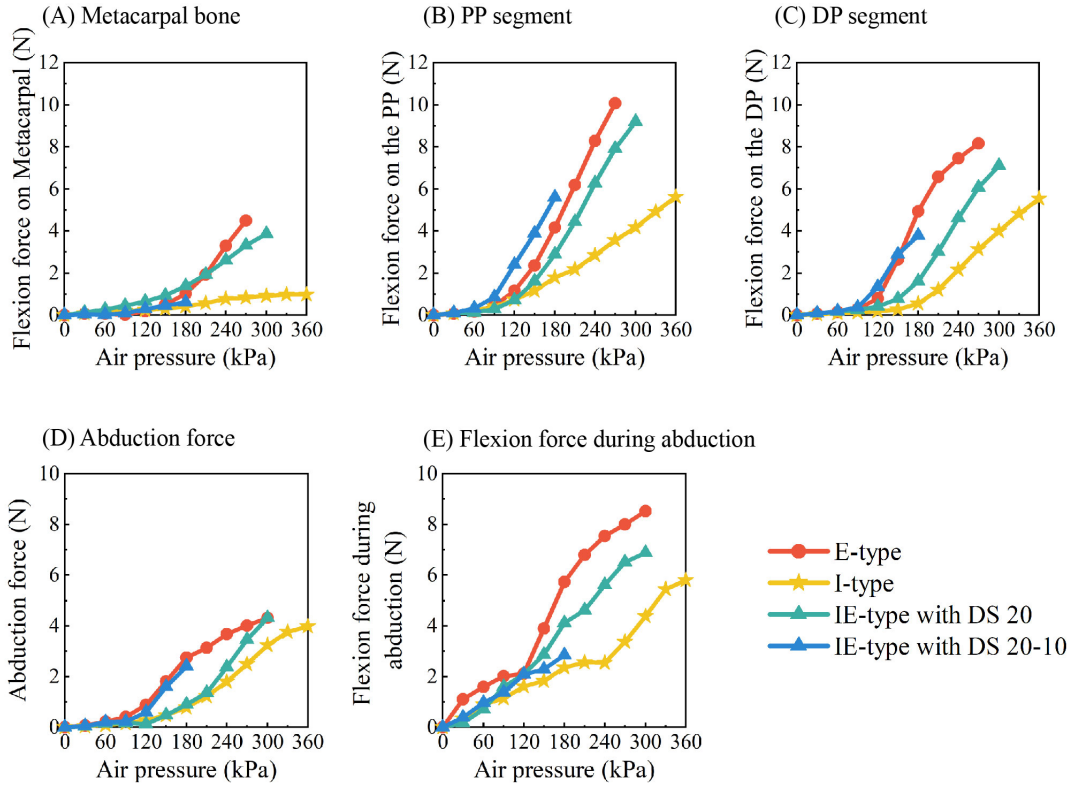

FIGURE 4.11: Flexion force (A-C), abduction force (D), and flexion force during abduction (E) measured with a dummy thumb.

Abduction force output results

The results of abduction force showed that the E-type, I-type, and the IE-type with DS 20 had a similar abduction force output (Fig. 4.11 (D)). However, the IE-type with DS 20 generated less unwanted flexion force during abduction compared with the E-type actuator (Fig. 4.11 (E)). As a result, it generated both a larger force in the desired direction and a lesser one in the undesired one.

4.6.5 Enhanced Kapandji test

Kapandji score

The E-type and IE-type with DS 20 had the same Kapandji score (score: 0-8) and a similar magnitude of thumb-finger pinching strength, which were greater than the I-type actuator (score: 0-5, Fig. 4.12 (A)).

Pinching strength

The maximum pinching strength of the E-type and IE-type with DS 20 was observed between the thumb and the middle finger. In contrast, the I-type generated the

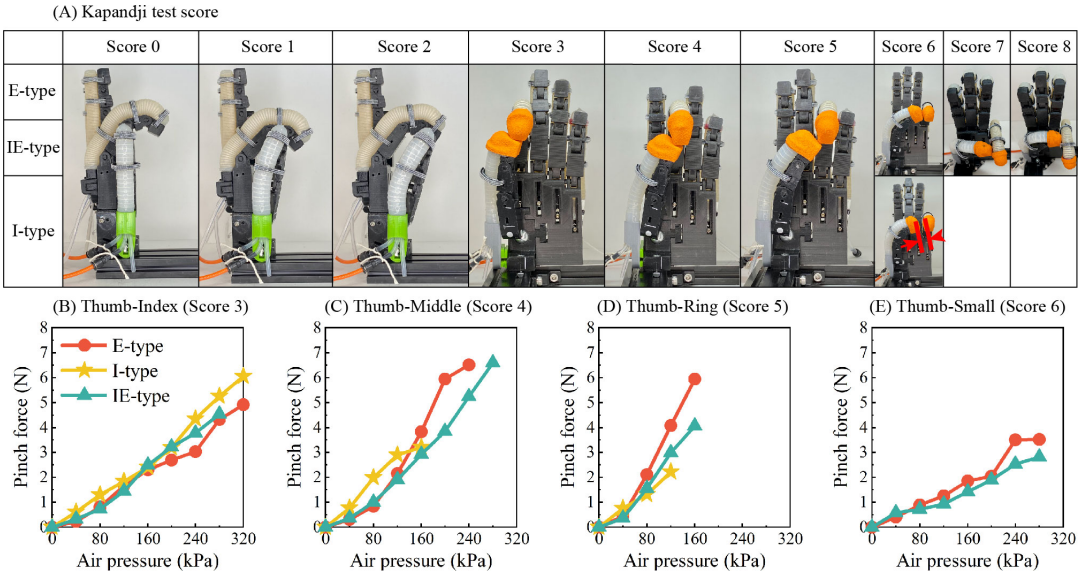

FIGURE 4.12: Kapandji score and pinching strength.

largest pinching force between the thumb and the index finger, with the magnitude decreasing as contact was made to a finger further from the thumb (Fig. 4.12 (B-E)).

4.7 Discussion

4.7.1 The validation of FEA results

The free bending results from the experiments and FEA exhibited similar tendencies (Fig. 4.5). The magnitude difference between experiments and FEA might be attributed to FEA modeling simplification (i.e., fiber nodes) and approximation of material properties of silicone rubber and reinforcement fiber. In general, the tendencies demonstrated in FEA results are instructional and predictive of experimental outcomes.

4.7.2 Comparison among three actuators with different fiber wrapping methods: exterior vs. interior vs. interior-exterior hybrid methods

RoM comparison

Both E-type and IE-type actuators could bend the finger joints close to their limit, whereas the I-type actuator was far from satisfactory, especially for the IP joint at the finger's distal tip (Fig 4.10 (A-D)). There are two possible reasons: One is in free bending. The I-type actuator had a smaller maximum flexion and abduction angles (Fig. 4.5 (A-B)), showing an inherent bending deficiency. Even if the I-type's inflated middle chamber tends to elongate, it has less impact on the surrounding silicone tissue owing to the intensive restriction of interior fibers and hence cannot drive the entire actuator to elongate. Another reason would be a lack of axial elongation upon pressurization. If a soft actuator could not elongate with finger flexion, its distal tip would go close to the IP joint, limiting flexion torque and making the IP joint unable to be bent. Let the flexed angles of the IP and MCP joints be α and β (in degrees, Fig. 4.13), respectively. During flexion, the thumb's surface elongation ΔL can be estimated as,

$$\Delta L = \frac{\pi}{180} (r_1 \times \alpha + r_2 \times \beta)$$

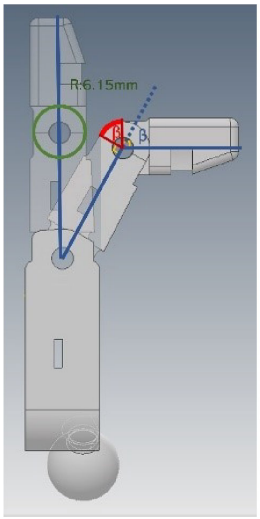

FIGURE 4.13: Flexion of the dummy thumb.

Where r_1 and r_2 are the radius of the two joints. When $r_1 = r_2 = 6.5$ mm (the radius of the IP and MCP joints of the dummy thumb), the maximum finger surface elongation would be 14.4 mm. The I-type actuator had less elongation in general, and its bottom surface even contracted during free bending (Fig. 4.6 (B, Lower)). We also measured the approximate elongation of the three actuators when they were mounted to the dummy thumb and inflated to 300 kPa. The E-type had the most elongation of 25 mm, the IE-type elongated 13 mm, which was the closest to 14.4 mm, and the I-type had the minimum elongation of 9 mm.

Accordingly, when supporting finger motion, actuator elongation during flexion is crucial for a finger actuator and should be taken into account throughout the design process.

Force comparison

Both E-type and IE-type actuators could provide more than 7.1 N to impel joint flexion (Fig. 4.11 (B-C)). There is a lack of data on the force needed for thumb flexion; as a reference, the muscular force of flexor pollicis longus, the muscle responsible for IP joint flexion, is in the range of 3-120 N during intensive pinching [83]. The 7.1 N force output would be adequate to induce full passive IP joint flexion for a motion assist device.

Overall, the E-type actuator could provide enough force to flex and abduct the thumb joints close to their requirements, but it produced more unwanted thumb flexion during side chamber pressurization. In contrast, the I-type actuator had the least flexion angle and force during the abduction, but it did not satisfy the joint's RoM requirements. Only the IE-type actuator had the ability to support full thumb flexion and abduction with fewer undesired actuator deformations (inter-chamber interference).

From a physiological perspective, the majority of contractile force (more than 75% in certain models, [84]) generated by contractile elements (e.g., myofibril) was transmitted laterally. Accordingly, the perimysium, which bundles muscle fibers, would transmit force across bundles while still inhibiting their excessive deformation. The epimysium encases multiple perimysiums to create a muscle, which would

protect the muscle from distortion and reduce muscular interference under high force loads. The existence of these internal and external membranes and their moderate binding effect may protect the muscles and, to some extent, facilitate force transmission.

Similarly, in terms of the stiffness of the chamber and the entire actuator and the stress distribution upon pressurization, a balance of interior and exterior stiffness, as adjusted by the interior-exterior hybrid fiber wrapping method, may be essential for enhanced finger bending performance.

4.7.3 An analysis of interference between neighboring air chambers

Adjacent chambers compress each other upon pressurization and thereby affect the deformation of the entire actuator. We investigated the relationship between stress applied to the surfaces of the inflated chamber and the elongation of different parts of the actuator using FEA results.

Middle-to-side chamber interference during middle chamber pressurization

The lower surfaces of the E-type's middle chamber extruded intensively toward the two side chambers corresponding to their greater stress and thus compressed the solid isosceles triangular portion at the bottom, resulting in elongation in both the top and bottom halves of the actuator (Fig. 4.6 (A)). In contrast, the bottom half of the I-type was hardly deformed due to the interior fiber restriction. Consequently, the stress and deformation were concentrated on its top half, with the bottom half shortened rather than elongated during flexion (Fig. 4.6 (B)). The IE-type actuator balanced the fiber restriction and actuator elongation of the other two types. The upper surfaces of its middle chamber had comparatively higher stress; meanwhile, its lower faces extruded to the side chambers due to a loose interior fiber restriction (8 mm fiber interval). As a result, the bottom half of the IE-type deformed more than that of the I-type, resulting in a smaller shortening (Fig. 4.6 (C)).

As aforementioned, a continuum actuator should elongate with finger flexion to provide sufficient force to the distal fingertip; hence, the effect of middle-to-side interference would enhance an actuator's finger flexion support performance.

Side-to-middle chamber interference during side chamber pressurization

In the aspect of the three actuator's internal structure, the dilatational deformation of the upper surface of the side-chamber was tolerated by its neighboring middle chamber, resulting in a minor elongation of the top part of the entire actuator (Fig. 4.8 (E)); the lower and lateral surfaces of the side-chamber can directly affect the length of the bottom and lateral parts of the entire actuator, respectively. Since the lateral surface has a bigger area and there is a solid isosceles triangular portion at the bottom of the actuator, the lateral part presented more elongation even though the average stress at the lateral side-chamber surface was smaller (E-type) than or equal to (IE-type) that of the lower surface (Fig. 4.8 (D-E)).

Consequently, all three actuators showed remarkable deformation in the abduction direction while exhibiting little deformation in the flexion-extension direction (Fig. 4.5 (C) solid lines).

Notably, the E-type's FEA can only calculate to 180 kPa for side chamber pressurization, even though in experiments with prototypes, the side chamber can be inflated to 300 kPa and the actuator start to flex while inflating air to 180 kPa (Fig.

4.5 (C)). Since the largest side-chamber stress of the E-type was observed on its upper surface (Fig. 4.8 (A) and (D)), it is reasonable to predict that if the side chamber is further inflated (> 180 kPa), its upper surface will protrude intensively towards the middle chamber, resulting in a large elongation of the actuator's top part and causing the entire actuator to flex. This behavior would be more obvious when the actuator is attached to the thumb for three reasons:

1) The fixing band would restrict deformation in the bottom and lateral chamber walls, amplifying deformation in the upper wall.

2) The actuator-finger friction would impede the elongation of the bottom part, increasing the length difference between the top and bottom parts.

3) The E-type showed a bigger overall actuator length change than the other types (Fig. 5 (A, lower) and Fig. 6 (G)). Excessive elongation may cause the actuator body to bulge and create flexion force at the binding locations. In contrast, I-type and IE-type actuators have interior reinforcement fibers, which limit the protrusion of the upper side-chamber surface toward the middle chamber. Consequently, the entire actuator would flex less when placed on the dummy thumb.

In general, the E-type actuator exhibits a greater negative impact of side-to-middle interference; the I-type actuator exhibits a less positive effect of middle-to-side interference; and the IE-type actuator overcomes the shortcomings of the other two.

4.7.4 Comparison among three actuators with different interior and exterior silicone materials: DS 20 vs. DS 10-20 vs. DS 20-10

IE-type with DS 20 generally had the best flexion and abduction performance of the three because the fiber loop interval was set by it. Actuators with DS 10-20 and DS 20-10 have inverted internal-external silicone materials but have the advantage in distinct deformations: DS 10-20 was superior in flexion (Fig. 4.10 (A-C)), while DS 20-10 was superior in abduction (Fig. 4.10 (D)). During middle chamber pressurization, unlike the deformation of DS 10-20 that focused on the exterior layer, the deformation of DS 20-10 occurred mostly within the internal chamber. It was not completely transmitted to the exterior due to a harder interior material (Fig. 4.7 (upper, A-B)). As a result, its top half had a shorter elongation than DS 10-20 (Fig. 4.7 (lower)) upon the same pressurization, resulting in an inferior flexion performance.

When abducted to the same angle of 45°, the side chamber of DS 10-20 extruded more intensely into the middle chamber because of the softer material of the interior chambers (Fig. 4.9). Since energy was consumed by side-to-middle interference, DS 10-20 exhibited an inferior performance in abduction.

An actuator's interior and exterior silicone material would significantly impact its bending performance, which could be utilized as a key design parameter in soft actuator design.

4.7.5 Comparison of actuator with different fiber wrapping methods in terms of the enhanced Kapandji test

Both the E-type and IE-type actuators could make thumb contact with all four other digits, implying that the two actuators could be used for basic opposition and precise

pinch support. Similar to an active pinching of a healthy hand, their maximum pinching force of 6.5 N was generated between the thumb and the middle finger, indicating that both actuators could assist the hand in gripping an object weighing no more than 1.3 kg ($2 \times 6.5 \times \mu$, μ: coefficient of finger-object friction).

On the other hand, the I-type actuator was unable to make the thumb reach the small fingertip because of its inadequate flexion ability.

4.7.6 Contribution

This study is the first attempt to utilize interior and interior-exterior hybrid fiber reinforcement in a soft finger actuator having multiple chambers and a non-axisymmetric structure. The causes and effects of interference caused between neighboring chambers, which has seldom been reported in previous research, were addressed in terms of the pressurized chamber surface stress and overall actuator deformation. Our findings highlight:

1) A positive effect of middle-to-side interference on thumb flexion support during middle chamber pressurization and a negative effect of side-to-middle interference on thumb abduction support during side chamber inflation.

1) The potential for utilizing interior-exterior hybrid fiber reinforcement to reduce negative chamber interference while maintaining good multi-DoF support performance.

4.7.7 Future work

In this study, only the fiber interval of the actuator with DS 20 was empirically optimized. For future tasks, analytical models containing interior and exterior silicone properties and fiber design parameters must be constructed to optimize actuators in other material combinations. Furthermore, the IE-type manufacturing process is prone to failure since the inner and outer fiber coils must be evenly staggered; any misalignment would result in uneven deformation. 3D automated printing technology capable of producing complex interior windings would be immensely beneficial.

4.8 Conclusion

E-type, I-type, and IE-type actuators with different fiber wrapping methods were designed and compared in terms of flexion, abduction, and opposition performances.

The E-type actuator had a greater flexion and abduction RoM and force output, but it also had more unwanted flexion during the abduction, rendering it unsuitable for full thumb abduction support. The I-type actuator could not achieve the thumb flexion RoM requirement due to intense constriction of internal fibers. Only the IE-type actuator demonstrated an RoM, force output, and thumb opposition support comparable to the E-type while exhibiting less flexion during the abduction.

The FEA results revealed a positive effect of middle-to-side interference during middle chamber pressurization for extending the entire actuator and improving thumb flexion performance, and a negative effect of side-to-middle interference during side chamber pressurization for inducing unwanted flexion during the abduction. The hybrid fiber wrapping approach conserved a portion of the positive

interference due to the effect of exterior fibers while limiting the negative interference owing to its interior fibers.

Accordingly, as compared to geometrical design, fiber reinforcement is an effective technique to improve inter-chamber interference of a multi-chamber actuator while maintaining excellent full support in independent DoF.

Chapter 5

Comparison between 3-chamber actuator vs. Interior-exterior hybrid fiber reinforced actuator

5.1 Preface

Model 2 of 3C-ACT and the IE-type actuator in DS 20 (IE-ACT) are the optimal versions from the study in Chapters 3 and 4, respectively. Both are cylindrical actuators with three interior air chambers. The difference is in the biomimetic design concepts. The 3C-ACT optimized the interior geometry structure in accordance with the RoM requirement of the thumb, while the IE-ACT optimized the fiber wrapping method to mimic the structure of skeletal muscle.

Since both are designed to support thumb movements, we compared the thumb support performance between them in this chapter using the results from Chapters 3 and 4. Results in the two studies are comparable because similar motion capture systems (Fig. 4.4 (B) vs. Fig. 6.2 (B)) were used for ROM measurement, and setups for force output measurement and the Kapandji test were identical ((Fig. 4.4 (C-E) vs. Fig. 6.2 (C-E)).

5.2 Comparison in one-DoF support performance

Table 5.1 and 5.2 summarize the RoM and force output results of the two actuators, respectively, recorded as the maximum value at each actuator's maximum air pressure (3C-ACT: 400 kPa, IE-ACT: 300 kPa).

The 3C-ACT could flex and abduct the thumb at a greater angle than the IE-ACT, particularly at the CMC joint. It did, however, have greater inter-chamber inference, as demonstrated by a significantly greater flexion angle during abduction (Table 5.1).

TABLE 5.1: RoM results of 3-chamber and hybrid fiber-reinforced actuators [°].

	Positive items				Negative items		
	Fleion RoM			Abudction	Flexion RoM during abduction		
	CMC joint	MCP joint	IP joint	RoM	CMC joint	MCP joint	IP joint
3C-ACT	31.8	36.7	84.3	37.1	38.9	39	52.5
IE-ACT	0.2	36.3	74.5	35.2	15.4	37.4	8.9

RoM: range of motion; CMC: carpometacarpal, MCP: metacarpophalangeal, IP: interphalangeal, 3C-ACT: 3-chamber actuator, IE-ACT: interior-exterior hybrid fiber reinforced actuator.

TABLE 5.2: Force output results of 3-chamber and hybrid fiber-reinforced actuators [N].

	Positive items				Negative items
	Fleion force			Abudction force	Flexion force during abduction
	Metacarpal	PP	DP		Metacarpal
3C-ACT	4.5	6.1	7.5	4.8	6.9
IE-ACT	3.9	9.2	7.1	4.3	6.9

PP: proximal phalanx, DP: distal phalanx, 3C-ACT: 3-chamber actuator, IE-ACT: interior-exterior hybrid fiber reinforced actuator.

TABLE 5.3: Kapandji test results of 3-chamber and hybrid fiber-reinforced actuators.

	Kapandji score	Pinching strength [N]			
		Index	Middle	Ring	Small
3C-ACT	0-8	2.2	4.4	4.2	3.1
IE-ACT	0-8	4.3	6.6	4.1	2.8

Accordingly, while the hybrid fiber wrapping method is effective at reducing interference, the more restricted fiber constraint may weaken the main deformation of the entire actuator. On the other hand, the maximum flexion angles of the CMC and IP joints measured in this doctoral study are 15° and 90°, respectively. According to the study in [85], the average functional RoM of the MCP and IP joints is 10–32° and 2–43°, respectively, which is less than the maximum angle we measured. Therefore, even if IE-ACT has a 15° deficit at these two joints, the RoM it achieved would be sufficient to support most daily movements.

The 3C-ACT had a slightly greater force output than the IE-ACT, with only a 0.5 N difference at the metacarpal bone and DP, as well as the abduction force. In contrast to the 3C-ACT, which has tapering inner chambers, the IE-ACT was designed with consistent inner chambers to facilitate discussion of inter-chamber interference. As a result, it does not have a force output that satisfies the Rom requirements for thumb joints but has a maximum flexion force output at the PP segment.

5.3 Comparison in multi-DoF support performance

The Kapandji test results of the two actuators are summarized in Table 5.3. Both actuators achieved a Kapandji score of 0–8, indicating their comparable capability in thumb opposition support. The IE-ACT had greater pinching strength when impelling the thumb to pinch with the index and middle fingers, which are relatively close to the thumb. Corresponding to its greater flexion RoM and force output, the 3C-ACT had slightly greater pinching strength when impelling the thumb to pinch with the ring and small finger, which required more thumb flexion to accomplish.

5.3.1 The merits and demerits of 3-chamber and hybrid fiber reinforced actuator

Generally, both actuators are capable of supporting thumb flexion and abduction and are comparable in opposition support. They have different but complementary strengths. The 3C-ACT has merit in finger flexion support. It could bend the

thumb with greater thumb compliance. The IE-ACT, on the other hand, could support thumb abduction with less inter-chamber interference, which is a deficit of the 3C-ACT.

Chapter 6

Comparison among soft thumb actuators: modular type vs. 3-chamber vs. interior-exterior hybrid reinforcement fiber actuators

6.1 Preface

We (Wang, Kokubu, Huang, Hsueh, and Yu) published this study in Applied science, on April 7th, 2022 [86]. I conducted the design and fabrication of the whole-type actuators, and the evaluation of all the prototypes and the analysis of the results. Kokubu designed the modular type of actuator for finger flexion. Prof. Yu provided comments and assistance in editing the manuscript. Other coauthors contributed to the collection and processing of data.

6.2 Introduction

Soft pneumatic actuators of soft robotic gloves can be categorized into two types in terms of construction: whole-finger actuators with air chambers that cover the entire finger and modular (or segmented) actuators with chambers only above the finger joints.

Different versions of whole-finger type actuators with multiple inner chambers were developed and optimized in Chapter 3 and 4. According to the comparison in the previous Chapter 5, both 3C-ACT and IE-ACT are applicable for thumb motion support. The IE-ACT has less inter-chamber interference; however, it has a slightly inferior flexion performance and needs a more complicated fabrication procedure. As a result, the whole-finger type of 3C-ACT was used for the comparison with modular actuators. In this chapter, we will introduce more details about the modular actuators.

6.2.1 Related research on modular actuators

In the early stages of the development of soft finger actuators, Pneu-Net [15] [12] and fiber-reinforced soft actuators [25] [23] [24] were designed in a whole-finger fashion. These actuators can impel a finger to perform flexion motions. However, they lack ergonomics and may impose a burden on the finger since they are deformed into a

curve that deviates from the finger outline, resulting in a high binding force at the phalanges (forces restricting the actuator to bulge) [16].

The modular or segmented type has chambers only above the finger joints, aiming to provide bending force at the finger joints instead of the phalanges. Wang et al. [16], Yap et al. [13], and Li et al. [65] shortened the air chamber of the Pneu-Net actuator in [15] [12] and connected chambers with solid silicon or inflexible components. Similarly, the fiber-reinforced actuators designed by Shiota et al. [44] and Heung et al. [58] [87] have chamber segments on the DIP joint, PIP joint, and MCP joint, respectively. The bellow-shaped actuator, another type of soft actuator popular in the past five years, is usually utilized in a modular fashion in a robotic glove. The even change of the bellow's peripheric zigzag angle results in longitudinal extension, whereas the uneven peripheral change results in radius bending. For example, Guo et al. [18] and Hu et al. [20] developed robotic gloves with three bellow modules on each of the four-finger digits and two modules on the thumb for finger flexion and extension. These actuator modules or segments can connect to separate air inlets, allowing them to control the independent bending of each joint.

6.2.2 Merits and demerits of modular and whole-finger soft actuators

The existing prototypes of whole-finger and modular actuators can provide adequate support for achieving a full range of motion (RoM) of finger flexion (1.2–3.6 N flexion force). Nevertheless, they are insufficient in thumb abduction and opposition support, and the two types of actuators have deficits in different aspects of thumb motion support.

The whole-finger type in [25] (fiber-reinforced), [24] (fiber-reinforced), and [15] (Pneu-net) have a specific unit for the thumb. These studies simplified thumb opposition as a coupled movement of flexion and twisting. As a result, the root part of the Pneu-Net actuator was designed with oblique chamber networks, and the root part of the fiber-reinforced actuator (or the entire actuator [15]) was coiled with fiber in a single-helix pattern. These actuators can make the thumb contact the fingertip of the small finger, but they lack independent support in the thumb abduction direction.

In [16] (Pneu-Net), [65] (Pneu-Net), and [20] (bellow-shaped), which designed modular or segmented types of actuators, the thumb opposition was simplified as a combination of flexion and abduction. The authors placed a mini version of their actuator transversely between the thumb and index finger's MCP joint to compel the thumb to abduct. These actuators can assist a hand to grip a large object; however, the initial length of the extra module prevents the thumb from reaching the lateral side of the index finger, restricting the thumb's abduction RoM.

We developed whole-finger thumb actuators in Chapter 3 and 4 and a modular finger actuator (M-ACT) designed by Kokubu in [88], which are fiber-reinforced soft actuators. The whole-finger thumb actuator developed in Chapter 3 (3C-ACT) has three tapering inner chambers designed to compensate for the hand's space limitation and cope with the unique RoM requirements of thumb joints. The air inflation of the middle chamber supports thumb flexion, the two side chambers support abduction and adduction, respectively; and the simultaneous pressurization of the middle and left-side chambers supports thumb opposition. This three-chamber actuator can assist the fingertip of the thumb in touching nearly all the positions recommended in the Kapandji test [63], which is used to access the thumb's opposition. However, it showed inter-chamber interference manifested as undesired flexion during left-side chamber pressurization.

The M-ACT was not specifically designed for the thumb or multi-DoF support, but we can arrange multiple modules while taking space constraint and inter-chamber interference into account to achieve support in different DoFs of the thumb's CMC joint, e.g., by attaching two modules vertically side by side. Air inflation of one of the modules would produce thumb abduction or adduction, and their simultaneous air inflation could cause joint flexion.

Based on the design concepts and results in previous studies, we suspect the modular type actuator has advantages for individual control of each joint because the module mounted on each joint can be connected to different air inlets and be controlled separately. Modular actuators can also deform to accommodate the contours of the fingers. However, this may no longer be its unique advantage, as we designed the whole-type actuator with tapering inner chambers in Chapter 3, which has force output that meets the RoM demands of finger joints. Moreover, multiple modules need to be connected head-to-tail, which may lead to interference between front and back modules upon pressurization.

The control method of the whole-finger actuator may be simpler than the modular type, with only 2 to 3 chambers to be controlled individually, each air chamber being capable of impelling the bending of all finger joints. It cannot, however, control each finger joint individually, and there will be interference between neighboring chambers during air pressurization.

Few studies have been conducted to develop effective soft thumb actuators; additionally, the advantages and disadvantages of whole-finger and modular types in thumb motion assist (multi-DoF assist) remain unknown.

6.3 Goals

Although several of the studies mentioned above accessed their thumb actuators or modules, the data cannot be directly compared because the actuators were designed, manufactured, and measured based on different schemes. The comparison of the two thumb actuator types would surely provide insights into soft-actuator-based thumb motion support and improvement of the function of soft robotic gloves.

Therefore, this study aimed to:

1) Design and evaluate the modular type of fiber-reinforced thumb actuator.

2) Compare the thumb assist performances of whole-finger actuators and designed modular actuators.

Thumb assist performances were assessed in terms of RoM and force output of thumb flexion and abduction, and an enhanced Kapandji test measured both the Kapandji score and thumb-tip pinch force.

6.4 Actuator prototyping

6.4.1 Functional requirements

The active thumb RoM of the participant was assessed using two methods: one with a goniometer and the other with a camera-based three-dimensional marker detection system (OpenCV with Python). The actuator RoM requirements were set to the same value as that measured using OpenCV, since the value of OpenCV was similar to that measured with a goniometer (Table 6.1), and the actuator RoM would be evaluated using the same system.

TABLE 6.1: RoM requirements of the thumb and actuators [°].

Thumb Motion	Real Thumb RoM [°]		Actuator RoM
	Goniometer Value	OpenCV Value	Requirement [°]
IP joint flexion	90	89	89
MCP joint flexion	37	32	32
CMC joint flexion	15	13	13
CMC joint abduction	43	38	38

RoM: range of motion; IP: interphalangeal; MCP: metacarpophalangeal; CMC: carpometacarpal.

6.4.2 Design parameters of the 3-chamber, hybrid fiber reinforced and modular thumb actuators

The 3C-ACT and M-ACT were designed in similar schemes. Specifically, based on the actuator design in Chapter 3, chamber thickness of all three actuators was set at 2 mm. Because of its more complicated multi-chamber inner structure, the 3C-ACT's height and width were 1 mm greater than the M-ACT's (Fig. 3.3 vs. Fig. 6.1). The M-ACT had a fiber loop interval of 2 mm, which was 0.5 mm greater than the 3C-ACT, since fiber wrapping that is too dense significantly hinders its bending capability [88].

3-chamber thumb actuator

The 3C-ACT is in a semi-cylindrical shape and has three tapering chambers. The middle chamber for thumb flexion was in a tapering-up fashion, with the maximum cross section area at the tip and the minimum at the root, matching the maximum flexion RoM requirement at the IP joint and the minimum at the CMC joint (Chapter 3, Fig. 3.3). The two side-chambers for abduction–adduction were in a contrary structure (tapering down) because thumb abduction only occurs at the CMC joint.

Modular type of thumb actuator

The actuator module was 23 mm long, which is long enough to fit into any of the thumb joints (Fig. 6.1). The fiber was wrapped in 12 loops of two-way hitching [88]. Two modules were connected head-to-tail, one for each of the IP joints and MCP joints, for impelling joint flexion. The bottom surface of the flexion module was made of stiffer silicon than the rest to limit the extension of the bottom surface, thus facilitating the module to flex.

The actuator unit for the CMC joint was designed based on the concept of utilizing pre-existing flexion modules to realize multi-DoF support without a noticeable sacrifice of ROM of abduction. According to the previous studies [16] [65] [20] that used a modular actuator for thumb abduction assistance, the modular unit cannot be simply placed transversely between the metacarpal bones of the thumb and the index finger because its initial length would diminish the thumb abduction RoM. Therefore, we designed a CMC unit by attaching the bottom surfaces of two modules via an inextensible nylon thread (1.2 mm in diameter) that ran longitudinally between them. The left module is responsible for CMC abduction, and the simultaneous air inflation of both modules induces CMC flexion. It is noteworthy that the two bottom surfaces cannot be completely attached because the two-module unit

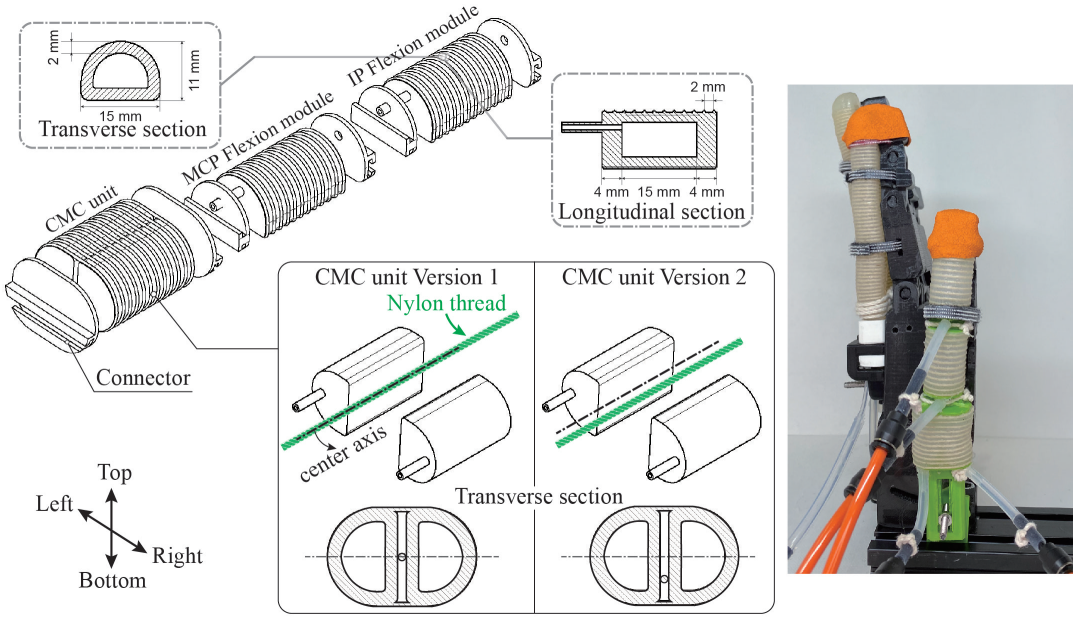

FIGURE 6.1: Actuator structures of modular type.

would have to overcome the elasticity of a shore 20A silicone (the stiffness of the silicone used in this study) block with a width of 4 mm (two times the chamber thickness) and a thickness of 15 mm (the width of the module), causing the unit to barely flex during simultaneous inflation of the two modules. Moreover, the CMC unit was wrapped with 12 loops of the single loop instead of two-way hitching because fibers in two-way hitching would restrict the elongation of the actuator surface that makes contact with the thumb, resulting in unwanted flexion during the air inflation of the left module (abduction). Accordingly, the optimization of the position of the inter-module thread would be important for effective multi-DoF support. We made two versions of the CMC actuator unit: one with the connective thread positioned at the center axis of the bottom surfaces (version 1), and the other with the thread located at a deeper position nearer to the thumb that equals 3/4 of the module's width (version 2).

6.4.3 Actuator fabrication

Smooth-Sil 940 (SmoothOn, Inc., Macungie, PA, USA) was used to make the bottom surface of the flexion module of the M-ACT. The rest of the M-ACT, as well as the entire actuator unit of 3C-ACT, was fabricated using DS 20. Ecoflex 00-30 was used for the final coating after fiber wrapping. The reinforcement fiber was a 0.7-mm-diameter cotton thread. The connector between modules and the root connector for fixing the actuators were printed by the 3D printer.

6.5 Thumb motion support evaluation

For the purpose of practical evaluation, all the measurements were carried out with the designed actuator mounted on the dummy thumb/hand (Fig. 6.2 (a)). The air pressure of the 3C-ACT and the flexion module of the M-ACT were increased in 10 kPa increments, and the CMC unit of the M-ACT was increased in 15 kPa increments (corresponding to a smaller RoM requirement of the CMC joint than the other joints)

until they reached their limit, at which point the actuator deformed extremely. Each measurement was repeated at least three times, and the mean value was evaluated.

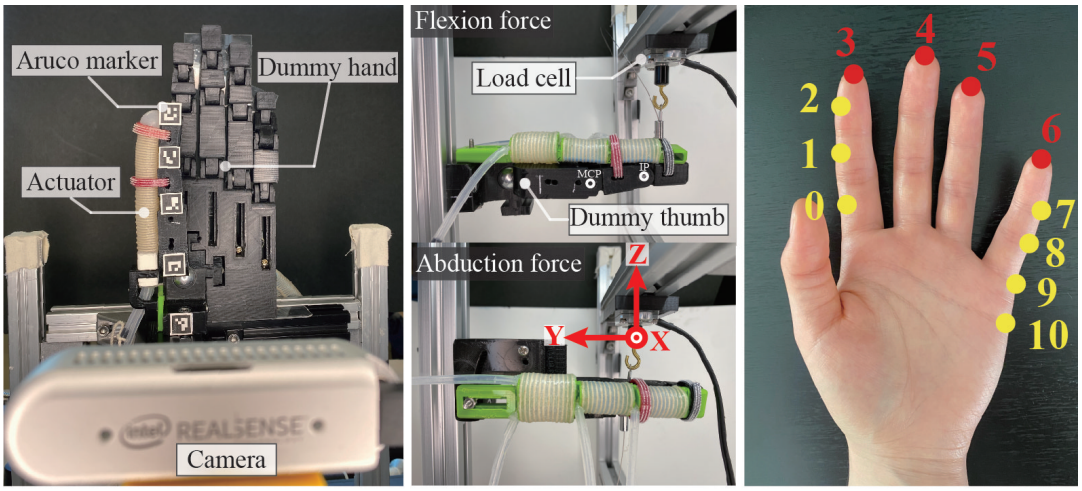

(a) RoM measurement (b) Force measurement (c) Kapandji score

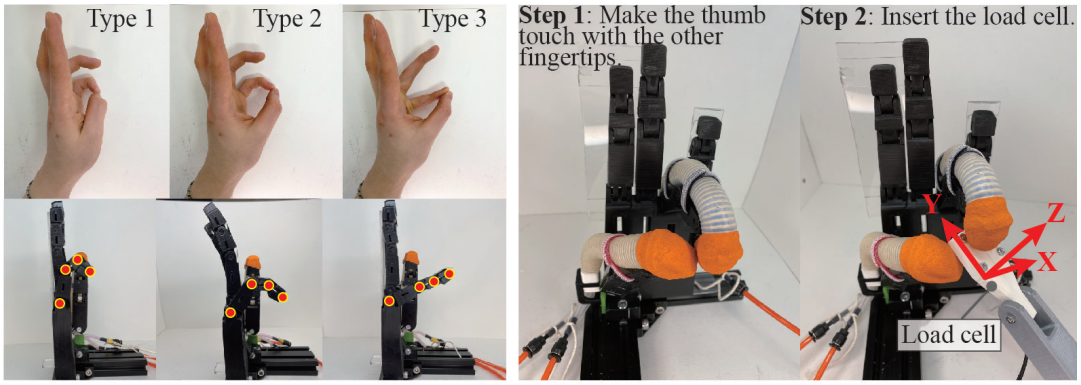

(d) Three types of thumb-small opposition (e) Pinch force measurement

FIGURE 6.2: Measurement setups

6.5.1 Bending RoM and force output measured with a dummy thumb

The methods and setups for measuring the bending angle and force output were the same as those demonstrated in Chapter 4. A camera-based angle calculator constructed with OpenCV was used to calculate the joint angle Fig. 6.2.

Force generated at each thumb segment (DP, PP, and metacarpal) was measured using a three-axis load cell (USL06-H5 Load cell, max: 100 N, Tec Gihan, Kyoto, Japan) (Fig. 6.2 (b)). The flexion force was calculated as the net force of F_Y (elongation force) and F_Z (flexion force). The overall abduction force of the 3C-ACT and IE-type was measured at the middle of the DP segment because the side chamber for abduction extends from the root to the fingertip. The abduction force of the M-ACT was measured at the middle of the PP segment. The abduction force was F_Z, and the flexion force during an abduction was the net force of F_X (flexion force) and F_Y (elongation force).

6.5.2 Enhanced Kapandji test and three specific thumb-small opposition assessment

The Kapandji test has a score range of 0 to 10, indicating where a thumb could touch [63] (Fig. 6.2 (C)). The scores of 9 and 10 were omitted because these movements are rarely used in daily life.

The Kapandji test was performed with various combinations of actuators:

1) A 3C-ACT for thumb assistance and a conventional single-chamber actuator for four-finger assistance.

2) An M-ACT for thumb assistance and a single-chamber actuator for four-finger assistance.

3) A whole-finger type actuator for thumb assistance and an M-ACT with three flexion modules connected in series for four-finger assistance.

Moreover, the clinical Kapandji test only focuses on whether the thumb tip can contact the ten scoring points, though there are multiple thumb–finger postures for achieving the thumb–finger opposition. Fig. 6.2 (d) shows three different thumb–small finger postures for scoring point 6. Therefore, for the most critical thumb–small finger opposition, we measured three postures illustrated in 6.2 (d), which require different degrees of thumb flexion and abduction.

The air pressure in the thumb actuator and the four-finger flexion actuator were carefully tuned to make the thumb reach the target positions specified by the Kapandji test. We inserted the three-axis load cell between fingers after confirming thumb-to-finger contact to record the change in pinch force with the pressurization of the thumb actuator and the four-finger flexion actuator (6.2 (e)). The pinch force was evaluated as the net force of F_X, F_Y, and F_Z.

Thumb opposition failure was defined as the inability of the thumb to reach the target position after a sequence of air pressure adjustments.

6.6 Results

All the RoM and force output results were presented with mean ± SD.

6.6.1 Bending angle results of modular and whole-finger thumb actuators

Flexion RoM

The three thumb joints were flexed to their required angles when using the 3C-ACT and M-ACTs (Fig. 6.3). The two M-ACTs bent the joints to the requirements at a lower air pressure compared with the 3C-ACT.

For the comparison between the two modular actuators, version 2, with a close-to-thumb bending axis, had a slightly larger flexion angle at each joint than version 1, with a bending axis in the center (CMC, MCP, and IP joints were flexed to 8.8°, 29.7°, and 84.1°, respectively, when using version 1, and flexed to 17.5°, 32.3°, and 88.1° when using version 2).

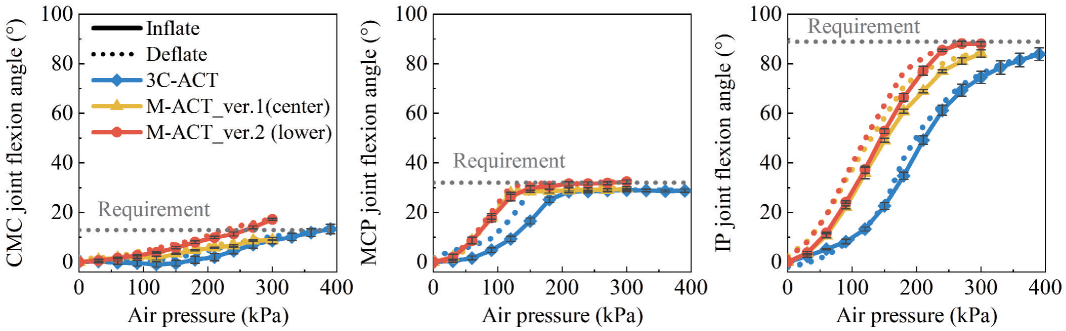

(a) CMC joint flexion angle (b) MCP joint flexion angle (c) IP joint flexion angle

FIGURE 6.3: Flexion RoM of whole-finger and modular actuators.

Abduction RoM

All three thumb actuators rotated the metacarpal of the dummy thumb to the required angle (38°) in the palmar direction (Fig. 6.4 (a)). The thumb flexed during an abduction, particularly for the 3C-ACT (Fig. 6.4 (b-d)). It made all the thumb joints flex at a notably larger angle than M-ACTs.

Only the CMC actuator unit of the M-ACTs was inflated during the abduction. As a result, the CMC joint was flexed the most, followed by the MCP, while the IP joint was barely flexed at all. The M-ACT version 2 generally flexed to a slightly larger angle during abduction than version 1 (Fig. 6.4 (b)).

6.6.2 Force output results of modular and whole-finger thumb actuators

Flexion force

The M-ACTs had a larger maximal flexion force at the metacarpal bone than the 3C-ACT; however, they had a lesser maximal force at the DP segment than the 3C-ACT (Fig. 6.5 (a and c)).

The two versions of the M-ACT exerted similar intensities of maximum flexion force at all three thumb segments (version 1: 3.69 N of flexion force at the metacarpal, 4.96 N at PP, and 4.85 N at DP; version 2: 3.97 N at the metacarpal, 5.16 N at PP, and 4.62 N at DP) (Fig. 6.5).

The 3C-ACT exhibited the greatest flexion force output at the DP, followed by the PP, and the lowest force output at the metacarpal, which is consistent with its design purpose.

Abduction force

The M-ACT and 3C-ACT both had similar maximum torque for thumb abduction (Fig. 6.6 (a)). The abduction torque of the two versions of the M-ACT did not differ significantly, showing that the two versions had a similar abduction force. Combining the results of flexion force output, both versions had similar force output capability.

Similar to the abduction RoM results (Fig. 6.4 (b-d)), the 3C-ACT showed the highest flexion force during thumb abduction, followed by M-ACT version 2; M-ACT version 1 had the lowest (Fig. 6.6 (b)).

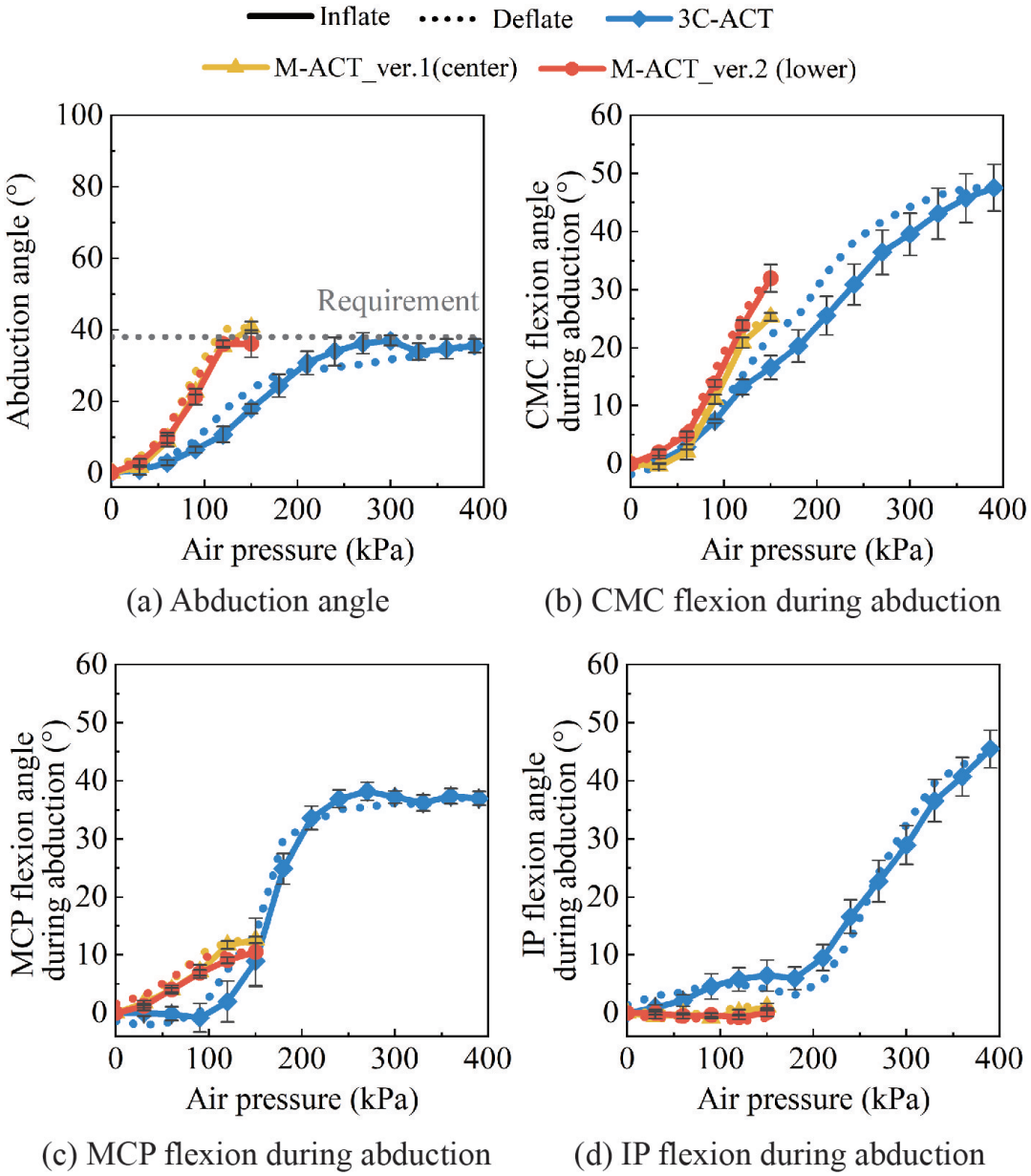

FIGURE 6.4: Abduction RoM of whole-finger and modular actuators

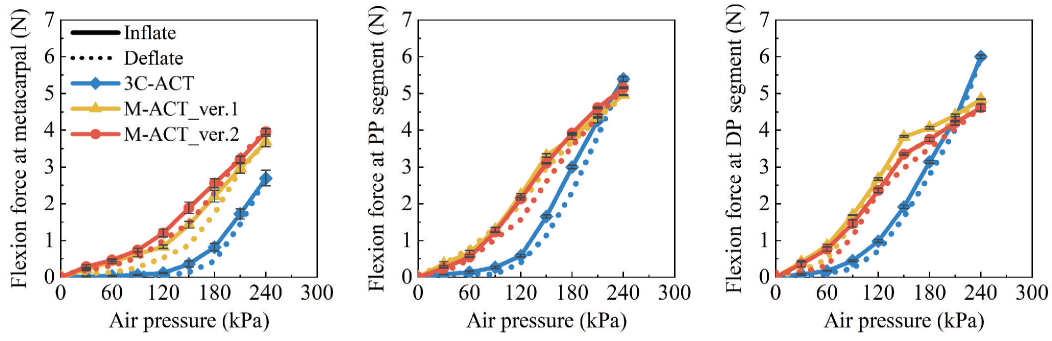

FIGURE 6.5: Flexion force of whole-finger and modular actuators

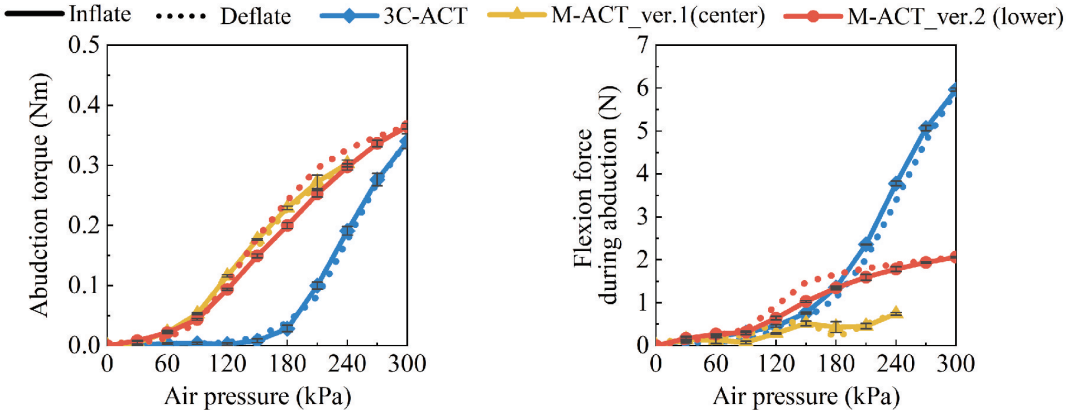

(a) Torque for thumb abduction

(b) Flexion force generated during abudction

FIGURE 6.6: Abduction force of whole-finger and modular actuators

6.6.3 Enhanced Kapandji test of modular and whole-finger thumb actuators

6.6.4 Kapandji Score

When using the same single-chamber actuator for four-finger flexion, the 3C-ACT was able to make the thumb's fingertip touch the 0–8 positions in the Kapandji test (Fig. 6.7 (a)), whereas the M-ACT was unable to realize positions six and seven, which require the most thumb flexion and a relatively larger abduction to make contact with (Fig. 6.7 (b)). Figure A1 (A, lower) illustrates an example of thumb opposition failure. When using the 3C-ACT as the thumb actuator and the M-ACT as the four-finger flex-ion actuator, the thumb achieved a Kapandji score of 0–8 (Fig. 6.7 (c)).

6.6.5 Thumb–Small Opposition

The 3C-ACT was successful in all three types of thumb–small opposition (Fig. 6.8 (a)). Both side chambers responsible for abduction and adduction were inflated to facilitate CMC joint flexion during type 1 and type 2 thumb–small oppositions.

However, the M-ACT was unable to accomplish types 2 and 3 of thumb–small opposition (Fig. 6.8 (b)) because both flexion and abduction were required for the CMC joint. It was challenging to adjust the air pressure of the two actuator modules in the CMC unit to get a stable actuator deformation for achieving multi-DoF thumb opposition. Only type 1 of the thumb–small opposition requires the flexion of all three joints; as a result, both of the modules in the CMC unit were inflated for the flexion of the CMC joint.

Thumb-Tip Pinch Force

The thumb and four fingers may form different arcs of closure at each thumb-tip opposition. In addition, the load cell placement (i.e., angle, contact position) varies from time to time, which affects the pinch force values. For a general assessment, the pinch force was calculated as the average of three times of measurements, and the value at the maximum air inflation was evaluated.

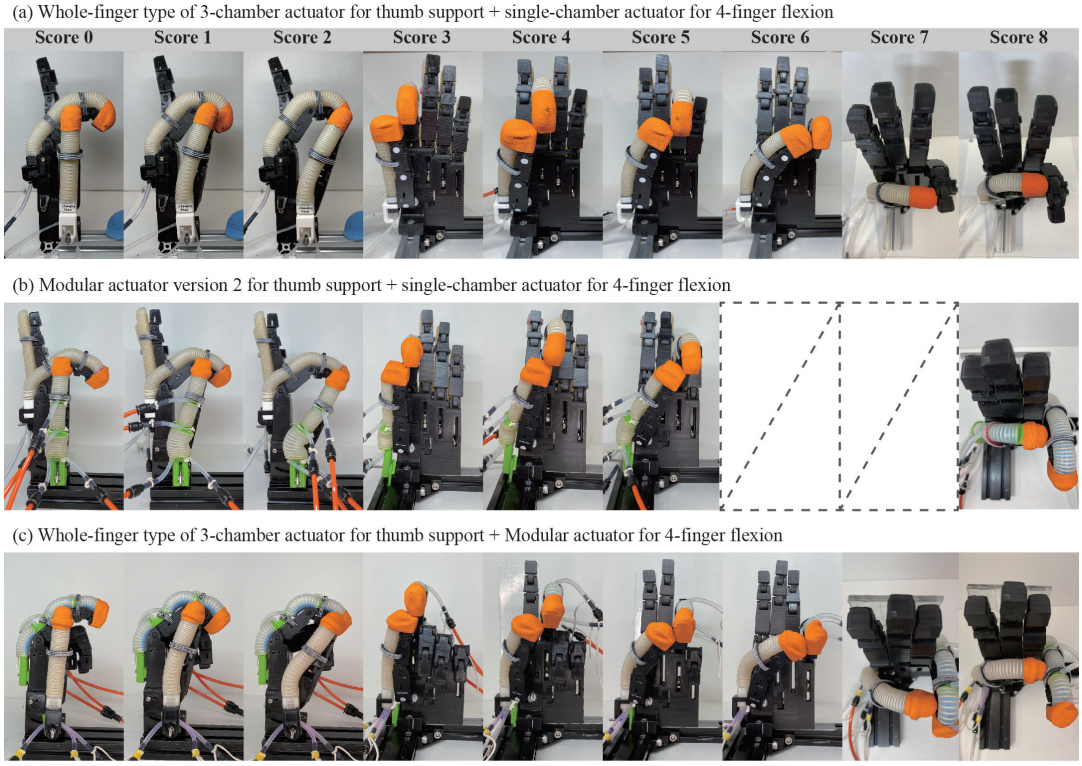

FIGURE 6.7: Kapandji test results of whole-finger and modular actuators

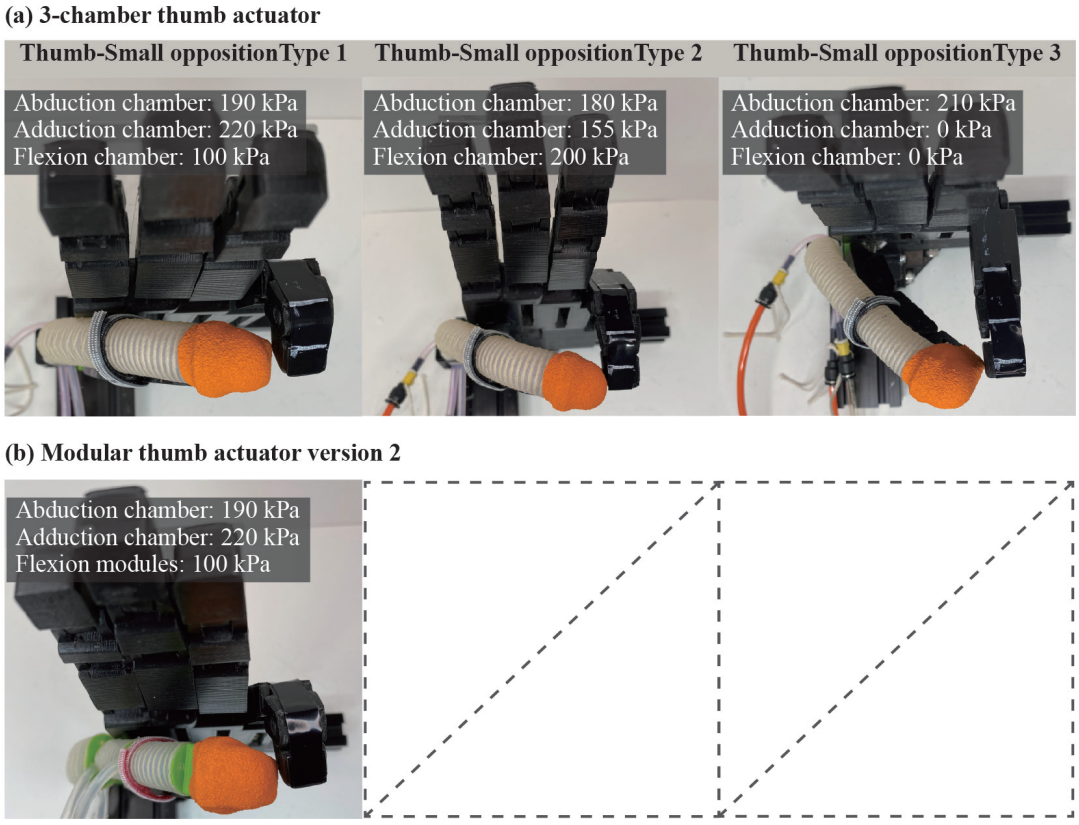

FIGURE 6.8: Three types of thumb–small opposition.

TABLE 6.2: The pinch force of the 3-chamber actuator and modular actuator [N].

Actuator Combination	Thumb-Index	Thumb-Middle	Thumb-Ring	Thumb-Small
3C-ACT (thumb) + single-chamber ACT (4-finger)	5.7	4.1	3.7	4.0
M-ACT (thumb) + single-chamber ACT (4-finger)	5.8	4.3	3.2	-
3C-ACT (thumb) + M-ACT (4-finger)	6.2	5.0	3.5	3.3

3C-ACT: 3-chamber actuator; M-ACT: modular type actuator.

In general, the thumb generated greater pinch forces with the index and middle fingers than with the ring and little fingers, the fingers furthest away from the thumb (Table 6.2).

When the identical single-chamber actuator was used for four-finger flexion, the thumb actuators of the M-ACT and 3C-ACT generated similar levels of pinch force with the three fingers, except for the small finger. The combination of the 3C-ACT and M-ACT produced a greater pinch force than the other two actuator combinations, particularly for the thumb and two fingers next to it (index and middle fingers).

6.7 Discussion

In this section, we evaluated the two M-ACT versions and determined which one works better in terms of thumb flexion and abduction assistance. The M-ACT was then compared with the 3C-ACT in terms of flexion, abduction, and opposition assistance.

6.7.1 Comparison between the two versions of modular thumb actuator

The two versions of the CMC unit of the M-ACT have a similar actuator structure, only differing in the position of the fiber axis (bending axis) for restricting the longitudinal elongation.

In line with the design purpose, version 2, with an off-center bending axis, showed a greater flexion RoM than version 1 (Fig. 6.1). Nevertheless, it did not exhibit a significant advantage in flexion force output, even at the metacarpal bone (corresponding to the CMC joint, Fig. 6.5). The force was measured by inflating all actuator modules simultaneously, including two flexion modules and the CMC unit. Therefore, the measured force was the two actuator modules' combined force before and after the measurement position. In contrast to the flexion module for the IP joint, which had both ends fixed, the connection part of the CMC unit and MCP flexion module was nearly impossible to fix on the hand's dorsal side (Fig. 6.9). As a result, during large air inflation, the root of the MCP flexion module would elevate the head of the CMC unit, thus reducing the flexion effect of the CMC unit.

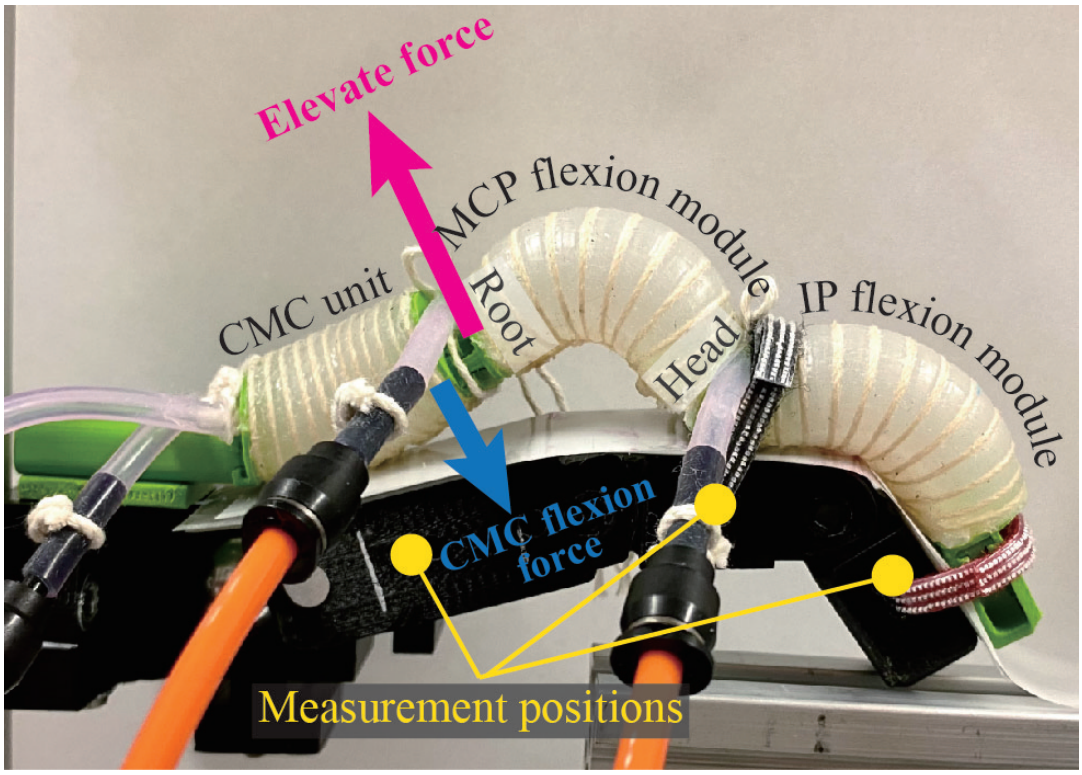

FIGURE 6.9: The deformation of a modular thumb actuator during excessive air inflation.

Additionally, the two versions of the M-ACT differed solely in the CMC unit, but the result showed that version 2 had a slightly greater flexion RoM in the CMC joint (the root section) and the IP joint (the tip section). Since the surface of a finger extends with finger flexion, mostly as the extension of the knuckle creases, the actuator modules need to move or elongate to maintain an efficient bending torque. Version 2 flexed more intensely than version 1 (Fig. 6.3), indicating a greater elongation of the top surface of version 2. The lengthened top part may push the two flexion modules toward the fingertip to some extent. Consequently, the mutual effects between adjacent modules may affect the bending performance of the whole actuator.

In terms of thumb abduction support, both versions of the M-ACT could impel the thumb to abduct to a similar angle (Fig. 6.4 (a)) and give comparable magnitudes of abduction torque (Fig. 6.6 (a)). However, due to its off-center bending axis, version 2 had a larger RoM (Fig. 6.4 (b–d)) and force output (Fig. 6.6 (b)) in the flexion direction during the air inflation of the left module of the CMC unit (abduction).

In general, though version 2 had an undesirable flexion during thumb abduction, it outperformed version 1 in thumb flexion support and may be helpful for the flexion of other joints (i.e., IP joint). Accordingly, the M-ACT version 2 was selected for the following comparison with the 3C-ACT.

6.7.2 Comparison between whole-finger and modular thumb actuators

Single-DoF Support Performance

Both the 3C-ACT and M-ACT were capable of bending the thumb joints to their limited angles (Fig. 6.3 and 6.4 (a)). The 3C-ACT could generate a maximum flexion force of 6.0 N at the DP segment (Fig. 3.7 (c)), and the M-ACT could generate a

maximum force of 5.2 N at the PP segment (Fig. 6.5 (b)). There has seldom been a study that assessed the force of intrinsic hand muscles required for passive finger flexion. As a reference, the extrinsic muscle group tendon force generated during passive finger motions could be up to 8.8 N [89]. The overall force output of the two actuators on the whole thumb would be intense enough to impel a passive thumb motion, thus demonstrating their capability to support thumb flexion motions.

As for the difference between the two thumb actuator types, the 3C-ACT had a lower flexion force at the metacarpal bone than the M-ACT (Fig. 6.5 (a)) because the middle chamber of the 3C-ACT has the smallest cross section area at the root part, resulting in a much smaller effective area which directly affects the bending angle of an actuator than the M-ACT. The maximum cross section of the 3C-ACT's middle chamber (at the fingertip) was still smaller than that of the M-ACT (Fig. 3.3 (b) and Fig. 6.1), but it produced a larger force output at the DP segment than the M-ACT (Fig. 6.5 (c)). The flexion force was calculated as the combined force of elongation and flexion forces. Due to its double-helix fiber wrapping method, the 3C-ACT may have a greater elongation force than the M-ACT. Such actuator elongation would also be helpful for improving the flexion angle of all three joints.

Moreover, compared with the M-ACT, the 3C-ACT had a significantly larger undesired flexion RoM (Fig. 6.4 (b–d)) and force output (Fig. 6.6 (b)) during thumb abduction. Unlike the CMC unit of the M-ACT, which has more than two symmetry axes in structure (symmetric in both top–bottom and left–right, Fig. 6.1), the 3C-ACT is only symmetric in left–right (Fig. 3.3 (b)). During left chamber pressurization, the curved top surface of the 3C-ACT would expand more vigorously than the bottom surface, resulting in deformation in the flexion direction. Accordingly, the M-ACT's CMC unit with two modules (or chambers) may be more structurally beneficial for independent flexion and abduction support than the actuator with three chambers.

In general, the two types of thumb actuators have equivalent thumb flexion assist capabilities. Structurally, both have the potential to provide sufficient support in thumb flexion and abduction with less sacrifice in RoM when compared with the soft finger actuators designed in previous studies [25], [24], [65], [20]. However, the M-ACT would be more suitable for independent flexion and abduction assistance due to less undesired flexion during an abduction.

Multi-DoF support performance

When using the identical single-chamber actuator to assist the four-finger flexion, the 3C-ACT achieved all the Kapandji scores (0–8, Fig. 6.7 (a)); however, the M-ACT was unable to make the thumb come in contact with the small finger (a Kapandji score of 0–5 and 8, Fig. 6.7 (b)). The result of the Kapandji test is affected by two factors: first, during the measurement of the two actuators, the four-finger flexion actuator may flex the four fingers at different angles; second, the M-ACT may be inferior in thumb opposition support. Table A1 shows that when using the M-ACT and 3C-ACT to perform thumb–finger opposition motions, the four-finger flexion actuator was inflated to similar air pressure ranges. Accordingly, the two actuators had to flex and abduct the thumb to similar angles during the Kapandji test. Therefore, the latter would be the reason for the lower Kapandji score of the M-ACT.

Unlike the air chambers in the 3C-ACT, which are in charge of the actuator bending in identical directions (the middle chamber for flexion, the left side-chamber for abduction, and the right side-chamber for adduction), each chamber of the M-ACT's CMC unit is responsible for the bending in two directions (the left module is responsible for flexion and abduction, and the right module for flexion and adduction).

There would be two strategies for manually inflating the M-ACT for realizing thumb opposition movements. One strategy is to inflate the left module first to abduct the thumb fingertip to the same height as the four-fingertip, then inflate the right module to flex the CMC joint (Fig. A.2 (A)). The pressurization of the right module did not flex the CMC joint on the basis of a certain degree of abduction; instead, it sacrificed the abduction for flexion. The air pressure in the two modules must be adjusted repeatedly until the thumb's fingertip reaches the objective position, which is a difficult procedure to complete manually, as even a minor alteration at the CMC joint would deviate the fingertip (distal part) from the objective position. The other strategy is to first inflate the two modules for CMC flexion and then increase the air pressure in the left module for thumb abduction (Fig. A.2 (B)). Either strategy makes it difficult to achieve a steady and fluent thumb–small opposition support, especially for postures that require both large thumb flexion and abduction because the deformation of the CMC unit in different DoF is not independent. The 3C-ACT, however, is simpler to manipulate. We could adopt either of the above-mentioned strategies to achieve thumb opposition with a less air tuning procedure because its deformation in different DoF is independent (additive), but not mutually depleting. Accordingly, the three-chamber structure of the 3C-ACT may be more beneficial to thumb opposition (multi-DoF) support.

For the same reason, the 3C-ACT can realize all three types of thumb–small positions (Fig. 6.8 (a)), whereas the M-ACT can only realize the first type of thumb–small opposition, which only requires thumb flexion (Fig. 6.8 (b)). Notably, both side chambers of the 3C-ACT were inflated to facilitate CMC joint flexion; otherwise, type 1 and type 2 thumb–small oppositions are impossible to achieve. Though the required angle for CMC joint flexion was 13° (Table 6.1), a rather minor value, it is critical for the thumb to make contact with the finger or position that is away from it.

Since the 3C-ACT outperformed the M-ACT in thumb opposition support and the M-ACT was proven to be proficient at single-DoF support in Section 6.7.2, we kept the 3C-ACT as the thumb actuator and utilized the M-ACT as the four-finger flexion actuator. This combination of 3C-ACT and M-ACT achieved all the Kapandji scores (Fig. 6.7 (c)) and a stronger pinch force than the other two combinations, especially for thumb–index pinch and thumb–middle pinch (Table 6.2). The greatest pinch force, 6.2 N, was generated between the thumb and index finger, demonstrating that the actuators can assist the hand in gripping an object weighing no more than 1.3 kg (12.4 N). Compared with a previous study [15] that measured 1.66 N of thumb–index pincer force using their designed actuator, our actuators could perform more powerful hand manipulation tasks.

Accordingly, utilizing the 3C-ACT as the thumb actuator and the M-ACT as the 4-finger actuator may be the best solution for the robotic glove.

Given the advantages of the two types of thumb actuators, they may be appropriate for distinct hand rehabilitation scenarios. For example, the M-ACT may be useful for patients with severe finger contracture because it can urge the thumb to perform independent abduction and flexion movements, allowing the targeted muscle groups and joints to be stretched and trained separately. The 3C-ACT may be beneficial for advanced exercises such as gross grip and finger pinch (tweezer grip) [90] to improve grip strength.

6.7.3 Contribution

This is the first study to comprehensively evaluate and compare whole-finger and modular soft actuators in terms of practical thumb assist performance. The advantages and disadvantages of the two actuator types for the thumb were analyzed, and an effective actuator combination for a soft robotic glove was provided. Our findings highlight:

1) The superior single-DoF support capability of the modular thumb actuator.

2) The superior multi-DoF support capability of the whole-finger thumb actuator.

Based on these findings, different thumb-assisting strategies could be used with the latest soft actuating technology depending on the degree of hand function impairment.

6.7.4 Future work

The thumb assist performance of the two actuators was examined using a dummy hand that imitated a participant's hand. Similar trials on real hands or patients' hands would be needed for a more practical evaluation. A long-term experiment is also required to assess the effect of the proposed actuator combination (three-chamber thumb actuator and modular four-finger flexion actuator) on the rehabilitation of hand functions. Most importantly, control methods for the three-chamber and modular actuators must be developed.

6.8 Conclusion

This study evaluated the design of the modular thumb actuator and compared it with the whole-finger thumb actuator in terms of thumb flexion, abduction, opposition, and pinch strength.

The CMC unit of the modular thumb actuator was designed into two versions, one with a center axis (version 1) and another with an off-center axis (version 2). Version 2 impelled the thumb joints to flex to a greater angle and provided a larger flexion force than version 1, in addition to its comparable abduction performance to version 1.

In the comparison between the M-ACT version 2 and 3C-ACT, both types achieved the required flexion angle and provided sufficient flexion force; however, the M-ACT had less undesired flexion during thumb abduction, thus making it more suitable for independent flexion and abduction (single-DoF) support.

In respect to thumb opposition support, the 3C-ACT obtained a Kapandji score of 0–8, whereas the M-ACT obtained a score of 0–5. The deficit of the M-ACT in thumb opposition support would be due to its multi-DoF support mechanism. Unlike the 3C-ACT, which can modify its deformation in different DoF by adjusting distinct chambers, the M-ACT cannot adjust the deformation in different DoF independently; an increase in CMC flexion angle reduces the abduction angle and vice versa. Therefore, the 3C-ACT would be more manipulable and easier to realize opposition support.

When the 3C-ACT was used for thumb assistance and the M-ACT was used for four-finger flexion support, the dummy hand performed all the opposition postures in the Kapandji test and achieved a higher pinch force than when the two actuators were used as thumb actuators and collaborated with a single-chamber actuator for

four-finger flexion, indicating that the combination of the 3C-ACT and M-ACT may be an optimal solution for a robotic glove.

Chapter 7

General discussion

7.1 Preface

In this section, we compared the three actuators designed in this doctoral project to each other and to preexisting prototypes to assess their benefits and limitations.

The features and usages of fan-ACT, 3C-ACT, and IE-ACT are summarized in Table 7.1.

7.2 Comparison between the designed actuators vs. preexisting actuators

Fan-ACT: The fan-ACT was designed to mimic the morphology and force application mechanism of hand muscles. It can generate a maximum abduction force of at least 32 N, which is substantially larger than the V-shaped actuator developed by Jiralerspong et al. [21], which has a similar shape and usage (0.9 N at 50 kPa, fan-ACT: 5 N at 50 kPa). Moreover, the fan-ACT can impel the thumb opposition with a significant pinching strength. This type of actuator, however, must have an initial sector angle to leave enough space for the inner chamber. Even though the angle was reduced to its maximum of 27.5° based on the hand structure, it still prevented the thumb from making contact with the lateral-lower part of the index finger. As a result, while this biomimetic approach significantly improved the abduction performance of a thumb abduction actuator, it can only be used at the expense of a portion of the thumb opposition support due to its geometrical limitations.

3C-ACT: The tapering interior chamber structure of the 3C-ACT was designed in accordance with the RoM requirement of thumb joints. It generated the greatest flexion force at the IP joint (fingertip) and the least at the CMC joint (root of the thumb), implying that the 3C-ACT can deform in compliance with the thumb. Compared with actuators that can deform in accordance with finger outline, for example, the segmented Pneu-Net actuator designed in [16] and the modular actuator discussed in Chapter 6, 3C-ACT can support movement in multiple directions using only one single actuator. Furthermore, the tapering chamber design reduced interference between neighbouring chambers. The preexisting cylindrical actuator with three consistent chambers in [22] showed a larger flexion torque during finger abduction. The flexion torque was approximately 2 times larger than the abduction torque. This interference was observed when using 3C-ACT, but the difference between flexion force during abduction and abduction force was diminished (flexion force during abduction: 6.9 N, abduction force: 4.8 N). Accordingly, the biomimetic design of tapering chambers improved the compliance of a multi-chamber actuator to the thumb

TABLE 7.1: Comparison of fan-ACT, 3C-ACT, and IE-ACT.

	Biomimetic approach	Advantage	Disadvantage	Application
Fan - ACT	Mimic the hand muscle morephology	Good thumb abduction (32N)	Less Kapandji score (0-6)	The early stage of rehabilitation that need large assistive force
3C - ACT	Coped with thumb joint RoM requirement	• Good compliance to thumb • High Kapandji score (0-8)	Inter-chamber interference	The mid-late stage of rehabilitation assisting fine motor movements.
IE - ACT	Mimic the skeletal muscle	• Small inter-chamber interference • High Kapandji score (0-8) • High pinching strength (6.6 N)	• Deficit in thumb flexion • Complicate fabrication	The mid-late stage of rehabilitation assisting fine motor movements.

and reduced inter-chamber interference to some extent. Moreover, the 3C-ACT realized the majority of the thumb opposition, indicating its capability of assisting most of the thumb movement in both rehabilitation and daily living.

IE-ACT: The IE-ACT was designed to reduce inter-chamber interference by mimicking the structure of skeletal muscles. In Chapter 5, we compared the IE-ACT and the 3C-ACT and confirmed that the IE-ACT was more effective at reducing interference. It may, however, sacrifice a small portion of flexion RoM due to a stricter fiber constraint. A combined biomimetic approach that integrates tapering chamber design and interior-exterior fiber wrapping method may result in an actuator with high thumb compliance and low inter-chamber interference.

From the physiological aspect, during thumb abduction, the CMC joint not only rotates away from the palm but also slides (the rotation axis is shifting); this causes a mismatch between the position of the actuator and the CMC joint, which may result in unwanted flexion during abduction. Therefore, it may be difficult or even impossible for soft finger actuators to achieve completely independent multi-degree of freedom deformation while maintaining high compliance with the thumb.

As an overview of all sorts of hand rehabilitation gloves, rigid mechanisms could support independent flexion and abduction but lacked finger compliance, oppositely, the thumb even need to compliance with the device in some cases, whereas the soft actuators had high compliance but struggled with independent flexion and abduction support. There may be a trade-off relationship between the two.

7.3 Comparison among fan-shaped vs. 3-chamber vs. interior-exterior hybrid fiber reinforced actuators

Three actuators have different advantages and disadvantages, and may be suitable for different stages of the hand rehabilitation process depending on their biomimetic design approaches (Table 7.1).

Actuators are frequently required to impel fingers with high joint rigidity during the early stages of hand rehabilitation. The fan-ACT, which has a much higher abduction force output than the other two cylindrical actuators (3C-ACT and IE-ACT), would be suitable for this stage. According to a study [91] that measured the joint rigidity of the thumb with osteoarthritis, the joint stiffness can increase to twice that of a normal joint. We converted the stiffness of the joints to the forces required to rotate the stiff joints. Flexion forces at the DP segment, PP segment, and metacarpal bone should be around 5.4 N, 4.0 N, and 1.8 N, respectively, and abduction forces should be around 5.0 N. Both the 3C-ACT and the IE-ACT could flex a rigid thumb, but their abduction force would be slightly insufficient. They could collaborate with a fan-ACT to support thumb movement. Besides, the right chamber for adduction could push the thumb closer to the palm, which may reduce the effect of the initial sector angle of the fan-ACT.

At the mid-late stage of hand rehabilitation, actuators with high dexterity are required to assist the hand in performing fine motor movements. Both 3C-ACT and IE-ACT are qualified owing to their high Kapandji scores. The IE-ACT may be applicable for an earlier stage of rehabilitation than the 3C-ACT because it has less inter-chamber interference so that it can impel independent thumb flexion and abduction, allowing the target muscle groups to be stretched and trained separately.

7.4 Insights into the biomimetic approach

The biomimetic approach, which mimics the morphology of muscle groups, can be applied to assistive devices that need to have a large force output and are used directly on the human body , such as four limbs and the shoulder. These muscle groups are much larger and more regular in shape, making them easier to mimic in shape. Actuators that mimic human muscle morphology and have large force output may also be applicable for activating humanoid robots.

The biomimetic approach, which optimized the size and shape of the interior air chamber cross-section in accordance with RoM requirements, can be applied to other fields in the industry. For example, pneumatic actuators (claws) for grippers used for picking large but light objects can be designed in a tapering down fashion, with the largest area of the air chamber at the fixed end and the smallest at the free end. Tapering chambers can also be made into chamber modules, allowing us to rearrange them as needed. Furthermore, the optimized tapering shape suggests that a soft actuator's cross-section can be designed to accommodate complex segmented deformations.

The interior and exterior hybrid fiber-reinforced actuator is made up of two layers: an air chamber on the inside and a silicone body on the outside. The silicone material of each layer, as well as the material and winding method of the reinforcing fibers, would have a significant impact on the overall actuator's bending ability. As a result of the silicone and fiber material optimization, as well as the use of human physiological mechanisms, functional novel actuators for different applications may be developed. Furthermore, this biomimetic approach achieves based on an understanding of both human physiology and mechanical design. Combining different areas of knowledge, such as physiology and botany, could generate novel biomimetic designs. For example, the flagella locomotion mechanism may provide insight into improving the swimming performance of underwater robots. Some plants, such as sesame and oxalis, can quickly pop out seeds through their structure, which may provide insight into fast response mechanisms.

Chapter 8

Contribution and future work

8.1 Preface

In this doctoral project, we developed biomimetic actuators that take advantage of the thumb's unique biomechanical features. With this goal in mind, we explored new methodologies for fiber-reinforcement soft thumb actuators capable of independent flexion and abduction, full thumb opposition, and a considerable thumb-tip pinch force for practical use.

8.2 Summary of contributions

We contribute to the advancement of soft robotic gloves toward real rehabilitation practice by improving thumb motion support in soft robotic gloves, providing various types of thumb actuators, and demonstrating their use in various stages of the hand rehabilitation process.

The novelties and contributions of the project were:

1. Designed novel geometrical structures and reinforcement fiber layouts for soft thumb actuators while considering the thumb's unique biomechanical features.

2. Enabled the soft thumb actuator to provide adequate support in thumb flexion, abduction, and opposition.

3. Developed systematic evaluation method for measuring both the kinematic aspect of the thumb and thumb-tip pinch force.

Furthermore, we believe the findings are not limited to the use of rehabilitation gloves; the cylindrical actuator with multiple chambers can be used in other devices that require dexterity, such as industrial grippers for sorting objects into different sizes and shapes, etc. The biomimetic design methodologies explored in this project would provide insights into designing robotic devices that interact with humans or are attached directly to the human body and assistive devices that are used in synergy.

8.3 Summary of future works

We improved the functionality of thumb actuators to augment the hand assist efficiency of the soft robotic hand. The following tasks need to be completed before the soft robotic gloves can be used in the real rehabilitation process:

- Active thumb joint extension, particularly for the IP and CMC joints, rather than passive thumb extension.

- Analytical models and mathematical (FEM) models of designed fiber-reinforced actuators with high accuracy are necessary for predicting bending performance when design parameters are changed.

- Compact soft sensors for acquiring the status of the soft actuator, such as bending sensors, force sensors for measuring tip force and joint load, and tactile sensors.

- The control mechanism coped with the viscoelasticity of the silicone material as well as coordinated movements of multiple fingers.

- Experiments were conducted with real hands and patients' hands over a long time span.

Furthermore, since a mismatch in the position of the actuator hand's finger would impair force transmission efficiency and cause discomfort over time, the method of attaching the soft actuator to the human hand must be investigated, such as attaching them directly to the finger or fixing them via a semi-rigid socket structure (i.e., exoskeleton). An entertaining and functional interface that helps the patient to conduct soft-robotic-glove-assisted rehabilitation needs to be constructed. Also, an interface connecting the patient and physical therapist is essential for at-home rehabilitation. 3D automated printing technology capable of producing complex fiber winding would be immensely beneficial for the rapid and mass production of the fiber-reinforced actuator.

8.4 Summary of conclusions

In conclusion, this doctoral project enhanced the dexterity of soft robotic gloves by improving the functionality of the thumb actuator. Our findings have contributed to the hardware aspect of soft robotic gloves, which is the foundation of soft robotic hand rehabilitation. Before the soft robotic gloves can be used on patients, certain tasks pertaining to the software and interface must be completed. Many researchers are currently working on soft robotic glove control, sensing, interface, and other aspects, and we believe the day when soft robotic gloves are used in actual rehabilitation practice will be approaching.

Appendix A

Supplementary figures

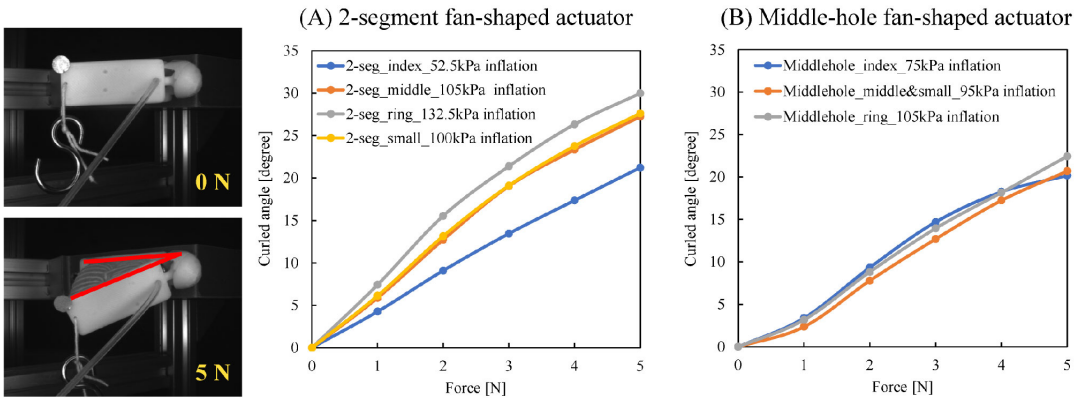

FIGURE A.1: Hand muscles for thumb abduction and opposition

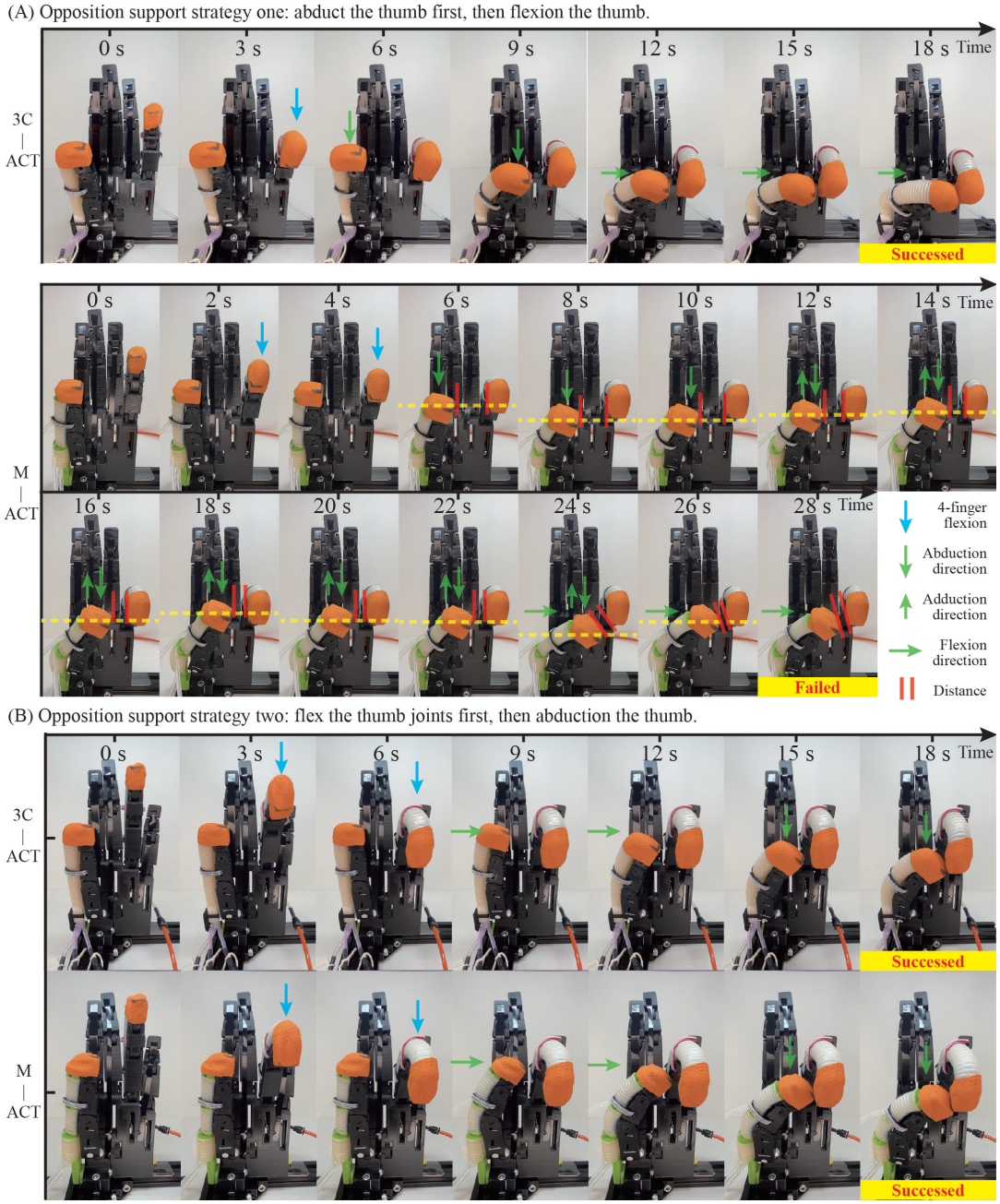

FIGURE A.2: Two strategies for thumb opposition.

Strategy one (Fig. A.2 (A)): abduct the thumb first, then flex the thumb joints. The 3C-ACT achieved thumb–small opposition in 18 s, whereas the M-ACT had to repeatedly adjust the air in-flation in the two modules of the CMC unit (from 12 to 28 s) and did not achieve thumb–small opposition after a sequence of air pressure adjustments. Strategy two (Fig. A.2 (B)): flex the thumb joints first, then abduct the thumb. Both the 3C-ACT and M-ACT realized thumb–ring opposition within 18 s. 3C-ACT: three-chamber actuator; M-ACT: modular type of thumb actuator.

Appendix B

Supplementary tables

TABLE B.1: The air pressure range of actuators during thumb to finger pinching [kPa].

Actuator combination	**Thumb-Index**			**Thumb-Middle**			**Thumb-Ring**			**Thumb-Small**		
	CH for Thumb *Abduction*	**CH for Thumb *Flexion***	**CH for 4-finger *Flexion***	**CH for Thumb *Abduction***	**CH for Thumb *Flexion***	**CH for 4-finger *Flexion***	**CH for Thumb *Abduction***	**CH for Thumb *Flexion***	**CH for 4-finger *Flexion***	**CH for Thumb *Abduction***	**CH for Thumb *Flexion***	**CH for 4-finger *Flexion***
3C-ACT + single-CH ACT	150	0-240	90-150	180	0-240	160-240	195	0-240	160-240	210	0-240	150-240
M-ACT + single-CH ACT	100	0-240	90-150	100	0-240	160-240	90	90-240	130-240	-	-	-
3C-ACT + M-ACT	90	0-240	230-300	150	0-240	280-300	170	120-240	300 (max)	190	150-240	260-300

3C-ACT: 3-chamber actuator, M-ACT: modular actuator, CH: chamber.

Bibliography

[1] W. S. O. (WorldStrokeOrganization). "Global stroke fact sheet." (2019), [Online]. Available: https://www.world-stroke.org/assets/downloads/WSO_Global_Stroke_Fact_Sheet.pdf. (accessed: 19.04.2022).

[2] P. Raghavan, "The nature of hand motor impairment after stroke and its treatment," *Current treatment options in cardiovascular medicine*, vol. 9, no. 3, pp. 221–228, 2007.

[3] F. Mawase, K. Cherry-Allen, J. Xu, M. Anaya, S. Uehara, and P. Celnik, "Pushing the rehabilitation boundaries: Hand motor impairment can be reduced in chronic stroke," *Neurorehabilitation and neural repair*, vol. 34, no. 8, pp. 733–745, 2020.

[4] S. Li, M. L. Latash, G. H. Yue, V. Siemionow, and V. Sahgal, "The effects of stroke and age on finger interaction in multi-finger force production tasks," *Clinical neurophysiology*, vol. 114, no. 9, pp. 1646–1655, 2003.

[5] H. C. Fischer, K. M. Triandafilou, K. O. Thielbar, *et al.*, "Use of a portable assistive glove to facilitate rehabilitation in stroke survivors with severe hand impairment," *IEEE Transactions on Neural Systems and Rehabilitation Engineering*, vol. 24, no. 3, pp. 344–351, 2015.

[6] C. E. Proulx, M. Beaulac, M. David, *et al.*, "Review of the effects of soft robotic gloves for activity-based rehabilitation in individuals with reduced hand function and manual dexterity following a neurological event," *Journal of rehabilitation and assistive technologies engineering*, vol. 7, p. 2 055 668 320 918 130, 2020.

[7] B. Radder, G. B. Prange-Lasonder, A. I. Kottink, A. Melendez-Calderon, J. H. Buurke, and J. S. Rietman, "Feasibility of a wearable soft-robotic glove to support impaired hand function in stroke patients," *J Rehabil Med*, vol. 50, no. 7, pp. 598–606, 2018.

[8] M.-G. Kang, S. J. Yun, S. Y. Lee, *et al.*, "Effects of upper-extremity rehabilitation using smart glove in patients with subacute stroke: Results of a prematurely terminated multicenter randomized controlled trial," *Frontiers in Neurology*, p. 1488, 2020.

[9] R Salazar, A Campos, V Fuentes, and A Abdelkefi, "A review on the modeling, materials, and actuators of aquatic unmanned vehicles," *Ocean Engineering*, vol. 172, pp. 257–285, 2019.

[10] J. M. Ochoa, Y. Jia, D. Narasimhan, and D. G. Kamper, "Development of a portable actuated orthotic glove to facilitate gross extension of the digits for therapeutic training after stroke," in *2009 Annual International Conference of the IEEE Engineering in Medicine and Biology Society*, IEEE, 2009, pp. 6918–6921.

[11] S. W. Lee, K. A. Landers, and H.-S. Park, "Development of a biomimetic hand exotendon device (biomhed) for restoration of functional hand movement post-stroke," *IEEE Transactions on Neural Systems and Rehabilitation Engineering*, vol. 22, no. 4, pp. 886–898, 2014.

[12] P. Polygerinos, S. Lyne, Z. Wang, *et al.*, "Towards a soft pneumatic glove for hand rehabilitation," in *2013 IEEE/RSJ International Conference on Intelligent Robots and Systems*, IEEE, 2013, pp. 1512–1517.

[13] H. K. Yap, J. H. Lim, F. Nasrallah, J. C. Goh, and R. C. Yeow, "A soft exoskeleton for hand assistive and rehabilitation application using pneumatic actuators with variable stiffness," in *2015 IEEE international conference on robotics and automation (ICRA)*, IEEE, 2015, pp. 4967–4972.

[14] G. Gu, D. Wang, L. Ge, and X. Zhu, "Analytical modeling and design of generalized pneu-net soft actuators with three-dimensional deformations," *Soft Robotics*, vol. 8, no. 4, pp. 462–477, 2021.

[15] H. K. Yap, B. W. Ang, J. H. Lim, J. C. Goh, and C.-H. Yeow, "A fabric-regulated soft robotic glove with user intent detection using emg and rfid for hand assistive application," in *2016 IEEE International Conference on Robotics and Automation (ICRA)*, IEEE, 2016, pp. 3537–3542.

[16] J. Wang, Y. Fei, and W. Pang, "Design, modeling, and testing of a soft pneumatic glove with segmented pneunets bending actuators," *IEEE/ASME Transactions on Mechatronics*, vol. 24, no. 3, pp. 990–1001, 2019.

[17] J. Zhou, Y. Chen, X. Chen, Z. Wang, Y. Li, and Y. Liu, "A proprioceptive bellows (pb) actuator with position feedback and force estimation," *IEEE Robotics and Automation Letters*, vol. 5, no. 2, pp. 1867–1874, 2020.

[18] N. Guo, Z. Sun, X. Wang, *et al.*, "Simulation analysis for optimal design of pneumatic bellow actuators for soft-robotic glove," *Biocybernetics and Biomedical Engineering*, vol. 40, no. 4, pp. 1359–1368, 2020.

[19] T Ashuri, A Armani, R Jalilzadeh Hamidi, T Reasnor, S Ahmadi, and K Iqbal, "Biomedical soft robots: Current status and perspective," *Biomedical Engineering Letters*, vol. 10, no. 3, pp. 369–385, 2020.

[20] D. Hu, J. Zhang, Y. Yang, Q. Li, D. Li, and J. Hong, "A novel soft robotic glove with positive-negative pneumatic actuator for hand rehabilitation," in *2020 IEEE/ASME International Conference on Advanced Intelligent Mechatronics (AIM)*, IEEE, 2020, pp. 1840–1847.

[21] T. Jiralerspong, K. H. Heung, R. K. Tong, and Z. Li, "A novel soft robotic glove for daily life assistance," in *2018 7th IEEE International Conference on Biomedical Robotics and Biomechatronics (Biorob)*, IEEE, 2018, pp. 671–676.

[22] T. V. J. Tarvainen, J. Fernandez-Vargas, and W. Yu, "New layouts of fiber reinforcements to enable full finger motion assist with pneumatic multi-chamber elastomer actuators," in *Actuators*, Multidisciplinary Digital Publishing Institute, vol. 7, 2018, p. 31.

[23] P. Polygerinos, K. C. Galloway, E. Savage, M. Herman, K. O'Donnell, and C. J. Walsh, "Soft robotic glove for hand rehabilitation and task specific training," in *2015 IEEE international conference on robotics and automation (ICRA)*, IEEE, 2015, pp. 2913–2919.

[24] P. Polygerinos, Z. Wang, K. C. Galloway, R. J. Wood, and C. J. Walsh, "Soft robotic glove for combined assistance and at-home rehabilitation," *Robotics and Autonomous Systems*, vol. 73, pp. 135–143, 2015.

[25] F. Connolly, C. J. Walsh, and K. Bertoldi, "Automatic design of fiber-reinforced soft actuators for trajectory matching," *Proceedings of the National Academy of Sciences*, vol. 114, no. 1, pp. 51–56, 2017.

[26] P. Maeder-York, T. Clites, E. Boggs, *et al.*, "Biologically inspired soft robot for thumb rehabilitation," *Journal of Medical Devices*, vol. 8, no. 2, 2014.

[27] C. Pearls. "Thumb terminology confusion." (), [Online]. Available: https://bracelab.com/clinicians-classroom/thumb-terminology-confusion. (accessed: 24.04.2022).

[28] D. A. Neumann, *Kinesiology of the musculoskeletal system-e-book: foundations for rehabilitation*. Elsevier Health Sciences, 2016.

[29] P. Brüser and A. Gilbert, *Finger bone and joint injuries*. CRC Press, 1999.

[30] D. A. Neumann and T. Bielefeld, "The carpometacarpal joint of the thumb: Stability, deformity, and therapeutic intervention," *Journal of Orthopaedic & Sports Physical Therapy*, vol. 33, no. 7, pp. 386–399, 2003.

[31] C. Cooper and C. Wietlisbach, *Fundamentals of hand therapy*. Elsevier, 2014.

[32] S. Standring, "Gray's anatomy e-book: The anatomical basis of clinical practice," in 42nd. Elsevier Health Sciences, 2021, pp. 955–989.

[33] K.-S. Lee and M.-C. Jung, "Ergonomic evaluation of biomechanical hand function," *Safety and health at work*, vol. 6, no. 1, pp. 9–17, 2015.

[34] M. Barakat, J Field, and J Taylor, "The range of movement of the thumb," *Hand*, vol. 8, no. 2, pp. 179–182, 2013.

[35] H. Hislop, D. Avers, and M. Brown, *Daniels and Worthingham's muscle Testing-E-Book: Techniques of manual examination and performance testing*. Elsevier Health Sciences, 2013.

[36] A. government. "Commission for the safety rehabilitation and compensation of commonwealth employee." (2011), [Online]. Available: https://www.comcare.gov.au/about/forms-publications/documents/publications/claims/assessment-of-degree-of-permanent-impairment.pdf. (accessed: 28.04.2022).

[37] L. A. Jones and S. J. Lederman, "Human hand function," in Oxford university press, 2007, pp. 141–143.

[38] A. Armstrong, M. C. Hubbard, *et al.*, "Aaos essentials of musculoskeletal care," in Jones & Bartlett Learning, 2021, pp. 508–510.

[39] F. Wang, M. Shastri, C. L. Jones, *et al.*, "Design and control of an actuated thumb exoskeleton for hand rehabilitation following stroke," in *2011 IEEE International Conference on Robotics and Automation*, IEEE, 2011, pp. 3688–3693.

[40] P. Aubin, K. Petersen, H. Sallum, C. Walsh, A. Correia, and L. Stirling, "A pediatric robotic thumb exoskeleton for at-home rehabilitation: The isolated orthosis for thumb actuation (iota)," *International Journal of Intelligent Computing and Cybernetics*, 2014.

[41] O. Lambercy, D. Schröder, S. Zwicker, and R. Gassert, "Design of a thumb exoskeleton for hand rehabilitation," in *Proceedings of the 7th International Convention on Rehabilitation Engineering and Assistive Technology. Singapore*, 2013, p. 41.

[42] J. Iqbal, H. Khan, N. G. Tsagarakis, and D. G. Caldwell, "A novel exoskeleton robotic system for hand rehabilitation–conceptualization to prototyping," *Biocybernetics and biomedical engineering*, vol. 34, no. 2, pp. 79–89, 2014.

[43] P. Agarwal, Y. Yun, J. Fox, K. Madden, and A. D. Deshpande, "Design, control, and testing of a thumb exoskeleton with series elastic actuation," *The International Journal of Robotics Research*, vol. 36, no. 3, pp. 355–375, 2017.

[44] K. Shiota, S. Kokubu, T. V. Tarvainen, *et al.*, "Enhanced kapandji test evaluation of a soft robotic thumb rehabilitation device by developing a fiber-reinforced elastomer-actuator based 5-digit assist system," *Robotics and Autonomous Systems*, vol. 111, pp. 20–30, 2019.

[45] J. Zhou, Y. Li, Y. Yang, H. Cao, J. Huang, and Y. Liu, "A 22-dofs bio-inspired soft hand achieving 6 kinds of in-hand manipulation," in *2021 IEEE International Conference on Real-time Computing and Robotics (RCAR)*, IEEE, 2021, pp. 20–26.

[46] H. Wang, F. J. Abu-Dakka, T. N. Le, V. Kyrki, and H. Xu, "A novel design of soft robotic hand with a human-inspired soft palm for dexterous grasping," *arXiv preprint arXiv:2009.00979*, 2020.

[47] A. Lakhtakia and R. J. Martín-Palma, *Engineered biomimicry*. Newnes, 2013, pp. 81–105.

[48] J. Shintake, V. Cacucciolo, H. Shea, and D. Floreano, "Soft biomimetic fish robot made of dielectric elastomer actuators," *Soft robotics*, vol. 5, no. 4, pp. 466–474, 2018.

[49] G. H. Kwon, J. Y. Park, J. Y. Kim, M. L. Frisk, D. J. Beebe, and S.-H. Lee, "Biomimetic soft multifunctional miniature aquabots," *Small*, vol. 4, no. 12, pp. 2148–2153, 2008.

[50] B. Liao, H. Zang, M. Chen, *et al.*, "Soft rod-climbing robot inspired by winding locomotion of snake," *Soft Robotics*, vol. 7, no. 4, pp. 500–511, 2020.

[51] M. Schaffner, J. A. Faber, L. Pianegonda, P. A. Rühs, F. Coulter, and A. R. Studart, "3d printing of robotic soft actuators with programmable bioinspired architectures," *Nature communications*, vol. 9, no. 1, pp. 1–9, 2018.

[52] J. Fras, M. Macias, Y. Noh, and K. Althoefer, "Fluidical bending actuator designed for soft octopus robot tentacle," in *2018 IEEE International Conference on Soft Robotics (RoboSoft)*, IEEE, 2018, pp. 253–257.

[53] C. Laschi, M. Cianchetti, B. Mazzolai, L. Margheri, M. Follador, and P. Dario, "Soft robot arm inspired by the octopus," *Advanced robotics*, vol. 26, no. 7, pp. 709–727, 2012.

[54] W. Wang, J.-Y. Lee, H. Rodrigue, S.-H. Song, W.-S. Chu, and S.-H. Ahn, "Locomotion of inchworm-inspired robot made of smart soft composite (ssc)," *Bioinspiration & biomimetics*, vol. 9, no. 4, p. 046 006, 2014.

[55] Q. Hu, E. Dong, G. Cheng, H. Jin, J. Yang, and D. Sun, "Inchworm-inspired soft climbing robot using microspine arrays," in *2019 IEEE/RSJ International Conference on Intelligent Robots and Systems (IROS)*, IEEE, 2019, pp. 5800–5805.

[56] T. Sun, Y. Chen, T. Han, C. Jiao, B. Lian, and Y. Song, "A soft gripper with variable stiffness inspired by pangolin scales, toothed pneumatic actuator and autonomous controller," *Robotics and Computer-Integrated Manufacturing*, vol. 61, p. 101 848, 2020.

[57] Y. Jiang, D. Chen, P. Liu, *et al.*, "Fishbone-inspired soft robotic glove for hand rehabilitation with multi-degrees-of-freedom," in *2018 IEEE International Conference on Soft Robotics (RoboSoft)*, IEEE, 2018, pp. 394–399.

[58] K. H. Heung, R. K. Tong, A. T. Lau, and Z. Li, "Robotic glove with soft-elastic composite actuators for assisting activities of daily living," *Soft robotics*, vol. 6, no. 2, pp. 289–304, 2019.

[59] M. de Kraker, R. Selles, T. Schreuders, H. Stam, and S. Hovius, "Palmar abduction: Reliability of 6 measurement methods in healthy adults," *The Journal of hand surgery*, vol. 34, no. 3, pp. 523–530, 2009.

[60] N. B. Reese and W. D. Bandy, *Joint range of motion and muscle length testing-E-book*. Elsevier Health Sciences, 2016.

[61] A. society for surgery of the hand. "Normal range of motion reference values." (2021), [Online]. Available: https://www.eatonhand.com/nor/nor002.htm. (accessed: 05.05.2022).

[62] D. A. N. P. P. FAPTA, "Kinesiology of the musculoskeletal system: Foundations for rehabilitation," 2010.

[63] A. I. Kapandji, "Clinical evaluation of the thumb's opposition," *Journal of Hand Therapy*, vol. 5, no. 2, pp. 102–106, 1992.

[64] Y. Wang, S. Kokubu, Z. Zhou, X. Guo, Y.-H. Hsueh, and W. Yu, "Designing soft pneumatic actuators for thumb movements," *IEEE Robotics and Automation Letters*, vol. 6, no. 4, pp. 8450–8457, 2021.

[65] M. Li, T. Wang, Y. Zhuo, *et al.*, "A soft robotic glove for hand rehabilitation training controlled by movements of the healthy hand," in *2020 17th International Conference on Ubiquitous Robots (UR)*, IEEE, 2020, pp. 62–67.

[66] T. Wang, L. Ge, and G. Gu, "Programmable design of soft pneu-net actuators with oblique chambers can generate coupled bending and twisting motions," *Sensors and Actuators A: Physical*, vol. 271, pp. 131–138, 2018.

[67] Y. Liu, W. Chen, and C. Xiong, "Simulation and fabrication of a pneumatic network actuator with capability of bending in multi-planes," in *2019 IEEE/ASME International Conference on Advanced Intelligent Mechatronics (AIM)*, IEEE, 2019, pp. 313–317.

[68] X. Liu, Y. Zhao, D. Geng, S. Chen, X. Tan, and C. Cao, "Soft humanoid hands with large grasping force enabled by flexible hybrid pneumatic actuators," *Soft Robotics*, vol. 8, no. 2, pp. 175–185, 2021.

[69] J. R. Boatright and G. M. Kiebzak, "The effects of low median nerve block on thumb abduction strength," *The Journal of hand surgery*, vol. 22, no. 5, pp. 849–852, 1997.

[70] W. P. Smutz, A. Kongsayreepong, R. E. Hughes, G. Niebur, W. P. Cooney, and K.-N. An, "Mechanical advantage of the thumb muscles," *Journal of biomechanics*, vol. 31, no. 6, pp. 565–570, 1998.

[71] P. Polygerinos, Z. Wang, J. T. Overvelde, *et al.*, "Modeling of soft fiber-reinforced bending actuators," *IEEE Transactions on Robotics*, vol. 31, no. 3, pp. 778–789, 2015.

[72] F. Liu, L. Carlson, and H. K. Watson, "Quantitative abductor pollicis brevis strength testing: Reliability and normative values," *The Journal of hand surgery*, vol. 25, no. 4, pp. 752–759, 2000.

[73] T.-H. Yang, S.-C. Lu, W.-J. Lin, *et al.*, "Assessing finger joint biomechanics by applying equal force to flexor tendons in vitro using a novel simultaneous approach," *PloS one*, vol. 11, no. 8, e0160301, 2016.

[74] T. Kuroiwa, K. Fujita, A. Nimura, T. Miyamoto, T. Sasaki, and A. Okawa, "A new method of measuring the thumb pronation and palmar abduction angles during opposition movement using a three-axis gyroscope," *Journal of Orthopaedic Surgery and Research*, vol. 13, no. 1, pp. 1–8, 2018.

[75] W. R. Frontera and J. Ochala, "Skeletal muscle: A brief review of structure and function," *Calcified tissue international*, vol. 96, no. 3, pp. 183–195, 2015.

[76] C. Gotti, A. Sensini, A. Zucchelli, R. Carloni, and M. L. Focarete, "Hierarchical fibrous structures for muscle-inspired soft-actuators: A review," *Applied Materials Today*, vol. 20, p. 100 772, 2020.

[77] G. Decroly, B. Mertens, P. Lambert, and A. Delchambre, "Design, characterization and optimization of a soft fluidic actuator for minimally invasive surgery," *International journal of computer assisted radiology and surgery*, vol. 15, no. 2, pp. 333–340, 2020.

[78] B. Zhang, Y. Fan, P. Yang, T. Cao, and H. Liao, "Worm-like soft robot for complicated tubular environments," *Soft robotics*, vol. 6, no. 3, pp. 399–413, 2019.

[79] H. Abidi, G. Gerboni, M. Brancadoro, *et al.*, "Highly dexterous 2-module soft robot for intra-organ navigation in minimally invasive surgery," *The International Journal of Medical Robotics and Computer Assisted Surgery*, vol. 14, no. 1, e1875, 2018.

[80] P. H. Nguyen, S. Sridar, W. Zhang, and P. Polygerinos, "Design and control of a 3-chambered fiber reinforced soft actuator with off-the-shelf stretch sensors," *International Journal of Intelligent Robotics and Applications*, vol. 1, no. 3, pp. 342–351, 2017.

[81] M. Shahzad, A. Kamran, M. Z. Siddiqui, and M. Farhan, "Mechanical characterization and fe modelling of a hyperelastic material," *Materials Research*, vol. 18, pp. 918–924, 2015.

[82] L. Marechal, P. Balland, L. Lindenroth, F. Petrou, C. Kontovounisios, and F. Bello, "Toward a common framework and database of materials for soft robotics," *Soft robotics*, vol. 8, no. 3, pp. 284–297, 2021.

[83] K. An, W. Cooney, E. Chao, L. Askew, and J. Daube, "Determination of forces in extensor pollicis longus and flexor pollicis longus of the thumb," *Journal of Applied Physiology*, vol. 54, no. 3, pp. 714–719, 1983.

[84] R. J. Bloch and H. Gonzalez-Serratos, "Lateral force transmission across costameres in skeletal muscle," *Exercise and sport sciences reviews*, vol. 31, no. 2, pp. 73–78, 2003.

[85] M. C. Hume, H. Gellman, H. McKellop, and R. H. Brumfield Jr, "Functional range of motion of the joints of the hand," *The Journal of hand surgery*, vol. 15, no. 2, pp. 240–243, 1990.

[86] Y. Wang, S. Kokubu, S. Huang, Y.-H. Hsueh, and W. Yu, "Towards an extensive thumb assist: A comparison between whole-finger and modular types of soft pneumatic actuators," *Applied Sciences*, vol. 12, no. 8, p. 3735, 2022.

[87] H. L. Heung, Z. Q. Tang, X. Q. Shi, K. Y. Tong, and Z. Li, "Soft rehabilitation actuator with integrated post-stroke finger spasticity evaluation," *Frontiers in bioengineering and biotechnology*, vol. 8, p. 111, 2020.

[88] S. Kokubu, Y. Wang, P. E. Tortós Vinocour, *et al.*, "Evaluation of fiber-reinforced modular soft actuators for individualized soft rehabilitation gloves," in *Actuators*, MDPI, vol. 11, 2022, p. 84.

[89] F. Schuind, M. Garcia-Elias, W. P. Cooney III, and K.-N. An, "Flexor tendon forces: In vivo measurements," *The Journal of hand surgery*, vol. 17, no. 2, pp. 291–298, 1992.

[90] K. Ellegaard, C. von Bülow, A. Røpke, *et al.*, "Hand exercise for women with rheumatoid arthritis and decreased hand function: An exploratory randomized controlled trial," *Arthritis research & therapy*, vol. 21, no. 1, pp. 1–9, 2019.

[91] J. Z. Wu, Z.-M. Li, R. G. Cutlip, and K.-N. An, "A simulating analysis of the effects of increased joint stiffness on muscle loading in a thumb," *Biomedical engineering online*, vol. 8, no. 1, pp. 1–9, 2009.